# Metallization of Carbon Fiber-Reinforced Polymers (CFRPs) using Cold Spray and Electrochemical Processes

By

Panteha Fallah

Department of Mining and Materials Engineering

McGill University, Montreal

September 2022



A thesis submitted to McGill University in partial fulfillment of the requirements of the degree of Doctor of Philosophy

© Panteha Fallah, 2022

#### **Abstract**

Carbon Fiber-Reinforced Polymers (CFRPs) have been a rapid alternative to aluminium (Al) in the aerospace industry due to their high-specific strength. However, their poor electrical conductivity makes them prone to structural damage during lightning strikes. This study aims to use combinations of the coating processes of cold spray, electroless plating, and electrodeposition to produce metallic coatings for lightning strike protection on CFRPs. Copper (Cu) was selected for cold spraying as it has superior electrical conductivity, making it suitable as a coating material for lightning strike protection.

Previous studies showed that direct cold spraying of Cu onto the CFRP is not possible due to substrate erosion. Cold spray deposition of Cu onto an epoxy-CFRP was then achieved via an interlayer of Cu electrodeposited on an electroless nickel (Ni) coating. It was found that the hardness similarity of the Cu powder to the underlying electrodeposited Cu coating allowed for the successful cold spray deposition of Cu onto the CFRP. Surface roughness and thermal conductivity were also found to play important roles in deposition efficiency of the Cu particle. Cold spray deposition of Cu was not possible on cold sprayed Sn and electroplated Ni interlayers due to the erosion and insufficient plastic deformation of the interlayer, respectively. The feasibility of the cold sprayed Cu coating build-up on the Cu electroplated interlayer was further studied using a two-step process with different gas pressures for each step. Copper coating build-up was possible under this two-step process, with lower deposition efficiency (DE) in the second deposition layer (i.e., the second step). This lower DE was associated with work hardening of the previously deposited layer. Finally, a duplex metallic coating comprising cold spray Sn followed

by electrodeposition of Cu was successfully developed, which had the main advantage of reducing the number of coating steps.

Tensile adhesion/cohesion strengths and electrical conductivity of the fabricated coatings were measured in accordance with ASTM Standard C-633-13 and the 4-point probe conductivity method, respectively. In the three-step coating system (i.e., Ni-Cu-Cu), Cu cold spraying led to the cohesive failure of the cold sprayed Cu coating due to the poor interparticle bonding and the fractured surfaces indicated that the bonding between the Cu particles is mainly mechanical. In the duplex Sn-Cu coating system, electrodeposition of Cu led to the cohesive failure of the cold-sprayed Sn coating. A "dissolution-deposition" mechanism has been established to explain the cohesive failure of the cold-sprayed Sn coating after electrodeposition. The electrical conductivity of the cold sprayed Cu coating was found to be almost two times lower than that of bulk Cu due to the presence of coating defects. However, the electrical conductivity of the electrodeposited Cu coating onto Sn interlayer was close to that of bulk Cu due to its dense and voids-free structure, as well as minimal oxygen content in the coating.

# Résumé

Les polymères renforcés de fibres de carbone (PRFC) ont rapidement remplacé l'aluminium (Al) dans l'industrie aérospatiale en raison de leur résistance spécifique élevée. Cependant, leur faible conductivité électrique les rend susceptibles d'être endommagés par la foudre. Cette étude vise à utiliser des combinaisons de procédés de revêtement par projection à froid, par dépôt chimique et par électrodéposition pour produire des revêtements métalliques de protection contre la foudre sur les CFRP. Le cuivre (Cu) a été choisi pour la projection à froid, car il a une conductivité électrique supérieure, ce qui le rend convenable comme matériau de revêtement pour la protection contre la foudre.

Des études antérieures ont démontré que la projection à froid directe de Cu sur le CFRP n'est pas possible en raison de l'érosion du substrat. Le dépôt par projection à froid de Cu sur un CFRP époxy a donc été réalisé par l'addition d'une couche intermédiaire de Cu déposée par électrolyse sur un revêtement de nickel (Ni) sans courant. Il s'est avéré que la similitude de dureté de la poudre de Cu avec le revêtement de Cu sous-jacent déposé par électrolyse a permis de réussir le dépôt par pulvérisation à froid de Cu sur le CFRP. La rugosité de la surface et la conductivité thermique ont également joué un rôle important dans l'efficacité du dépôt de la particule de Cu. Le dépôt de Cu par pulvérisation à froid n'a pas été possible sur les couches intermédiaires de Sn pulvérisées à froid en raison de l'érosion ni des couches de Ni électroplaquées à cause de la déformation plastique insuffisante de la couche intermédiaire. De plus, la faisabilité de la formation d'un revêtement de cuivre par pulvérisation à froid sur l'intercalaire de cuivre électrodéposé a été étudiée en utilisant un procédé en deux étapes avec différentes pressions de gaz pour chaque étape. La formation d'un revêtement de cuivre a été possible dans ce procédé en deux étapes, avec une efficacité de dépôt (DE) plus faible dans la deuxième couche de dépôt (c'est-à-dire la deuxième étape). Cette efficacité

de dépôt plus faible était associée à un durcissement par travail de la couche déposée initialement. Enfin, un revêtement métallique duplex comprenant une projection à froid de Sn suivie d'une électrodéposition de Cu a été développé avec succès, ce qui a pu réduire le nombre d'étapes de revêtement.

Les forces d'adhésion/cohésion en traction ont été mesurées à la norme ASTM C-633-13 et la conductivité électrique des revêtements fabriqués a été mesurée conformément à la méthode de conductivité par sonde à 4 points. Dans le système de revêtement en trois étapes (c'est-à-dire Ni-Cu-Cu), la pulvérisation à froid de Cu a conduit à la rupture cohésive du revêtement de Cu pulvérisé à froid en raison de la faible liaison interparticulaire et les surfaces fracturées ont indiqué que la liaison entre les particules de Cu est principalement mécanique. Dans le système de revêtement duplex Sn-Cu, l'électrodéposition de Cu a entraîné la rupture cohésive du revêtement de Sn pulvérisé à froid. Un mécanisme de « dissolution-dépôt » a été établi pour expliquer la rupture cohésive du revêtement de Sn pulvérisé à froid après l'électrodéposition. La conductivité électrique du revêtement de Cu projeté à froid était presque deux fois inférieure à celle du Cu brut en raison de la présence de défauts dans le revêtement. Cependant, la conductivité électrique du revêtement de Cu déposé par électrolyse sur l'intercalaire de Sn était proche de celle du Cu massif en raison de sa structure dense et sans vides, ainsi que de la teneur minimale en oxygène dans le revêtement.

# Acknowledgements

As my Ph.D. journey is approaching the end, I would like to express my gratitude to people who have always supported me and made this experience exceptional for me during my Ph.D. studies. This amazing adventure would not have been possible without their help and support.

First and foremost, I would like to thank my supervisor, Professor Stephen Yue, for giving me the opportunity to join his research group and explore the world of cold spray. He has always been supportive and open to any ideas that I had, allowing me to be creative in conducting the project. His unique discipline in supervising helped me improve my skills in several aspects, not only in my professional life but also in my personal perspective. Words cannot describe how grateful I am to have been supervised by him over the period of my Ph.D. studies, Thank you for everything, Professor!

I would also like to thank my co-supervisor, Professor André McDonald for providing me with his constant support and exceptional guidance over this journey. I have learnt a lot from his constructive advice and insightful suggestions. His exceptional dedication to research and professional skills allowed me to grow my academic skills such as writing, editing, and being able to comprehensively explain phenomena and broad-minded thinking. Thank you, Professor!

I wish to thank the collaborators at the National Research Council of Canada (NRC) in Boucherville, namely Dr. Phuong Vo for providing technical support and feedback and Kévin Bricault. This project would not have been possible without their assistance and support.

Green Surface Engineering for Advanced Manufacturing (Green-SEAM) Network, directed by Prof. Christian Moreau from Concordia University, and managed by Simon Durham is gratefully acknowledged. Being part of this network allowed me to expand my academic and industrial connections and interact with people in the thermal spray society. Bombardier Aerospace is also acknowledged for providing us with composite substrates.

I am grateful for the funding source of my project, the Natural Sciences and Engineering Research Council of Canada (NSERC) through Green-SEAM, that allowed me to conduct this project.

I would like to extend my sincere thanks to the administrative members of the department of Mining and Materials Engineering, namely Barbara, Leslie, June, Genny, Heather and Diti.

From the technical support staff, I would like to thank Dr. Florence Paray, Dr. Lise Guichaoua, Robert Paquette, Alexandra Djuric and Stéphanie Bessette for their help in the lab.

Many thanks to my friends and colleagues, namely Evelin, Christina, Andre, Yang, Meixin, Hanqing, John, Lori, Manoj, Masoud and Sriraman for their continuous support and sharing of ideas.

Finally, I would especially like to thank my husband, lovely Ali, for his endless support and for always listening to me. You have always made me feel proud of my effort to achieve my goals.

I particularly thank my second half, my twin sister, Parastoo, from the bottom of my heart who has always been a leader for me! Without you, nothing would have been possible for me!

I am especially grateful for the unending support of my parents, Naser and Niloufar, who have always motivated me with love to keep up the good work through this journey! This dissertation is dedicated to my beloved ones...

# **Contribution of Authors**

The current thesis is comprised of a manuscript-based format that includes three publications and one manuscript ready for submission, respecting the thesis preparation guidelines of McGill University. This thesis is the work accomplished from January 2019 to August 2022 over the program of the author's Ph.D. at McGill University. The contribution of authors for the four manuscripts that are included in chapters 3, 4, 5, and 6 is as follows:

Chapter 3: Panteha Fallah, Sriraman Rajagopalan, André McDonald, Stephen Yue, "Development of hybrid metallic coatings on carbon fiber-reinforced polymers (CFRPs) by cold spray deposition of copper-assisted copper electroplating process", J. Surf. Coat. Technol. 400 (2020), 126231, https://doi.org/10.1016/j.surfcoat.2020.126231.

Chapter 4: Panteha Fallah, Rohan Chakrabarty, Jun Song, André McDonald, Stephen Yue, "Effect of Metallic Interlayer Hardness on Deposition Characteristics of Cold-sprayed Copper Particles on Carbon Fiber-Reinforced Polymers", J. Therm. Spray Technol. 31 (2022), 559–573, https://doi.org/10.1007/s11666-021-01313-9.

Chapter 5: Panteha Fallah, Sima A. Alidokht, Phuong Vo, Richard R. Chromik, André McDonald, Stephen Yue, "Properties of Multilayered Metallic Coatings Deposited on Carbon Fiber-Reinforced Polymers (CFRPs) through Electrochemical and Cold Spray Processes", J. Therm. Spray Technol. (2022), https://doi.org/10.1007/s11666-022-01475-0.

Chapter 6: Panteha Fallah, André McDonald, Stephen Yue, "Development of a Duplex Sn-Cu Coating on Carbon Fiber-Reinforced Polymers (CFRPs) through Cold Spray and Electrodeposition Processes", ready to be submitted.

Panteha Fallah designed and developed experiments, conducted all the experiments (except for the cold spraying and scratch adhesion testing) and material characterization, analyzed and investigated the research results and findings for establishing the discussion points of the manuscripts and wrote all the manuscripts. Cold spraying experiments were performed by the cold spray system operator at the National Research Council of Canada in Boucherville, Québec. Dr. Sriraman Rajagopalan helped in the design of the electrochemical experiments conducted in Chapter 3 and provided comments and feedback for this manuscript. Dr. Rohan Chakrabarty performed all the numerical simulations (FEA analysis), provided FEA results and the corresponding discussion, and wrote the simulation methodology, its results, as well as discussion in Chapter 4. Prof. Jun Song helped with the numerical simulations in Chapter 4 and provided feedback and insights for the FEA part of this manuscript. Dr. Sima A. Alidokht conducted the scratch adhesion testing in **Chapter 5** and provided feedback for this manuscript. Dr. Phuong Vo from the National Research Council of Canada (Boucherville, QC) provided assistance with all the cold spray experiments and comments on the manuscript in Chapter 5. Prof. Richard R. Chromik provided feedback and useful insights for the manuscript in Chapter 5. Prof. Stephen Yue and Prof. André McDonald defined the project, supervised the research, actively provided feedback and valuable insights, discussed the results, and edited all the manuscripts.

# **Table of Contents**

Abstract	I
Résumé	III
Acknowledgements	V
Contribution of Authors	VII
List of Figures	XII
List of Tables	XV
Chapter 1: Introduction	1
1.1 General background	1
1.2 Aims and Objectives	2
1.3 Thesis Overview	3
Chapter 2: Literature Review	6
2.1 Applications and interest in metallizing CFRP	6
2.2 Cold spray process	7
2.2.1 Bonding mechanisms	9
2.2.2 Critical velocity	12
2.2.3 Cold spray onto polymeric substrates	14
2.3 Electrochemical deposition	19
2.3.1 Electroless deposition of polymeric substrate	19
2.3.2 Electrodeposition	22
Chapter 3: Development of Hybrid Metallic Coatings on Carbon Fiber-reinforced Pol (CFRPs) by Cold Spray Deposition of Copper-assisted Copper Electroplating Process	•
Abstract	25
3.1 Introduction	27
3.2 Experimental methodology	29
3.2.1 Feedstock powder and substrates	29
3.2.2 Cu electroplating of CFRPs	32
3.2.3 Cold spray deposition of Cu on the fabricated Cu interlayer	34
3.2.4 Coating characterization	35
3.2.5 Electrical resistivity	35
3.3 Results and discussion	36
3.3.1 Coating characterization	36
3.3.2 Comparison of cold spray on CFRP and Cu panel substrates	43

3.3.3 Hardness effect	45
3.3.4 Surface topology effect	47
3.3.5 Thermal conductivity effect	49
3.3.6 Electrical characterization of cold-sprayed coatings	50
3.4 Conclusion	52
3.5 Acknowledgment	52
Chapter 4: Effect of Metallic Interlayer Hardness on Deposition Characteristics of Cold-specific Copper Particles on Carbon Fiber-Reinforced Polymers	•
Abstract	55
4.1 Introduction	56
4.2 Experimental procedure	58
4.2.1 Feedstock powders and the substrates	58
4.2.2 Fabrication of Sn, Ni, and Cu interlayers on CFRP substrates	60
4.2.3 Cold spray deposition of Cu on various metallic interlayers	
4.2.4 Characterizations of coating and cold spray process	64
4.2.5 Finite element simulations	64
4.3 Results and discussion	66
4.3.1 Cold-sprayed coatings and deposition characteristics	66
4.3.2 Modeling results	71
4.3.3. Single particle impact	79
4.4 Discussion on the deposition behavior	82
4.5 Conclusion	84
4.6 Acknowledgements	85
Chapter 5: Properties of Multilayered Metallic Coatings Deposited on Carbon Fiber-Reinfo	
Polymers (CFRPs) through Electrochemical and Cold Spray Processes	86
Abstract	
5.1 Introduction	87
5.2 Experimental Methodology	
5.2.1 Materials, Metallization Steps, and Conditions	
5.2.2 Coating Properties and Characterization	
5.3 Results	
5.3.1 Tensile Adhesion/Cohesion Bond Strengths	96
5.3.2 Characterization of fractured surfaces in the EN and EN-Cu <sub>1</sub> coating configurations	98
5.3.3 Effect of CFRP surface characteristics on EN coating formation mechanisms	
5.3.4 Characterization of fractured surfaces in the EN-Cu <sub>1</sub> -Cu <sub>2</sub> coating configuration	106
X	

5.3.5 Scratch adhesion bond strength	107
5.3.6 Microstructure analysis	109
5.4 Discussion	112
5.4.1 Adhesion/Cohesion Bond Strengths of Multilayered Coatings	112
5.4.2 Coating Microstructure	114
5.5 Conclusion	115
5.6 Acknowledgement	116
Chapter 6: Development of a Duplex Sn-Cu Coating on Carbon Fiber-Reinforced Polymers	
(CFRPs) using Cold Spray and Electrodeposition Processes	
Abstract	117
6.1 Introduction	119
6.2 Experimental Methodology	120
6.2.1 Materials, Metallization Steps, and Conditions	120
6.2.2 Coating Characterization and Properties	122
6.3 Results and Discussion	124
6.3.1 Coating microstructure	124
6.3.2 Tensile Adhesion/Cohesion Bond Strength	127
6.3.3 Fractured surfaces	128
6.3.4 Dissolution-deposition mechanism	131
6.3.5 Electrical resistivity	134
6.4 Conclusion	135
6.5 Acknowledgement	136
Chapter 7: Concluding Remarks	137
7.1 Global discussion and conclusions	137
7.2 Suggestions of future work	141
7.3 Contributions to original knowledge	143
References	145
Appendix A	155

# **List of Figures**

<b>Figure 2- 1:</b> Schematic presentation of a) high-pressure cold spray (HPCS) and b) low-pressure cold spray (LPCS) [31]
<b>Figure 2- 2:</b> (a) High magnification image of copper coating on ground and annealed aluminium substrate showing aluminium extruded in between copper particles. (b) Fracture surface (coating side) after pull-off test on the same coating-substrate combination showing rim of Al (dark) around Cu particles (bright) [9]
Figure 2- 3: Simulation results of a Cu particle impacting a Cu substrate at a velocity of 600 m/s [32] 11
<b>Figure 2- 4:</b> Schematic illustration of the deposition efficiency in a function of particle velocity [37] 12
<b>Figure 2- 5:</b> Critical impact velocity for a 25 μm particle calculated for different materials [38]
<b>Figure 2- 6:</b> SEM images (a and b) and cross-section optical micrographs (c and d) of the epoxy-CFRP sample after cold spray of spherical Cu powder [12]
<b>Figure 2- 7:</b> Optical micrographs of cross-section view of copper coating on PC/ABS and glass-fiber composites [46]
<b>Figure 2- 8:</b> Optical micrographs of the cross-section view of tin coating on various polymeric substrates [46]
Figure 2- 9: Schematic of the crack filling mechanism [12]
Figure 2- 10: Schematic representation of electroless metal deposition [54]
Figure 2- 11: Mechanism of electroless plating on a non-conductive surface [57]
<b>Figure 2- 12:</b> Migration of metal ions from a sacrificial anode to the cathode with the formation of a metal deposit on the substrate [58]
<b>Figure 2- 13</b> : Schematic of the developed hybrid coatings
<b>Figure 3- 1:</b> The particle size distribution of the copper powder
Figure 3- 2: SEM image of the feedstock copper powder
Figure 3- 3: The image of electroless Ni plated CFRP (a) before and (b) after conducting cold spray Cu33
<b>Figure 3- 4:</b> SEM micrographs of Ni-P deposit on CFRP (a): from the top view, (b): from the cross-section view (white arrows represent the nodular structure)
<b>Figure 3- 5:</b> SEM micrographs of the Cu deposit on CFRP (a): from the top view, (b): from the cross-section view
<b>Figure 3- 6:</b> SEM top (a) and cross-sectional (b) images of the cold sprayed Cu coatings at P= 0.41 MPa on a Cu electroplated CFRP (white arrows show the presence of pores and inter-particle defects)
<b>Figure 3-7:</b> SEM top (a) and cross-sectional (b) images of the cold sprayed Cu coatings at P= 0.45 MPa on a Cu electroplated CFRP (white arrows show the presence of pores and inter-particle defects)

<b>Figure 3- 8:</b> SEM top (a) and cross-sectional (b) images of the cold sprayed Cu coatings at P= 0.46 MPa on a Cu electroplated CFRP (white arrows show the presence of pores and inter-particle defects)
<b>Figure 3- 9:</b> (a) Delaminated copper coating from the CFRP at a pressure of 0.48 MPa (b) SEM image of the delaminated coating
<b>Figure 3- 10:</b> EDS results of the (a) Cu powder, (b) electroplated Cu coating, and (c) cold-sprayed Cu coating at various pressures (0.41, 0.45, 0.46 MPa)
Figure 3- 11: Oxygen content in feedstock material and the coatings (EP Cu and CS Cu coatings) 43
<b>Figure 3- 12:</b> Comparison of deposition efficiency of Cu at various pressures (0.41, 0.45, 0.46 MPa) for two different substrates (Cu electroplated CFRP and grit blasted Cu panel)
<b>Figure 3- 13:</b> Microhardness comparison of feedstock powder, electroplated Cu coating, Cu panel, and cold-sprayed Cu coatings at various pressures (0.41, 0.45, 0.46 MPa)
<b>Figure 3- 14:</b> Indentation micrographs of deformed zones of (a) Cu powder, (b) electroplated Cu coating, (c) Cu panel, and cold-sprayed Cu coatings at various pressures (d) $P = 0.41$ MPa, (e) $P = 0.45$ MPa, and (f) $P = 0.46$ MPa under 10 gf load for a penetration time of 15 seconds
Figure 3- 15: Surface topologies of (a) Cu electroplated interlayer, and (b) grit-blasted copper panel 48
<b>Figure 3- 16:</b> Electrical resistivity comparison of Cu Cs CFRP, Oxygen-free copper, Al, PVC polymer cold sprayed by Cu with Sn and Cu as the interlayers
Figure 4- 1: Particle size distribution of the (a) Cu and (b) Sn powders
Figure 4- 2: SEM images of the feedstock powders: (a) Cu and (b) Sn
<b>Figure 4- 3:</b> (a) Schematic diagram of the meshed model with the substrate dimensions (b) Magnified view of the meshing
Figure 4- 4: SEM micrographs of the Sn interlayer (a) before and (b) after cold spraying Cu
<b>Figure 4- 4:</b> SEM micrographs of the Sn interlayer (a) before and (b) after cold spraying Cu
<b>Figure 4- 5:</b> Comparison of deposition efficiency of the Cu particle sprayed on the electroplated CFRP substrates and mild-steel panels (MS) at various pressures (Substrate refers to: Mild-steel for P1-P2 (MS) and P1 (MS), first cold-sprayed layer for P2*, Cu electroplated CFRP for P1-P2* (EP-CFRP) and P1 (EP-
<b>Figure 4- 5:</b> Comparison of deposition efficiency of the Cu particle sprayed on the electroplated CFRP substrates and mild-steel panels (MS) at various pressures (Substrate refers to: Mild-steel for P1-P2 (MS) and P1 (MS), first cold-sprayed layer for P2*, Cu electroplated CFRP for P1-P2* (EP-CFRP) and P1 (EP-CFRP)). (Note: Standard deviations are indicated in yellow vertical lines (SD = 0.1 to 0.2 for $n = 3$ )) 69 <b>Figure 4- 6:</b> SEM micrographs of the Cu cold sprayed coatings after two-pass pressures of (a and d) 65-

<b>Figure 4- 9:</b> Comparison between (a) temporal evolution of recoverable strain energy (rebound energy) of the entire model for different substrate materials, (b) the particle crater depth and the (c) particle $PEEQ$ at $t = 60$ ns for the different substrate materials (d) the temperature profile of the copper particle and deformed tin substrate
<b>Figure 4- 10:</b> (a) SEM micrograph of Cu deposit on Sn interlayer by individual particle impact (b) and (c): EDS mapping SEM micrographs of the Sn interlayer after single particle impact cold spray
<b>Figure 4- 11:</b> SEM micrographs of the Cu deposits on (a) electroplated Cu interlayer and (b) electroplated Ni interlayer by an individual particle impact (c), and craters on the Ni interlayer surface 82
<b>Figure 5- 1:</b> SEM images of the feedstock Cu powder from (a) top and (b) polished cross-section views
Figure 5- 2: (a) Adhesion strength testing setup and (b) machined steel block
<b>Figure 5- 3:</b> Adhesion/cohesion bond strength of the coatings obtained after electroless Ni deposition (EN), Cu electrodeposition (EN-Cu <sub>1</sub> ), and Cu cold spraying (EN-Cu <sub>1</sub> -Cu <sub>2</sub> ) at three different gas pressures of 60, 65, and 68 psi
<b>Figure 5- 4:</b> Keyence digital microscope images of the (a) CFRP substrate and (b) backing surface of the EN coating after performing the adhesion strength test
<b>Figure 5- 5:</b> (a) top and (b) cross-section views of as-received CFRP, (c) SEM image, (d) EDS map and (e) EDS results of the CFRP surface after the adhesion strength test. SEM images of the (f) peeled EN coating and (g) polished cross-section of the carbon fiber region of CFRP
<b>Figure 5- 6:</b> SEM images of the CFRP after Pd activation in the (a) epoxy and (b) carbon fiber regions. (c) corresponding EDS data of the image (b)
<b>Figure 5- 7:</b> Height profile of the epoxy-CFRP substrate before Pd activation
<b>Figure 5- 8:</b> High magnification SEM images of EN coating fabricated for (a) 15 s and (b) 1 min. Low magnification SEM images of the EN coating fabricated on carbon fibers after (c) 15 s and (d) 15 min. (Note: the red and white arrows indicate Pd particles and EN coating in (a) and (c), respectively) 106
<b>Figure 5- 9:</b> (a-c) SEM images of the backside of the removed coatings and (d-f) corresponding remained Cu coatings cold-sprayed at 60, 65, and 68 psi, respectively
<b>Figure 5- 10:</b> (a) and (b) SEM images of the scratch tracks in the cold-sprayed coatings, (c) and (d) OM images of the cone-shaped fracture in the cold sprayed coatings, (e) and (f) SEM images of the scratch tracks in the electroplated regions after cold spraying at 60 and 68 psi, respectively
<b>Figure 5- 11:</b> ECCI micrographs of the cross-section of the feedstock Cu powder with (a) low and (b) high magnifications
<b>Figure 5- 12:</b> ECC images of cross-sections of (a) Cu electroplated coating, (c) and (e) Cu coatings sprayed at 60 and 68 psi, respectively. (b), (d), and (f) are enlarged views of the white rectangles in (a), (c), and (e), respectively. (Note: the impact direction of the Cu powder is from top to the bottom) 111

<b>Figure 6- 1:</b> SEM images of the feedstock Sn powder from (a) top and (b) polished cross-section vie	
<b>Figure 6- 2:</b> Top surface images of the (a) Sn coating, Sn coating after (b) electrodeposition, and (b) the immersion test	
<b>Figure 6- 3:</b> Top view SEM images of the (a) cold sprayed Sn, (b) electrodeposited Cu coatings, and and d) Sn coating after the immersion test in the plating solution	
<b>Figure 6- 4:</b> (a) and (b) cross-sectional SEM images of the Sn <sub>cs</sub> -Cu <sub>ep</sub> coating and (c)-(f) EDS maps at results of the image (a)	
<b>Figure 6- 5:</b> Adhesion/cohesion bond strength of the cold sprayed Sn coating before and after electrodeposition of Cu and immersion test in the plating solution	128
Figure 6- 6: OM image of the substrate side of a tested Sn coating on epoxy-CFRP	129
<b>Figure 6-7:</b> SEM image and EDS mapping of the coating side of a tested Sn coating in the absence of Cu coating	
<b>Figure 6- 8:</b> (a) and (d) SEM images of the coating and substrate sides of the tested $Sn_{cs}$ - $Cu_{ep}$ coating CFRP, respectively (b) and (e) EDS mapping of the image (a) and (b), respectively, (c) and (f) enlarg views of the rectangles in images (a) and (d), respectively	ed
<b>Figure 6- 9</b> : Schematic of the immersion, dissolution, and deposition mechanism in the absence of current	132
<b>Figure 6- 10:</b> Electrical resistivity of the cold sprayed Sn, electrodeposited Cu coatings on CFRP substrate, bulk Cu and Sn materials	135
List of Tables	
Table 3- 1: Properties of the feedstock powder used in this work	31
Table 3- 2: Cold spray parameters	35
<b>Table 3- 3:</b> Skewness and kurtosis of the electroplated CFRP and grit-blasted Cu panel substrates	48
Table 4- 1: Properties of the feedstock powders used in this work	59
<b>Table 4- 2:</b> Cold spray parameters for the fabrication of Sn interlayers	61
Table 4- 3: Microhardness of the substrates	62
Table 4- 4: Cu cold spray parameters for Sn and Ni coated CFRP substrates	63

Cable 4- 5: Cu cold spray parameters for Cu coated CFRP substrates	63
Cable 4- 6: Descriptions of the simulations	72
<b>Cable 4- 7:</b> Material parameters for copper particles and the substrates of different hardness values. (* efers to experimental hardness values determined for the particle and first deposited layers. ** signifies the modified values of <i>A</i> according to Eq. 2)	
<b>Table 4- 8:</b> Copper particle velocity measurements at 482 °C for different pressures	74
Table 5- 1: Properties of the feedstock Cu powder	92
Cable 5- 2: Cu cold spray parameters for Cu coated CFRP substrates	93
Cable 6- 1: Properties of the feedstock Sn powder	21
Cable 6- 2: Sn cold spray parameters for CFRP substrates         1	22
Cable 6- 3: Solution analysis of the plating solution before and after immersion and electrodeposition for min	

# **Chapter 1: Introduction**

#### 1.1 General background

Metallizing polymeric substrates has gained significant interest in recent decades [1] due to its extensive applications in microelectronics and as heating elements for de-icing applications [2], [3]. As well, attention has been given to polymers and polymeric composite materials such as carbon fiber-reinforced polymers (CFRPs) to be used as structural components in aerospace industry due to their high-specific strength as compared to aluminum (Al) alloys [4]. However, one of the main drawbacks of these materials is their poor electrical conductivity, which make them susceptible to structural damage during the lightning strike [5]. Thus, lightning strike protection (LSP) methods are required for these materials [6]. Current LSP strategies are to bond a metallic foil or a metallic mesh to the outer surface of the composite materials or to metallize the C fibers in the composite structures [5, 7]. However, these structures are not easy to manufacture or, in case of damage, to repair. An alternative LSP approach is to apply electrically conductive metallic coatings onto these materials [6].

Cold spray is a solid-state thermal spray process that has been a suitable coating technique for heat-sensitive materials, such as polymers and polymeric composites, as it uses relatively low temperature, limiting the oxidation risk of the sprayed particles and the substrate heat damage [8]. In this process, micron sized particles are accelerated to a high velocity through a converging-diverging nozzle. The high velocity particles undergo plastic deformation upon impact and bond to a substrate to build up a coating [9].

Cold spraying onto metallic substrates has been extensively studied [10]; however, cold sprayed coatings onto polymers and polymer-based composites is difficult to achieve due to the substrate erosion with poor erosion resistance [11, 12]. Thermoplastic polymers/polymer-based composites are more amenable to cold spraying, and this is attributed to the local thermal softening and its better ductility than brittle thermosets. Whereas thermoset polymers/polymer-based composites are degraded at high temperatures rather than softening and suffer from erosion problem, thus, it is more difficult to achieve coating on these substrates [13]. It was reported that cold spray Cu onto thermoset epoxy polymer and CFRP with epoxy as the matrix material is not possible due to the observed localized fracture and severe erosion rather than deposition [13].

Limited studies have proposed a hybrid coating approach to be used as an alternative solution to metallization of polymeric substrates [13, 14]. This hybrid coating approach involves deposition of an interlayer prior to cold spraying to not only protect the substrate from erosion but to may also enable subsequent cold spray deposition of metals. Although the interlayering concept has been proved to be a promising metallization approach for polymers/polymer-based composites, limited studies are available, and thus more investigations are required to explore this interesting hybrid metallization path.

# 1.2 Aims and Objectives

The aim of this study is to examine the feasibility of the cold spray deposition of Cu onto an epoxy-CFRP. The main method was through a hybrid coating process involving fabrication of a metallic interlayer before cold spraying. Ultimately, since Cu is of a great interest to be used as the coating material on CFRP, a final hybrid approach is proposed that includes electrodeposition of Cu on a cold sprayed Sn interlayer. Therefore, the work provides a better understanding of how

different coating approaches perform with each other. The objectives were achieved by the following scientific approaches:

- Fabricating an interlayer that includes electroless Ni coating (EN) followed by electrodeposition of Cu to determine the feasibility of the subsequent cold spray Cu and to understand the mechanisms affecting deposition efficiency of the Cu particle.
- Fabricating an interlayer comprising electroless Ni followed by electrodeposited Cu coatings for the subsequent cold spray Cu with a two-step gas process to investigate the feasibility of coating build-up and its associated mechanism.
- Fabricating interlayers of cold sprayed Sn and electrodeposited Ni coatings prior to cold spray Cu to understand the effect of their hardness on cold spray deposition of Cu.
- Fabricating a cold sprayed Sn coating  $(Sn_{cs})$  as an interlayer followed by electrodeposition of Cu  $(Cu_{ep})$  to understand the effect of coating processes on mechanical properties of the duplex  $Sn_{cs}$ -Cu<sub>ep</sub> coating.
- Assessing the adhesion strength and electrical conductivity of all the successfully fabricated coatings to correlate the coating process mechanism to mechanical properties of the coatings.

#### 1.3 Thesis Overview

Chapter 2 is the literature review, which includes an overview of the applications requiring metallization of composite materials, a review of the current strategies for metallizing polymers and polymer-based composites through cold spray, an explanation of the fundamentals and basics of the cold spray and electrochemical processes.

In Chapter 3, an interlayer which includes electroless Ni and electrodeposited Cu coatings is developed onto an epoxy-CFRP. Subsequently, cold spray deposition of Cu onto a Cu-coated CFRP and bulk Cu is achieved. Coating characterization is performed and possible mechanisms and influential parameters affecting the deposition efficiency are investigated and discussed.

In Chapter 4, various interlayers are fabricated onto CFRP prior to cold spraying Cu to understand the effect of interlayer hardness on deposition and deformation behavior of the Cu particles. The single particle impact experiment is performed, and the observations are supported by the finite element simulations to examine the particle retention behavior upon impact. Thus, a correlation between the particle deformation behavior and coating deposition is established.

In Chapter 5, properties of the successfully fabricated multilayered coatings (i.e., electroless Ni- electrodeposited Cu- cold sprayed Cu) are characterized, such as adhesion strength, electrical conductivity, and microstructure. The importance of the substrate surface characteristics on coating formation is highlighted. Fractured surfaces are analyzed, and possible bonding mechanisms are explored and discussed.

Chapter 6 is focused on the feasibility of fabricating a duplex metallic coating onto an epoxy-CFRP through cold spray deposition of Sn followed by electrodeposition of Cu. The idea is to reduce the number of coating steps and to possibly enhance the properties of the coating as compared to that of the previously multilayered coating developed in Chapter 3. Adhesion properties and electrical conductivity performance of the duplex Sn<sub>cs</sub>-Cu<sub>ep</sub> coating are evaluated, and the results are compared with coatings fabricated in Chapter 3. Fractured surfaces are analyzed and a mechanism affecting the adhesion properties is described.

A global discussion and conclusions, suggestions of future work and contributions to original knowledge are presented in Chapter 7.

# **Chapter 2: Literature Review**

In this chapter, potential applications and interest in metallizing polymeric substrates are presented. Fundamentals behind the cold spray and electrochemical processes (i.e., electroless and electrodeposition) are explained. The recent developments in metallizing polymeric substrates using cold spray are also reviewed.

#### 2.1 Applications and interest in metallizing CFRP

Metallizing polymeric substrates has gained significant interest in the food packaging and microelectronics industries [2]. In the aerospace industry, there is interest in applying a metallic coating on polymeric composites using plasma spray as the heating element for the de-icing applications [3], but the main interest in the aerospace sector is in relation to carbon fiber-reinforced polymers (CFRPs) that have been extensively used as an alternative to metallic structures due to their low density and high strength [15]. As an example, Boeing 787 DreamLiner is composed of 50 wt% composites (80% in volume) [16].

Aircraft can get struck by lightning, on average once per year, usually on an extremity, such as the wingtip, the nosecone, and the tail [17]. The lightning current then passes through the shortest and the least electrically resistant path of the aircraft, exiting from another extremity, and may cause structural damage to the contact point [17]. Polymer-based composites, such as carbon fiber-reinforced polymers (CFRPs), are composed of carbon fibers and (epoxy) polymers, which are 1 000 and 1000 000 times more electrically resistive than aluminum, respectively [18]. Since the electrical conductivity of CFRP is significantly lower than that of metals, lightning strike protection (LSP) of these materials is required [19]. The LSP is currently provided by applying a copper or aluminum mesh over the outer skin of the aircraft [7]. However, delamination between

layers or burning of the composite material (carbon fiber, resin, or mesh material) may still take place [20]. Another proposed LSP solution is using metalized fibers in the composite structure. This method has been developed to improve the adhesion between carbon fibers and the resin matrix and to enhance the electrical conductivity of the composite material [21]. Metallization of these fibers has been performed by various coating methods such as electroless plating or physical vapor deposition (PVD) with variety of materials such as gold, silver, and copper [5].

Metal coatings is another proposed LSP approach. High-temperature thermal spray processes such as wire-arc spray [22], plasma spray [23], and flame spray [24] have been used to produce electrically conductive metallic coatings to composite structures. However, oxidation of metallic powder and thermal degradation of polymeric substrates may occur [8]. Among thermal spray processes, cold spray has been found to be a suitable approach for fabrication of metallic coatings on polymeric substrates since it uses relatively lower operating temperature (below the melting point of sprayed material), limiting the oxidation of metallic powder and the damage to heat sensitive CFRP [12].

#### 2.2 Cold spray process

Cold spray (CS) is a coating process also known as cold gas-dynamic spray, kinetic spray, micro cold spray, and supersonic particle deposition [25]. Cold spray was first discovered in early 1980s by Dr. Anatolii N. Papyrin at the institute of Theoretical and Applied Mechanics of the Siberian Branch of the Russian Academy of Sciences in Novosibirsk, Russia [26]. The discovery was made while performing experiments of supersonic two-phase flow (gas and solid particles) in a wind tunnel; a transition from erosion by particles to deposition and coating formation was noticed on increasing the particle velocity. Since the recognition of this process, cold spray has

become a promising coating approach to deposit a wide range of pure metal, metallic alloys, and composite materials onto various substrates [27].

Cold spray is a solid-state deposition process in which micron-sized powder particles (1 to 50 µm in diameter) are accelerated to a high velocity through a converging-diverging nozzle ("De Laval"), impact with a substrate, deform plastically and bond to the surface [27, 28]. The powders are inserted into a high-temperature and pressurized gas (nitrogen, helium, or air) and depending on the cold spray process parameters, the particle velocity can be varied from 300 m/s to 1500 m/s for a high-pressure cold spray system (HPCS) and 300 m/s to 550 m/s for a low-pressure cold spray system (LPCS) [29]. The gas temperature is normally well-below the melting point of the feedstock material; thus, the particles are not melted in the carrier gas flow [30]. A schematic of both HPCS and LPCS is presented in Fig 2.1 [31]. In HPCS, the powder particles are pre-mixed with the carrier gas inside the pre-chamber zone and the mix is introduced into the upstream of the converging part of the nozzle, while in the LPCS system, particles are injected to the diverging section of the nozzle (downstream) [31].

The primary advantage of HPCS over LPCS is wider range of materials selection and better quality of the deposit due to its higher particle velocity [31]. Low residual stresses, lack of oxide inclusions and voids, high deposition efficiency and the minimal heat transfer to the substrates are the advantages of cold spraying technique over high-temperature thermal spray processes [26]. Common parameters affecting the particle deformation and the subsequent coating properties is divided into 'materials', i.e., powder and substrate characteristics, and 'process' (including gas type, gas temperature and pressure, standoff distance, etc.) [32].

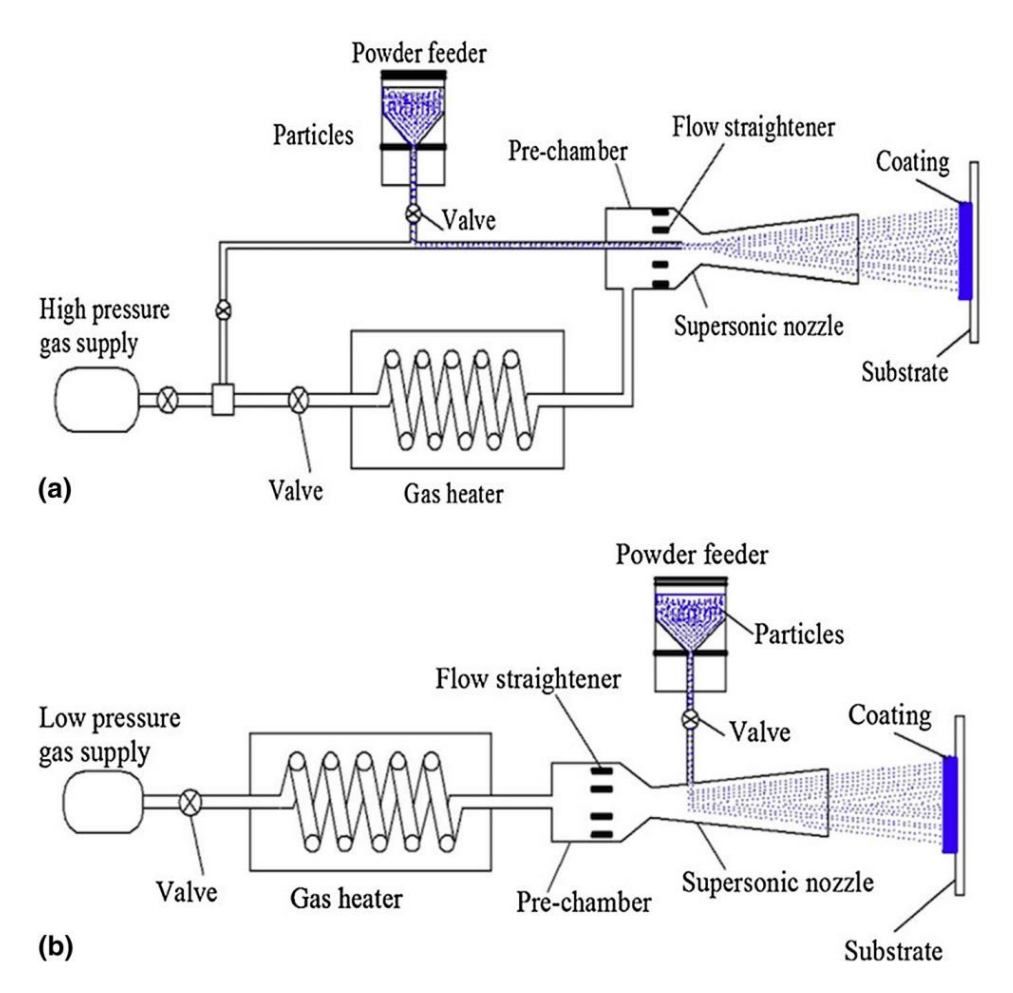


**Figure 2- 1:** Schematic presentation of a) high-pressure cold spray (HPCS) and b) low-pressure cold spray (LPCS) [31]

# 2.2.1 Bonding mechanisms

Bonding processes during cold spray of metal powders onto metallic substrates have been widely studied, but the true bonding mechanism is not still clear [9, 32, 33]. It has been considered that mechanical interlocking and metallurgical bonding are the two main mechanisms associated with the deformation of particle/substrate and particle/particle upon impact [25].

Mechanical interlocking [9] occurs when two 'rough' surfaces are self-interlocked through, e.g., grit-blasting of the substrate or using irregular powder morphology [34]. Mechanical

interlocking can also be formed when hard particles are cold sprayed onto a relatively softer substrate, such as Cu particles on Al substrate (Fig 2-2) [9]. According to Fig 2-2, soft material has been extruded and enveloped the hard Cu particle and the Al rim can be clearly seen in the fracture surface after the pull-test, indicating mechanical interlocking between the soft Al and hard Cu particle (Fig 2-2 (b)). The way to enhance mechanical interlocking is by increasing the gas temperature and pressure, leading to higher particle impact velocity which allows the particles to deeply embed into the substrate. Thus, an enhanced mechanical interlocking and superior bond strength are expected [31].

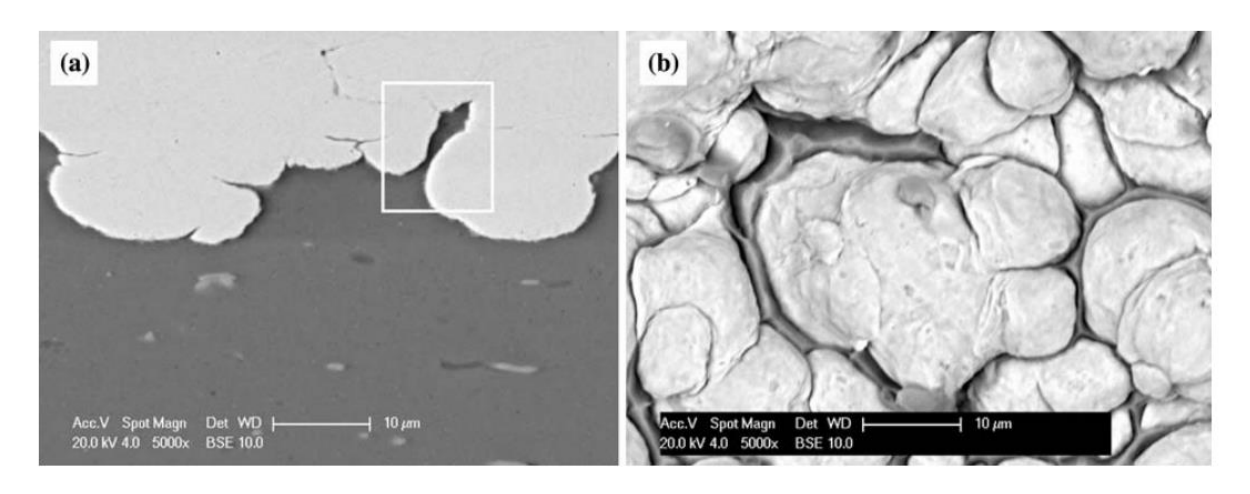


**Figure 2- 2:** (a) High magnification image of copper coating on ground and annealed aluminium substrate showing aluminium extruded in between copper particles. (b) Fracture surface (coating side) after pull-off test on the same coating-substrate combination showing rim of Al (dark) around Cu particles (bright) [9]

When cold spraying onto a non-metallic substrate such as polymeric substrates, mechanical interlocking is the only possible bonding mechanism at the coating/substrate interface [13].

Adiabatic shear instability (ASI) has been proposed to be the main mechanism of metallurgical bonding, which is illustrated in Fig 2-3 [32]. When a particle impacts with sufficiently high velocity a significant level of plastic deformation takes place in a narrow region

close to the particle-substrate interface. At the highly strained interfaces, thin oxide surface films are disrupted, allowing for an intimate contact between the two fresh/clean surfaces of particle-substrate or particle-particle at the atomic level, thus, forming metallurgical bonds across the interfaces. Plastic deformation occurs in a very short time and can be considered as adiabatic, thus leading to a dramatic rise in temperature at the interface [13, 35]. As a result, the material loses its shear strength as the temperature locally approaches the melting point, and the interfaces undergo extensive plastic deformation and behave like viscous fluids, forming metal 'jets'; this phenomenon is modelled in Fig 2-3 [32].

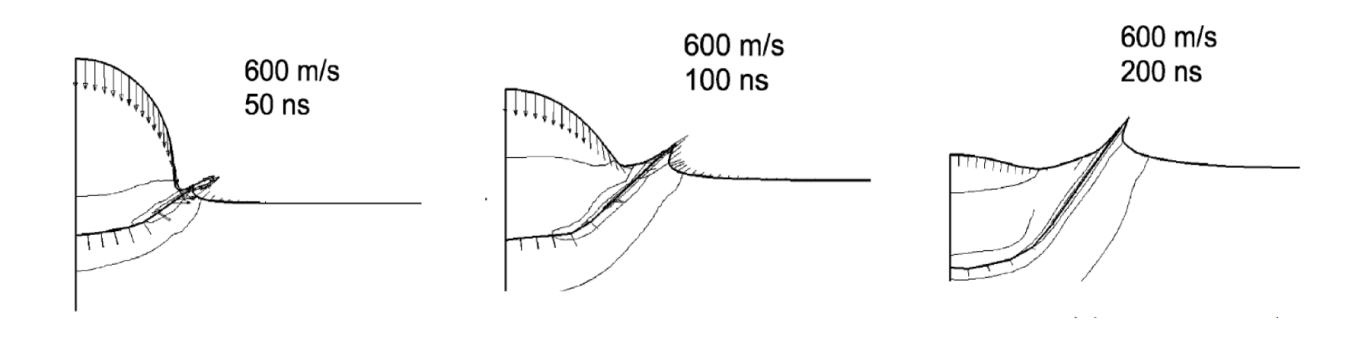


Figure 2- 3: Simulation results of a Cu particle impacting a Cu substrate at a velocity of 600 m/s [32]

As the coating continues to grow layer by layer, impacting particles cause further densification and work hardening of the previously deposited layers through the shot peening mechanism [36].

#### 2.2.2 Critical velocity

Critical velocity ( $V_{crit}$ ) is a minimum particle velocity in which a particle can adhere to a substrate and a coating cannot be obtained until the critical velocity has been exceeded [30]. As demonstrated in Fig 2-4, substrate abrasion occurs below the critical velocity, while above the critical velocity, deposition and coating formation will take place [37].

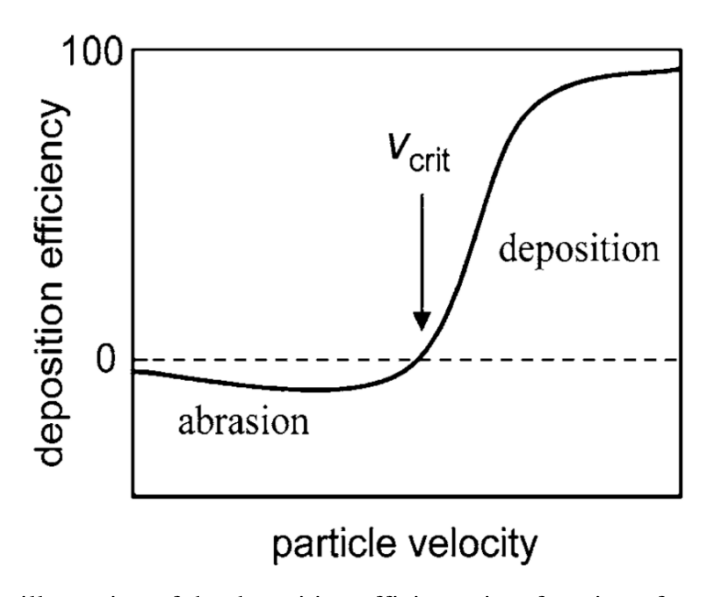


Figure 2- 4: Schematic illustration of the deposition efficiency in a function of particle velocity [37]

Critical velocity for various metal powders have been determined in many studies through experiments or numerical simulations [32]. Schmidt *et al.* [38] proposed one of the first semi-empirical equations to predict the critical velocity of a powder with different properties. According to the equation (Eq. (1)),  $\sigma_{Ts}$  is the tensile strength of the powder material,  $T_i$  the particle temperature at impact,  $T_m$  the melting temperature of the powder material,  $T_R$  the reference temperature (293 K),  $C_p$  the specific heat of the powder material,  $\rho$  the density of the particle, and  $F_1$  and  $F_2$  the empirical factors [38].

$$v_{crit} = \sqrt{\frac{F_1 \cdot 4 \cdot \sigma_{Ts} \cdot \left(1 - \frac{T_i - T_R}{T_m - T_R}\right)}{\rho} + F_2 \cdot c_p \cdot (T_m - T_i)}$$
 Eq. (1)

The critical velocities of 25 µm particles of different materials were calculated based on the semi-empirical equation (Eq. (1)). As shown in Fig 2-5, the dark area represents the range of uncertainty with respect to the range of available materials data [38]. It is noted that materials with low melting points such as tin, lead and zinc or ductile materials resistant to oxidation such as gold and silver, require relatively low critical velocities, while materials that are naturally passivated by an oxide layer (e.g., magnesium, aluminum, titanium) require relatively higher velocities [39].

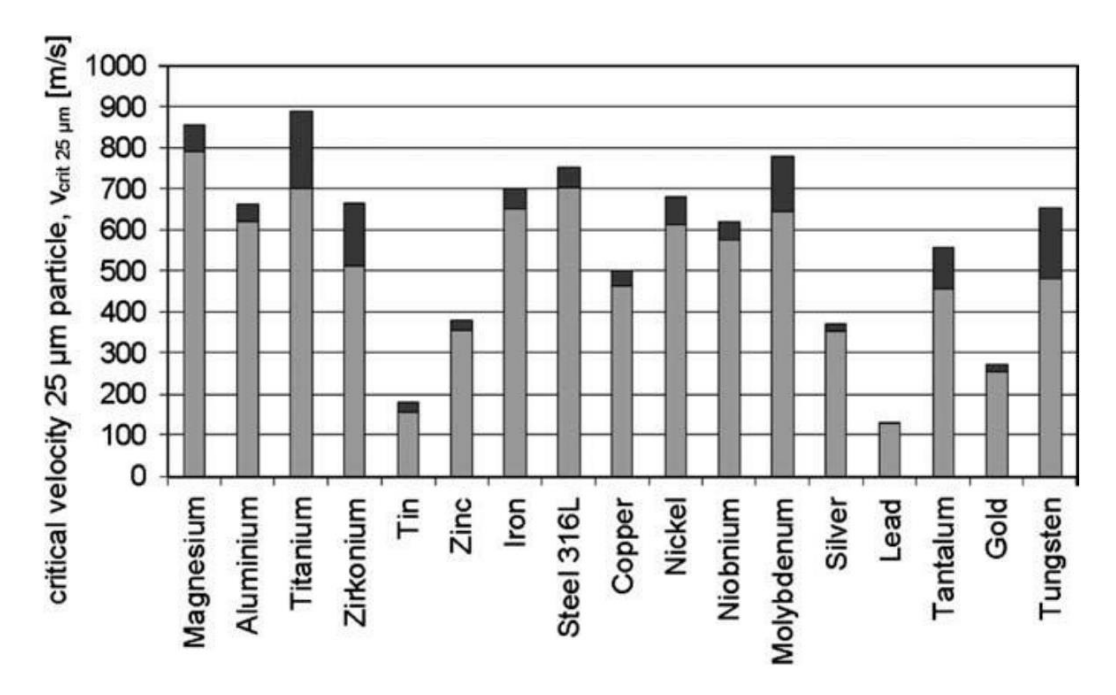


Figure 2- 5: Critical impact velocity for a 25 μm particle calculated for different materials [38]

# 2.2.3 Cold spray onto polymeric substrates

Polymers can be divided into three categories based on their thermal properties: 1) thermoplastics (e.g., acrylonitrile butadiene styrene (ABS), polyvinyl chloride (PVC), polyether ether ketone (PEEK), etc.), 2) thermosets (e.g., epoxy, Bakelite, polyimide, etc.), and 3) elastomers (e.g., natural rubbers) [40].

Thermoplastics contain long molecular polymeric chains held together with relatively weak forces that allows thermoplastics to be softened and melted upon heating and to be reformed when cooled. However, unlike thermoplastics, thermosets are stiffer, harder, and more brittle. Thermosets cannot be softened during heating as they are held together with complex tridimensional cross-linking bonds (covalent bonds) that may break when heated. Thus, thermosets can only be heated and formed once. In elastomers, polymer chains are held together by relatively weak intermolecular forces that allow them to stretch in response to stresses [41].

Carbon fiber-reinforced polymers (CFRPs) contain thermoplastics or thermosets as the polymer matrix and carbon fiber as the reinforcement mainly due to its very high strength, but also low density and low thermal expansion coefficient [42].

Cold spraying onto polymers and polymer composites is more challenging as compared to metallic substrates since they have two or three orders of magnitude less erosion resistance than metals [43]. Normally, thermosets and thermoplastics show brittle and ductile erosive behavior, respectively [44]. Possible mechanisms of solid particle erosion could be surface melting and plastic deformation for thermoplastics and erosion, fracture, or cracks for thermosetting polymers [45]. Therefore, deposition on polymeric substrate is dependant on the nature of the substrate. Cold

spraying onto thermoplastics and its composites is more successful than that of thermosets due to the local thermal softening of thermoplastics [13].

Che *et al.* [12] have attempted to cold spray Cu on an epoxy-CFRP with both spherical and irregular Cu particles. No coating was achieved, and substrate erosion was found to be the main obstacle for deposition. As shown in Fig 2-6, embedded Cu particles were observed within the epoxy area with no obvious plastic deformation and carbon fibers were not only exposed but they also fractured.

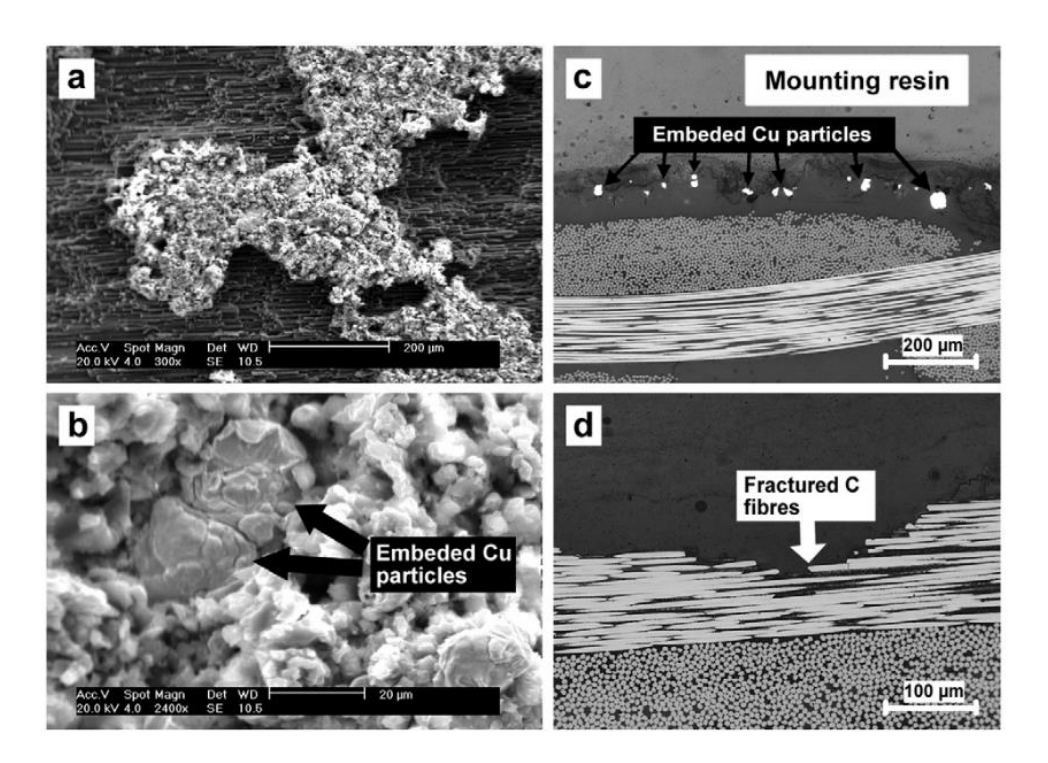


**Figure 2- 6:** SEM images (a and b) and cross-section optical micrographs (c and d) of the epoxy-CFRP sample after cold spray of spherical Cu powder [12]

Cold spray of Cu was attempted at various gas pressures (1 and 2 MPa) on thermoplastic ABS and PEEK polymers. A thick Cu coating was successfully deposited on PEEK polymer at 2 MPa, whereas no coating was achieved on ABS polymer due to the substrate erosion. Mechanical

properties and glass transition temperature ( $T_g$ ) of the polymeric substrates were found to be the primary parameters affecting the deposition [12].

Lupoi and O'Neill [46] have attempted cold spraying copper, tin and aluminum powders on various thermoplastics (Polycarbonate/ABS, polyamide-6, polypropylene and polystyrene) and on a glass-fibre composite material. Deposition of aluminum was unsuccessful, leading to no deposition or erosion, and cold spraying of Cu also led to substrate erosion (Fig 2-7) and was also unsuccessful, while cold spraying of tin led to successful deposition, as shown in Fig 2-8.

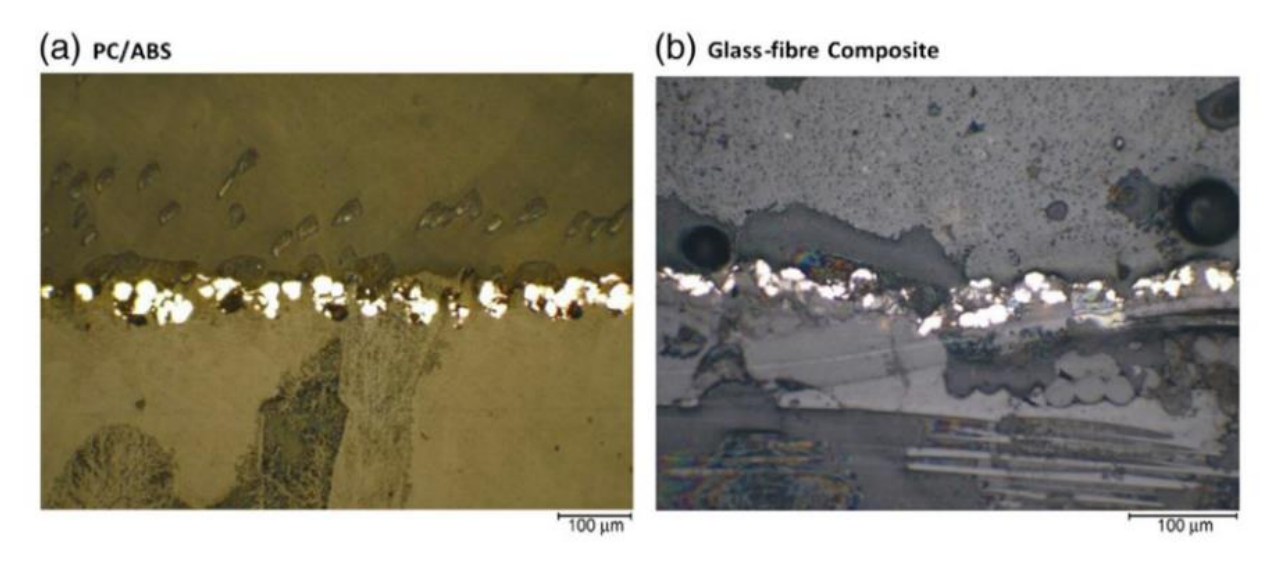


**Figure 2- 7:** Optical micrographs of cross-section view of copper coating on PC/ABS and glass-fiber composites [46]

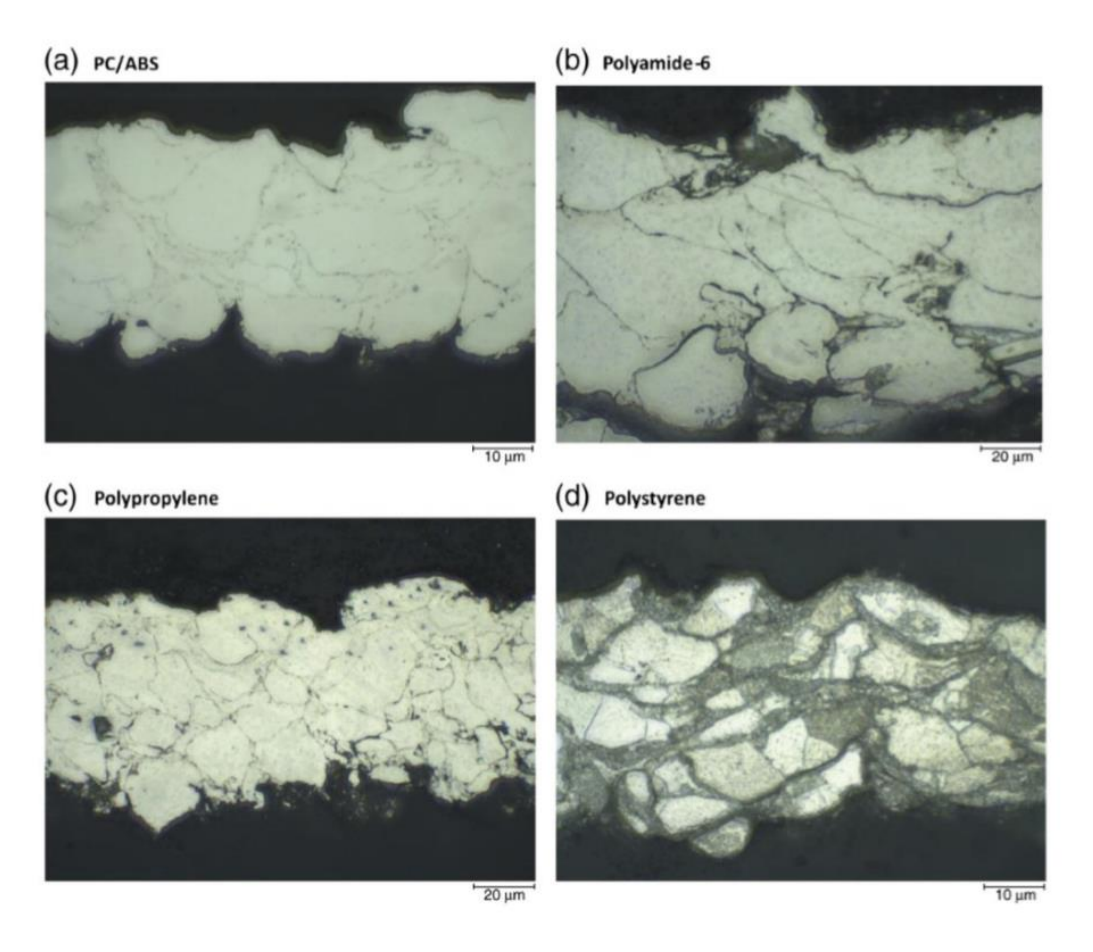


**Figure 2- 8:** Optical micrographs of the cross-section view of tin coating on various polymeric substrates [46]

Ganesan *et al.* [13] studied the difference of cold spray deposition mechanism between thermoplastic and thermosetting substrates. It was found that deposition was possible on thermoplastics through mechanical interlocking and only localized fracture was observed on thermosetting substrates. Therefore, cold spraying on thermosets substrates is more difficult than that of thermoplastics.

Affi *et al.* [8] could not directly cold spray Al onto an epoxy-CFRP substrate due to the substrate erosion. A thin plasma-sprayed Al coating prior to cold spraying was deposited onto CFRP that facilitated the deformation of the upcoming cold sprayed Al particles.

Robitaille *et al.* [47] have attempted to cold spray zinc powders onto carbon-epoxy composites, but deposition was not possible due to the substrate erosion. When the substrate surface was co-cured with a thin layer of copper particles, coating formation was possible with good adhesion strength to the substrate.

Che *et al.* [12] attempted to cold spray carbon fibre-reinforced epoxy composites with tin, copper and aluminum powders at various gas pressure and temperature. Only deposition of tin was successfully performed, and the associated bonding mechanism was suggested to explain the "crack-filling" mechanism, as shown in Fig 2-9. In this mechanism, tin particles are softened or partially melted due to the higher gas temperature than the melting temperature of tin (about 300 °C vs 232°C). When they impact the substrate, the solid core of the tin particle would generate microcracks on the brittle epoxy, while the molten part of the particles would be squeezed into these cracks, limiting erosion, and providing mechanical anchoring with the substrate.

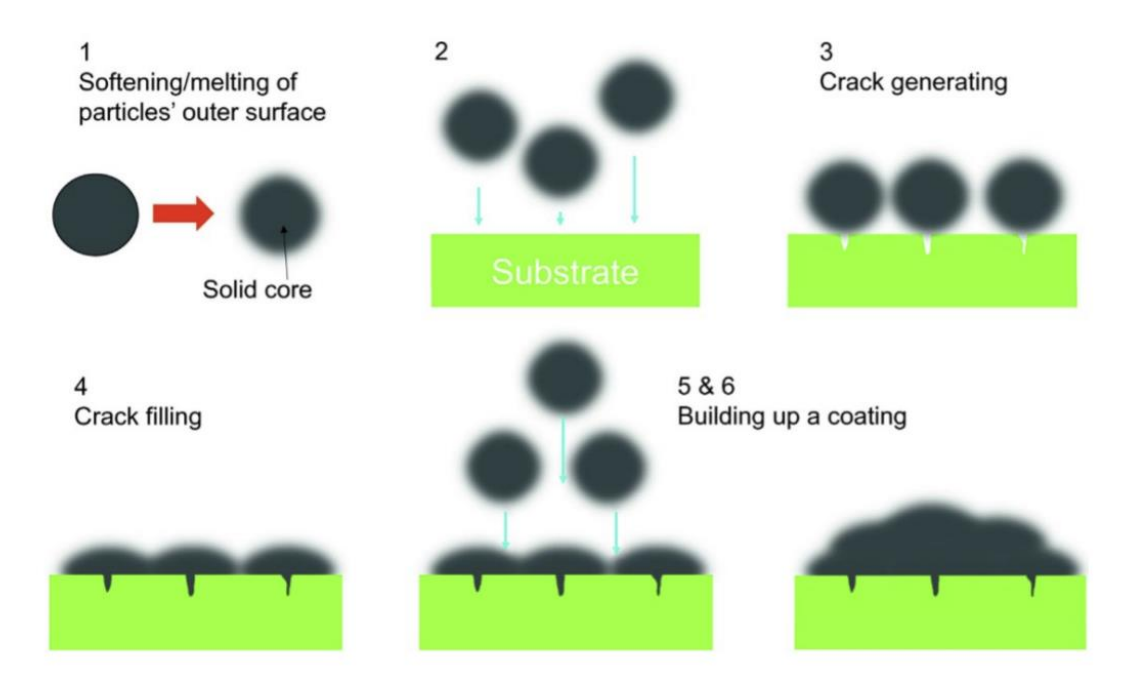


**Figure 2- 9:** Schematic of the crack filling mechanism [12]

One possible deposition approach to avoid substrate erosion during cold spraying of polymeric substrates is the interlayer concept prior to cold spray (i.e., hybrid coating process). The interlayer approach may not only protect the substrate from erosion, but it may also permit successful formation of a subsequent cold sprayed coating. Ganesan *et al.* [13] successfully cold sprayed dendritic Cu on an epoxy polymer substrate using a cold sprayed Sn interlayer. Małachowska *et al.* [14] also applied an interlayer made of a mixture of Sn and Al<sub>2</sub>O<sub>3</sub> particles for the metallization of thermoplastic polyamide 6 polymer before cold spraying of dendritic Cu powders. They found that several contact points of the dendritic Cu particles with the Sn interlayer minimized the overall impact energy and erosion, enabling a successful deposition of Cu coating.

# 2.3 Electrochemical deposition

Electrochemical deposition is defined as the reduction of metal ions from aqueous, organic, and salt electrolyte. The reduction of metal ions from an aqueous solution is represented by  $M_{\text{solution}}^{z+} + ze^- \rightarrow M$ . There are two broad types of electrochemical deposition: (i) electroless and (ii) electrodeposition. In electroless deposition process, there is no external power supply (i.e., no electricity involved) and electrons are supplied by the reducing agent in the solution. However, electrons are supplied by external power supply in electrodeposition process [48]. These two electrochemical deposition processes are described in below.

# 2.3.1 Electroless deposition of polymeric substrate

The term electroless plating, also known as autocatalytic plating, refers to the method of depositing metals through electrochemical reactions without the use of electric current [49]. This process is being able to produce a thin layer and uniform metallic coating with excellent step coverage [50]. Electroless plating has been developed over the past fifty years and among

electroless processes, electroless nickel and copper have been extensively used for a variety of applications [49].

The nature of the substrate determines the surface preparation steps prior to electroless deposition. In case of non-conductive surfaces such as polymers, an activation treatment is required to enable the subsequent electroless deposition, as the non-conductive surfaces lack catalytic properties [51]. During the activation step, catalysts which are usually precious metals such as palladium (Pd), are dispersed on the surface, acting as the nucleation sites for the subsequent electroless plating to enhance the adhesion between the coating and the substrate [52].

The electroless plating bath mainly contains a source of ions, reducing agent and other secondary components such as complexing agent, buffer, and stabilizer [53]. Electroless deposition is a result of two partial reactions; oxidation of reducing agent ( $R + H_2O \rightarrow OX + H^+ + e^-$ ) and reduction of metal ions ( $M^+ + e^- \rightarrow M$ ), where M is metal,  $e^-$  is electron, R is the reducing agent, and OX is the oxidized product [53]. A schematic of the electroless plating process is shown in Fig 2-10.

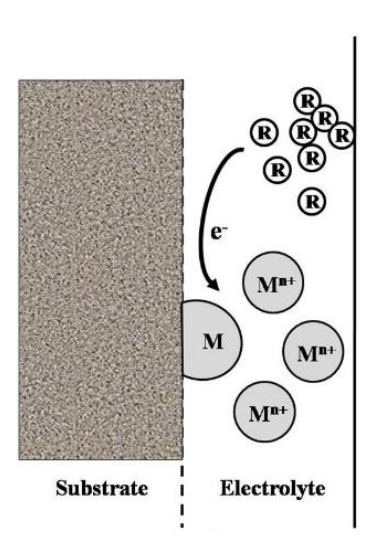


**Figure 2- 10:** Schematic representation of electroless metal deposition [54]

Nowadays, electroless Ni plating (EN) has been the most used autocatalytic plating process due to its superior physical and chemical properties. In an electroless Ni bath, the source of ions and the reducing agent are typically nickel sulfate (NiSO<sub>4</sub>) and sodium hypophosphite (NaH<sub>2</sub>PO<sub>2</sub>), respectively [49].

Three chemical mechanisms can be distinguished during EN process [55]: 1) reduction of Ni ions, 2) oxidation of the hypophosphite and its reduction to phosphorus, and 3) evolution of hydrogen. Reactions involved in the EN process are as follows:

(1) 
$$Ni^{2+} + 2e^- + 2H^+ \rightarrow Ni^0 + 2H^+$$

(2) 
$$H_2PO_2^- + H_2O \rightarrow H_2PO_3^- + 2H^+ + 2e^-$$

(3) 
$$Ni^{2+} + H_2PO_2^- + H_2O \rightarrow Ni^0 + H_2PO_3^- + 2H^+$$

(4) 
$$H_2PO_2^- + \frac{1}{2} H_2 \rightarrow H_2O + OH^- + P$$

(5) 
$$2H^+ + 2e^- \rightarrow H_2$$

Reactions (1) to (4) are responsible for the formation of Ni-P alloy coating, indicating that the produced coating is not pure nickel and phosphorus is present in the coating [49]. The amount of phosphorus in the coating determines the microstructure, physical, mechanical and corrosion properties. From the reactions, nickel ions are reduced to Ni atoms due to its more positive redox potential than that of hypophosphite ion (-0.25 V vs. -0.5 V). According to reaction (5), electroless Ni deposition is accompanied by hydrogen evolution [56].

Shang *et al.* [55] proposed the deposition mechanism of the electroless Ni plating on activated non-conductive surfaces. According to this mechanism, nickel and hypophosphite ions rapidly move forward to the activated surface and adsorb on the surface in the vicinity of the palladium particles. Simultaneously, nickel ions are reduced to metallic nickel and hypophosphite

ions are oxidized to supply electrons for the reduction reaction of the nickel ions. Nucleation of Ni in the vicinity of Pd particles and the subsequent growth, leads to the formation of a uniform and continuous Ni-P alloy coating. A schematic diagram of the electroless deposition on a non-conductive surface is presented in Fig 2-11.

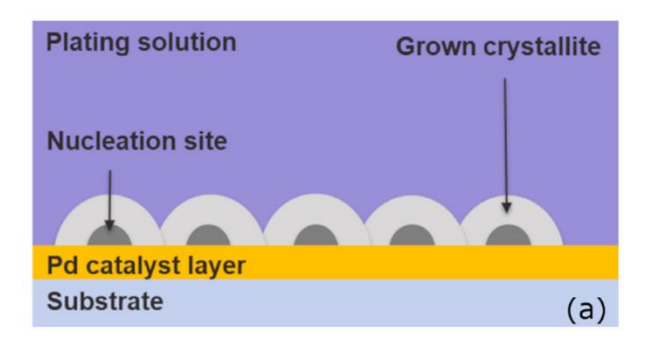


**Figure 2- 11**: Mechanism of electroless plating on a non-conductive surface [57]

# 2.3.2 Electrodeposition

Electrodeposition is a result of cathodic and anodic reactions occurring simultaneously on the cathode and the anode surfaces, respectively, by passing an electric current. Reaction at the cathode follows the equation  $M^{n+} + ne^- \rightarrow M$ , and for the sacrificial anode, the anodic reaction is  $M \rightarrow M^{n+} + ne^-$ [53], resulting in a formation of a metal deposit on the cathode surface [63]. A schematic diagram of the electrodeposition is shown in Fig 2-12:

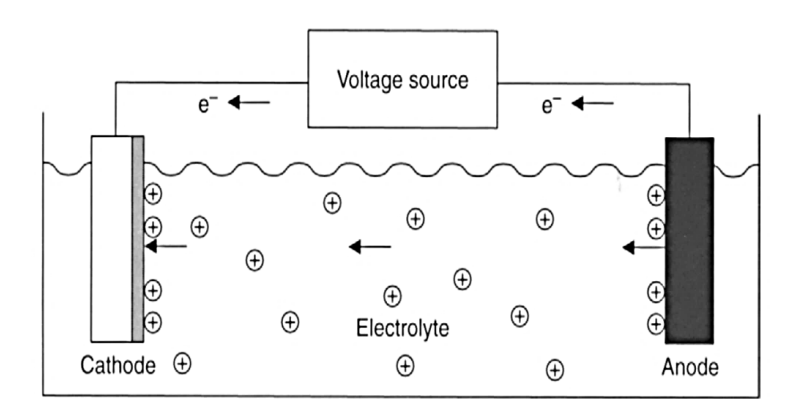


**Figure 2- 12:** Migration of metal ions from a sacrificial anode to the cathode with the formation of a metal deposit on the substrate [58]

Electrodeposition possesses several advantages when compared with physical vapour deposition and chemical vapour deposition such as cost effectiveness, ease of use, being able to customize the properties by modifying the composition of the electroplating bath and conditions (i.e., temperature, current density, PH, and time), while physical vapour deposition is a high-cost process with very low deposition efficiency and chemical vapour deposition requires high-temperature which may cause substrate damage or softening. When compared with electroless deposition, electrodeposition provides higher deposition rate to form a thick coating (<1mm) by applying an external current and takes place at modest temperatures (room temperature to 60°C) which makes it suitable for industrial scale-up. However, autocatalytic surface and high temperature bath are required to ensure continuing deposition in electroless deposition [59].

According to the literature, cold spray deposition of Cu was not successfully performed on epoxy-CFRP due to substrate erosion. Thus, this study mainly aims to enable cold spray deposition of Cu on an epoxy-CFRP by fabricating a metallic interlayer prior to cold spraying. For the abovementioned purpose, this study uses a hybrid metallization approach that includes electrochemical methods for fabrication of a Ni-Cu metallic interlayer followed by cold spray Cu.

The effect of interlayer hardness on cold spray characteristics of the Cu particle is further investigated by varying the interlayer material. Three different interlayers of Sn, Cu and Ni are fabricated prior to cold spray deposition of Cu. After successful cold spray deposition of Cu on an epoxy-CFRP, another hybrid metallization approach is finally proposed that includes two consecutive coating steps of cold spray Sn followed by electrodeposition of Cu to improve properties of the coatings and to take advantage of reducing the number of coating steps. This study also includes an investigation of adhesion properties and electrical conductivity/resistivity performance of the fabricated multilayered hybrid coatings. For a better understanding, an evolution schematic of the different coating systems is summarized in Fig 2-13, representing the coatings developed in this thesis.

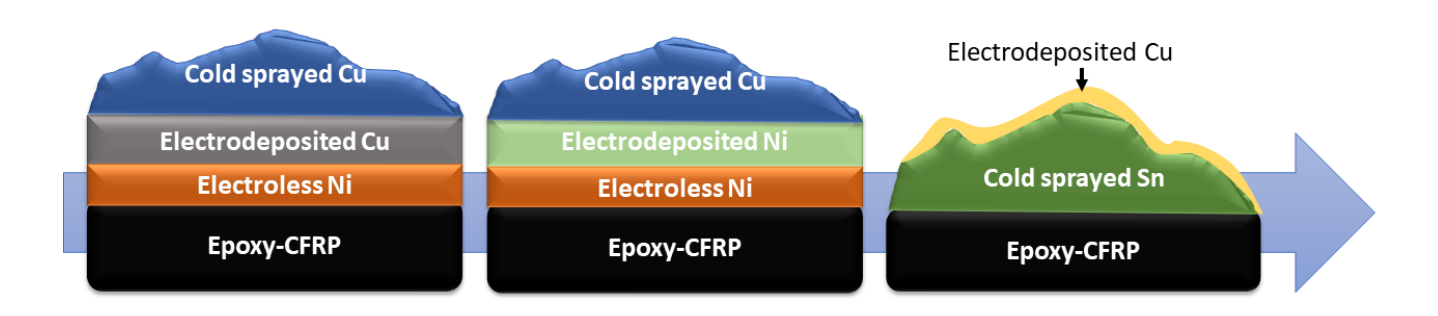


Figure 2- 13: Schematic of the developed hybrid coatings

# Chapter 3: Development of Hybrid Metallic Coatings on Carbon Fiberreinforced Polymers (CFRPs) by Cold Spray Deposition of Copper-assisted Copper Electroplating Process

#### Preface

This chapter aimed to understand how the presence of a metallic interlayer could enable cold spray deposition of Cu onto an epoxy-CFRP which was not successfully performed in previous studies. The effect of surface roughness, thermal conductivity, and substrate hardness on deposition efficiency (DE) of the Cu coating was investigated. Electrical resistivity performance of the cold sprayed Cu coating was also studied and compared with that of bulk Cu.

# This chapter has been published as:

Panteha Fallah, Sriraman Rajagopalan, André McDonald, Stephen Yue, "Development of hybrid metallic coatings on carbon fiber-reinforced polymers (CFRPs) by cold spray deposition of copper-assisted copper electroplating process", J. Surf. Coat. Technol. 400 (2020), 126231, https://doi.org/10.1016/j.surfcoat.2020.126231. (Reprinted by permission from Elsevier)

#### **Abstract**

Metallization of polymeric materials such as carbon fiber-reinforced polymers (CFRPs) by the cold spray technique has gained significant interest to enhance their electrical conductivity. Copper is a very good electrical conductor, which makes it favorable for applications that require high electrical conductivity. However, previous studies showed that continuous copper coatings could not be fabricated directly on CFRPs by cold spraying. In this study, a hybrid fabrication process was used to enable cold spray deposition of copper onto CFRPs, making them electrically conductive. The CFRP substrate was first metallized with an electroless Ni coating; subsequently, a thick copper layer was electroplated onto the Ni interlayer. Copper was then cold spray deposited onto the electroplated CFRP as well as on a Cu control panel. Deposition efficiency (DE) of the cold-sprayed coatings was measured for both the CFRP and the control Cu coupons to determine optimal deposition conditions. Surface and cross-sectional morphologies of the coated CFRP were investigated, and both the electroplated CFRP and control panels were characterized for mechanical properties and surface roughness before cold spray deposition. The electrical resistivity of the cold-sprayed CFRPs was evaluated. It was found that the DE of copper particles is sensitive to the surface characteristics of the substrate. The electrical resistivity of the coldsprayed coatings was slightly higher than that of the bulk copper due to porosity and small defects on the coating surface. The results suggest that Cu coatings can be successfully fabricated onto CFRPs if a copper inter-layer is present. This layer not only protects the CFRP from any possible damage, but also improves the cold sprayability of copper particles as compared to the conventional cold spraying copper powder/copper panel due to its favorable mechanical, thermal and surface properties. The fabricated coatings can serve as conductive surfaces for application as lightning strike protection coatings.

**Keywords**: Carbon fiber-reinforced polymer; Cold spray; Deposition efficiency; Electrical conductivity; Hybrid fabrication process.

#### 3.1 Introduction

Carbon fiber-reinforced polymers (CFRPs) have been increasingly used in the aerospace and automotive industries as they have better strength to weight ratio than typical aluminum alloys (e.g., 2000 and 7000 series) [4]. On the other hand, their use is restricted due to poor electrical conductivity, erosion resistance, and low operating temperature [60, 61]. This makes CFRPs prone to damage during lightning strikes when they are used as airfoil structures or as construction components for aircraft or wind turbines [18]. Additionally, integration of dissimilar materials such as CFRPs with metals using conventional joining processes is still challenging. Metallized coatings may be useful for joining zones (e.g., rivet and screw connections) of the CFRP/metal materials as a substitute for common joining methods [62]. Hence, metallization of composite materials (e.g., CFRPs) is required to ensure structural integrity and safety.

Amongst deposition methods, physical vapor deposition (PVD) [63] and chemical vapor deposition (CVD) [64] have been utilized to attain metallic coating on polymer surfaces. However, low deposition rate as well as the high expense of the processes would limit the applications of these methods [65]. Many researchers have attempted metallizing polymeric materials such as CFRP by high-temperature spraying processes. Nevertheless, thermal degradation of polymeric substrates may occur depending on the temperature of the metal particles and gases during thermal spray process [66]. Huonnic *et al.* [67] studied the influence of Al coatings that were flame-spray deposited onto glass fiber composite tubes. Considerable damage to the composite material was reported because of the heat input during the process.

Owing to the lower operating temperature, cold spray may be a suitable approach to apply metallic coatings on polymeric materials, including thermosets, thermoplastics and CFRPs, since oxidation of metallic particles and heat destruction of the substrate are limited. Therefore, the main

advantages of using cold spray to deposit metal coatings on polymer structures is to prevent damage of temperature-sensitive polymeric substrates that require metallization. This process also allows for the fabrication of electrically conductive coatings due to limited particle oxidation during the deposition process, which is an added advantage compared to high-temperature thermal spray processes [65].

Sturgeon et al. [68] successfully cold sprayed aluminum on carbon fiber reinforced PEEK substrates with helium gas at 300°C and 20 bar. Lupoi and O'Neill [46] attempted cold spray deposition of copper, aluminum, and tin on various thermoplastics (PC/ABS, polyamide-6, polypropylene, and polystyrene) and on a glass-fiber composite material. Deposition of aluminum was accompanied by erosion, but cold spraying of tin resulted in successful deposition due to its low critical velocity, which led to a low theoretical impact energy (10.7 times lower than copper), while erosion of the polymer was the most predominant effect in the case of copper. Barletta et al. [69] successfully deposited a thin copper coating on a thermoplastic substrate (PA66), but after the initial deposition layer, erosion took place, preventing any further increase in thickness. Ganesan et al. [70] cold-sprayed tin and copper (spherical and dendritic) onto thermoplastic PVC substrates. Higher deposition efficiency (DE) was obtained for tin compared to both copper powders due to the lower yield strength of tin. Ganesan et al. [13] also showed that a thick copper coating could be cold sprayed on thermoplastic PVC and thermoset epoxy substrates by using interlayers of copper and tin. They also studied the difference between the deposition mechanisms on thermoplastics and thermosetting substrates. They found that deposition was possible on thermoplastics through mechanical interlocking (particle embedment), while localized fracture was observed for thermosetting substrates.

As described above, few successful attempts have been made for cold spray deposition of copper on polymeric materials (thermosets and thermoplastics), however, cold-sprayed copper coatings have not been achieved on thermosetting epoxy CFRPs. Che *et al.* [12] attempted cold spray deposition of copper onto thermosetting epoxy CFRPs with both high-pressure and low-pressure cold spray systems. They found that erosion was a critical barrier for coating development on the CFRP substrates since exposed and fractured carbon fibers were observed after impacting particles. Thus, only individual particles were embedded into the epoxy matrix.

The objectives of this present work were to: (1) determine the feasibility of cold spray deposition of copper onto CFRP without damaging the composite, (2) investigate the cold spray deposition of copper powder particles on a non-metallic substrate through hardness, surface topology and thermal conductivity effects, (3) describe the electrical performance of the coating through measurements of the electrical resistivity.

## 3.2 Experimental methodology

## 3.2.1 Feedstock powder and substrates

The copper feedstock powder (PG-PMP-1012, Plasma Giken Co., Ltd, Saitama, Japan), and its properties are listed in Table 3-1. The particle size of the feedstock powder was evaluated using a laser scattering particle size analyzer (LA-920, Horiba, Japan), and the distribution is presented in Figure 3-1. A scanning electron microscope (SEM, Hitachi SU 3500) was used to capture images of the copper powder particles, which is presented in Figure 3-2. The copper powder was largely spherical, and the average particle size (D50) of the copper particles was estimated to be 18.93 µm, where 50% of the particles are smaller than 18.93 µm.

Two types of substrates were employed in this study: CFRP substrates and oxygen-free copper panels. The CFRPs fabricated by Bombardier Aerospace (Montreal, Canada) consisted of a thermosetting epoxy matrix with continuous carbon fiber reinforcements. The CFRP panels were made of four plies of 5276-1/G30-500 epoxy carbon prepreg ([0/90]2s). The CFRP dimensions were 7 x 3 cm<sup>2</sup> during the cold spray campaign.

Oxygen-free copper panels (McMASTER-CARR, USA, 99.99%) were used as a benchmark control to compare with the conventional metal-metal cold sprayed coatings on electroplated CFRPs. The copper plates were grit blasted with #24 alumina grit before cold spray deposition.

A Clark CM-100AT Vickers Microhardness Tester (Sun-Tec, Novi, USA) was used to measure the micro-hardness of the substrates (fabricated electroplated coating and Cu panels), cold-sprayed Cu coatings and as-polished feedstock powder for a penetration time of 15 s under a load of 10 gf according to the ASTM standard E384 [71]. Vickers hardness measurements were conducted on the cross-section of the samples and ten measurements were taken for each sample. Vickers hardness of the feedstock material was measured by mounting and polishing the powder. A thin layer of powder was spread over the mold and a small amount of mounting material was mixed with the powders; once the mixture was semi-cured, the rest of the mounting material was added. When the mounted sample was completely set, it was polished until the cross-sections of the particles were exposed.

A 3D optical surface profiler (ZYGO, Connecticut, USA) was used to determine the roughness and topology of the substrate surfaces before cold spray deposition of Cu to support the DE analysis of the cold spray process. Skewness ( $S_{sk}$ ) and kurtosis ( $S_{ku}$ ) parameters were also obtained; the  $S_{sk}$  indicates the symmetry of the surface profile with regards to the mean line, while

 $S_{ku}$  measures the degree of sharpness of the surface asperities [72, 73]. Therefore,  $S_{sk}$  and  $S_{ku}$  can provide details about the shape of asperities.

**Table 3-1:** Properties of the feedstock powder used in this work

Powder	Morphology	Supplier	D <sub>50</sub>	Hardness
Cu	Spherical	Plasma Giken	18.93 µm	65 ± 8.71 HV

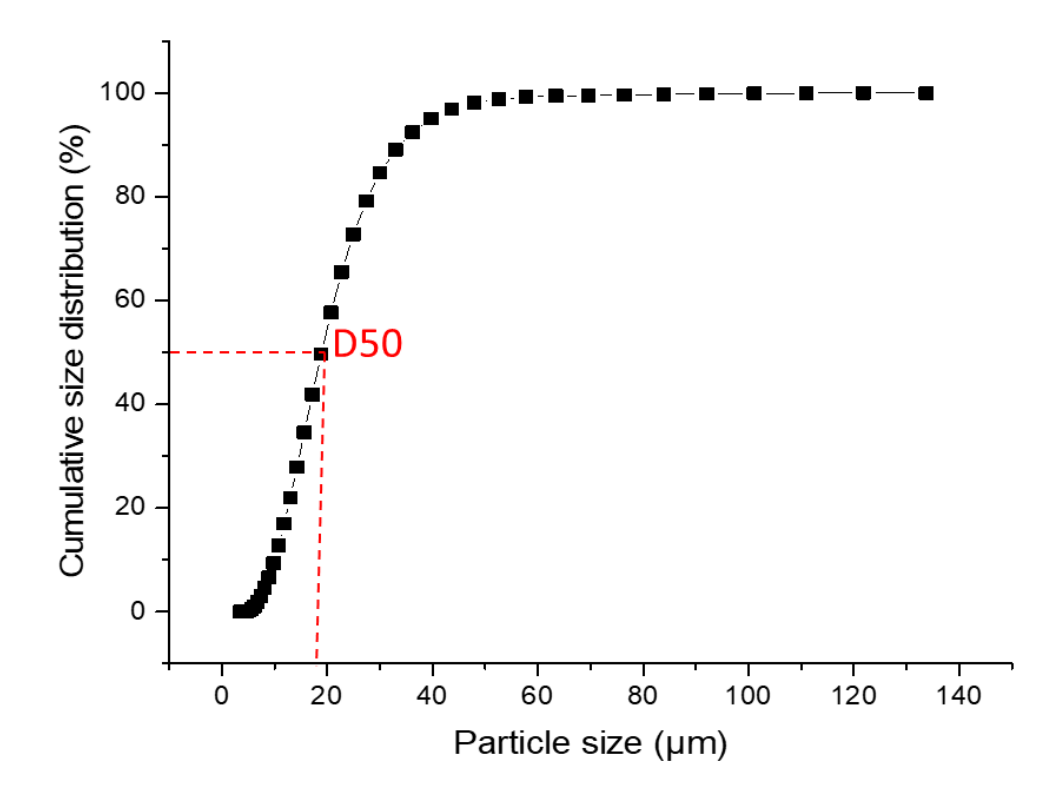


**Figure 3-1:** The particle size distribution of the copper powder

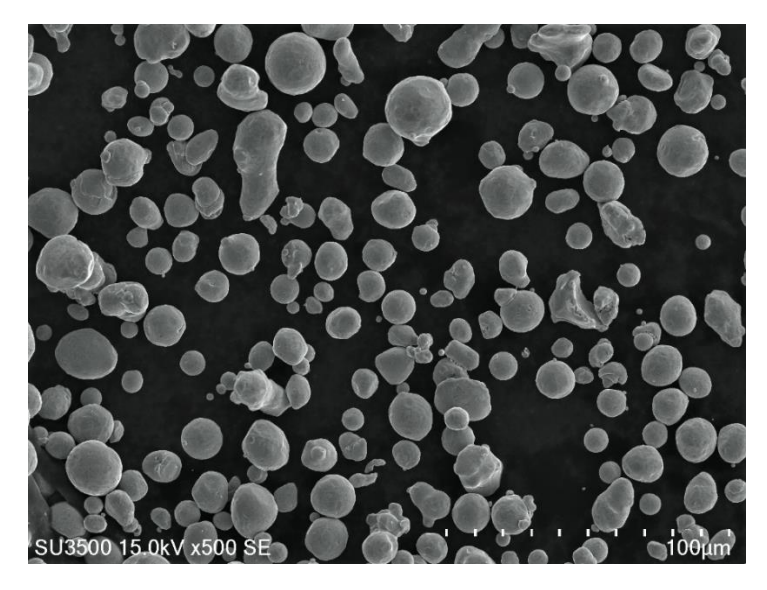


Figure 3- 2: SEM image of the feedstock copper powder

# 3.2.2 Cu electroplating of CFRPs

The first metallization stage is a two-step electroplating process: electroless Ni plating followed by Cu electroplating on to the Ni. Ni was chosen as the initial metallic layer due to its good electrical conductivity and feasibility for electroless plating on catalyzed polymeric surfaces [74].

Electroless plating is a method of depositing metals from an electrolyte without the use of electric current [53]. Therefore, this process was used to increase the conductivity of non-conductive surfaces such as CFRP to enable subsequent electroplating. Hence, the aim was to produce a continuous conductive coating with minimum thickness. For the electroless step, the CFRP substrates needed to be 'activated'. The CFRP surfaces were degreased with histoprep ethyl alcohol (95%), followed by catalysis in a colloidal solution that contained 0.3 g/L PdCl<sub>2</sub>, 5 g/L SnCl<sub>2</sub>·2H<sub>2</sub>O, 15 mL/L H<sub>2</sub>SO<sub>4</sub> (37%) and 250 g/L NaCl at room temperature for about 10 minutes. Catalyzed samples were immersed in an activation solution containing 100 mL/L HCl (density =

1.19 g/mL) at 40°C for about 2 minutes [52]. Water rinsing for about 20 seconds was necessary between each step. As a result, palladium particles served as the nucleation sites to initiate chemical reactions taking place on the activated surface during the electroless plating process. Activated CFRP substrates were then electroless nickel-plated in a bath that contained 20 g/L NiSO<sub>4</sub>.6H<sub>2</sub>O, 20 g/L NaH<sub>2</sub>PO<sub>2</sub>.H<sub>2</sub>O (reducing agent), 35 g/L Na<sub>3</sub>C<sub>6</sub>H<sub>5</sub>O<sub>7</sub> and 30 g/L (NH<sub>4</sub>)2SO<sub>4</sub> at 71°C for about 20 minutes [75]. Electroless deposition can take place after the surface was activated by Pd particles according to the following autocatalysis reaction (Equation 1) to form the Ni-P film [76].

$$Ni^{2+} + 4H_2PO_2^- + H_2O \rightarrow Ni + 3H_2PO_3^- + P + H^+ + \frac{3}{2}H_2$$
 Equation 1.

Electroplating Cu was utilized to increase the thickness of the interlayer since the removal of the Ni-P film took place after conducting the cold spray process (see Figure 3-3), and no cold spray deposition was possible.

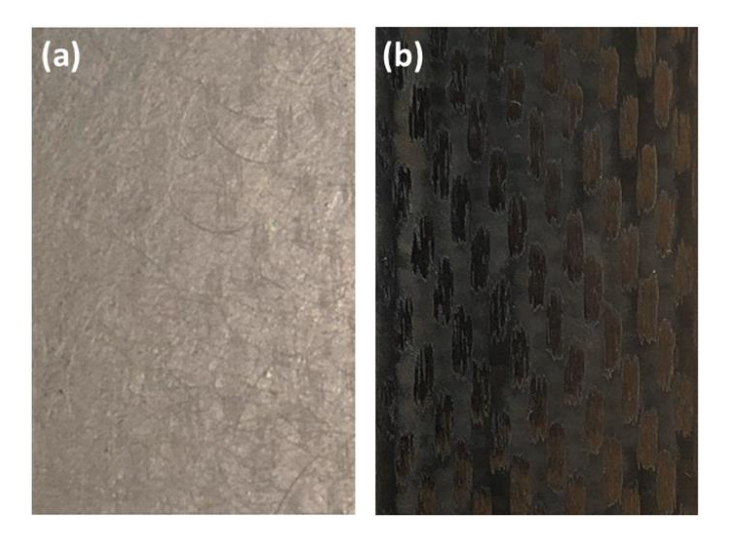


Figure 3-3: The image of electroless Ni plated CFRP (a) before and (b) after conducting cold spray Cu

Copper electroplating of electroless Ni-plated CFRPs was then performed in voltage control mode in a cell containing 1 M H<sub>2</sub>SO<sub>4</sub> and 0.5 M CuSO<sub>4</sub>.5H<sub>2</sub>O with two electrodes connected to the rectifier (XTS 7-6 XANTREX, Canada) at room temperature. Ni-plated CFRP was the working electrode, and a rectangular copper sheet was the sacrificial anode. The applied voltage was -200 mV, and the corresponding deposition rate was 30 µm/hr. Therefore, 3 hours of plating was required to achieve approximately 100 µm copper coating.

## 3.2.3 Cold spray deposition of Cu on the fabricated Cu interlayer

Cold spraying has been used as the last step in the coating process given its high deposition rate, scalability, and limited adverse impact on the environment. Low-pressure cold spray deposition of Cu was performed with a commercially available cold spray system (Inovati KM CDS 2.2, Santa Barbara, California, USA). The cold spray parameters are listed in Table 3-2. Only one pass was attempted for each experiment with a step size of 1 mm (18 steps). Deposition efficiency (DE) is defined as the weight of the deposited powder onto the substrate divided by the overall weight of the powder sprayed during the time that the nozzle was effectively over the sample (see Equation 2 [8]).

$$DE = \left[\frac{M - M_0}{\frac{(d)(N)(f)}{V_{\text{gun}}}}\right] (100),$$
 Equation 2.

where M and  $M_0$  are the mass of the substrate after and before spray, respectively, which were measured using an Ishida scale with a precision of 0.005 g, d is the length of the substrate, N is the number of steps on the substrate, f is the feeding rate of the powder, and  $V_{gun}$  is the gun travel speed.

**Table 3- 2:** Cold spray parameters

Carrier	Carrier gas	Gas pressure,	Stand-off	Gun travel	Powder feeder
gas	temperature,	MPa	distance, mm	speed, mm/s	rate
	°C				
$N_2$	482	0.41, 0.45,	35	25	1 RPM
		0.46, 0.48			(11.5 g/min)

# 3.2.4 Coating characterization

After electroless plating, electroplating, and cold spray processes, samples were characterized by using a scanning electron microscope for top view observation. For imaging of the cross-sections, samples were cut by using a manual abrasive cutter (ISOMET 5000, Buehler, Lake Bluff, Illinois, USA). Then the specimens were metallurgically mounted in epoxy resin and cured at room temperature. The sample was subsequently ground using #600 and #800 grit SiC polishing papers and finally polished with 6 and 3 µm diamond suspension. Compositional analysis of the Ni-P layer, electroplated Cu coating, cold sprayed Cu coatings and the Cu powder were conducted using Energy-Dispersive X-ray Spectroscopy (EDS) in the SEM. To avoid surface charging during SEM imaging, a thin layer of carbon was sputtered on mounted samples by a carbon sputter coater (EMS 150T ES, PA, USA).

## 3.2.5 Electrical resistivity

The electrical resistivity of the cold-sprayed coatings was measured using the four-point probe method (Everbeing Int'l Corp, Hsinchu City, Taiwan), where an electric current was applied onto the coating through the two outer probes, and the voltage drop was measured using the two inner probes. The measurement system consisted of a Xantrex power supply and Keithley

multimeter (199 system DMM scanner, Cleveland, Ohio, USA) with a precision of 0.001mV. Measurements were made on three different locations on each of the three samples tested. For each location, three measurements ranging from 100 mA to 120 mA with a 10-mA step were performed.

The electrical resistivity of the coatings was measured using collinear, equally spaced, 4-point probe system and calculated according to Equation 3 [77]:

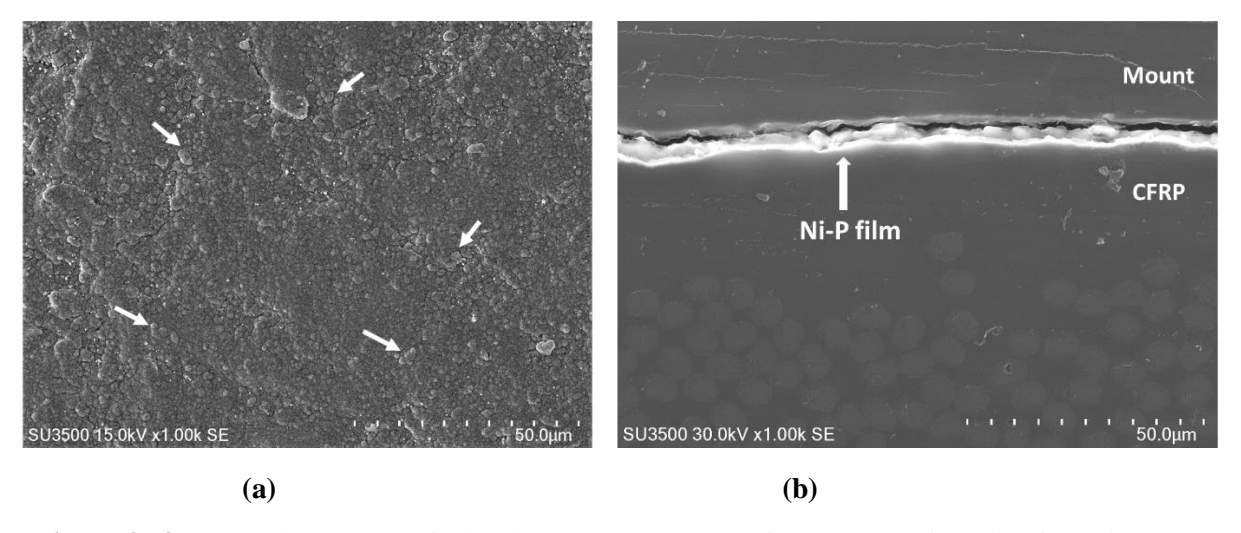
$$\rho_{\rm R} = \frac{\pi}{\ln(2)} t \frac{V}{I} f,$$
Equation 3.

where  $\rho_R$  is the resistivity, t the coating thickness, V the measured voltage, I the applied current and f the finite width correction factor. The correction factor, f, may be varied depending on the dimensional characteristics of the sample and probe spacing (i.e. a/d, the ratio of the sample length to width and d/s, the ratio of the sample width to probe spacing). In this present study, the distance between all four probes was fixed at 3 mm and f was estimated to be 0.85. The value for f was based on the sample geometry and the given spacing probe. The average of the electrical resistivity was determined for each sample.

### 3.3 Results and discussion

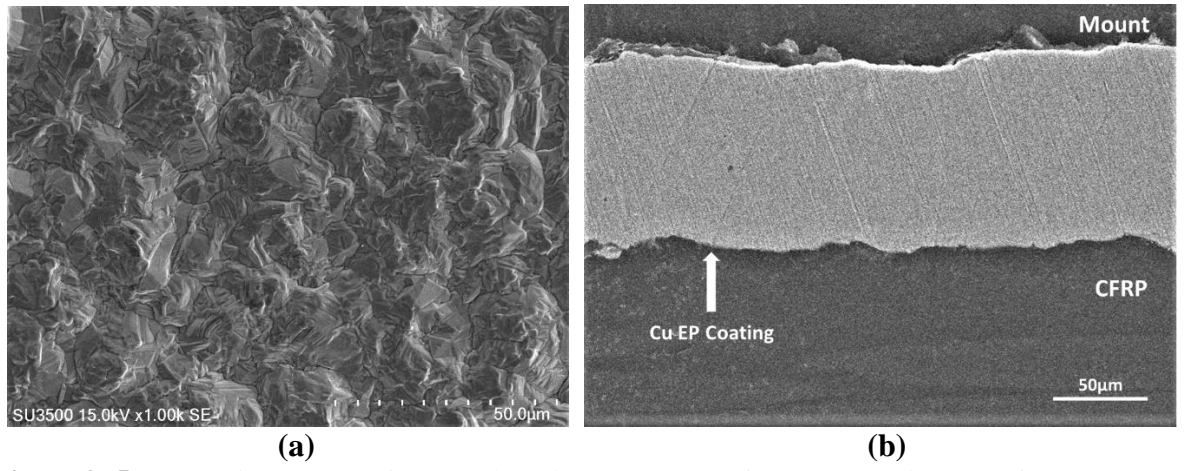
## 3.3.1 Coating characterization

Figure 3-4 presents SEM micrographs of the electroless Ni-P deposit onto the CFRP. These SEM images show deposits that are fine-grained, compact, continuous and dense, with an average thickness of about 5 μm. Spherical nodular features can be observed on the surface (white arrows), that are similar to previous studies [78, 79]. From the EDS measurements, it was observed that the binary Ni-P deposit contained approximately 10 wt.% of phosphorus and 90 wt.% nickel.



**Figure 3- 4:** SEM micrographs of Ni-P deposit on CFRP (a): from the top view, (b): from the cross-section view (white arrows represent the nodular structure)

Copper coating with a thickness of 100 µm on the electroless Ni interlayer was successfully fabricated by electroplating (see Figure 3-5). The surface morphology of the copper electroplated layer was a rounded cauliflower type structure, which is typical of any aqueous electroplated processes [80, 81]. The cross-sectional SEM image indicated a very dense and uniform coating.



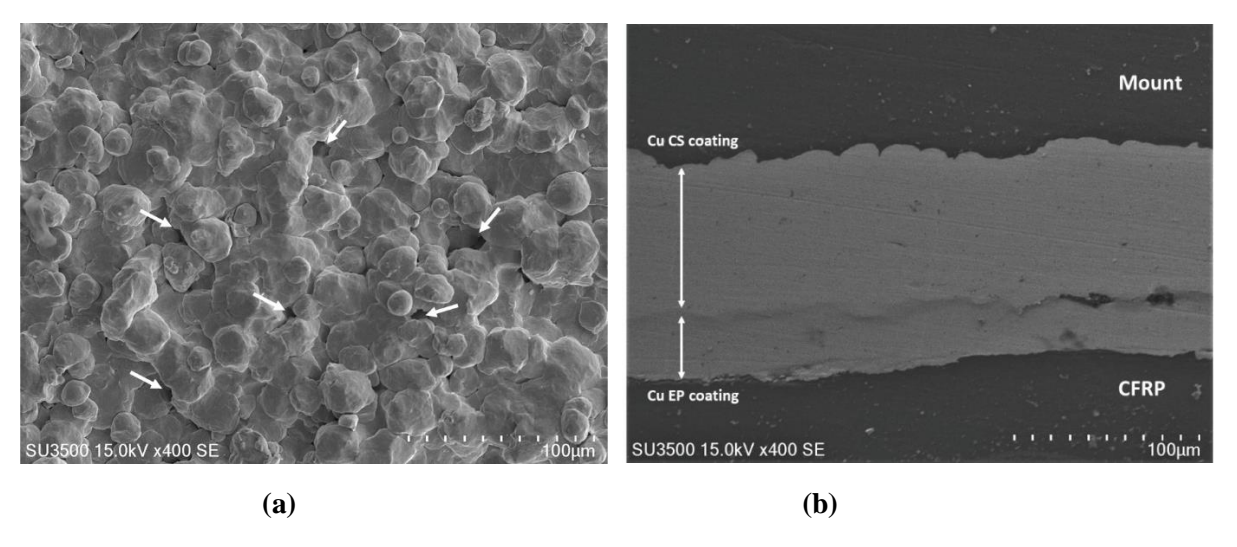
**Figure 3- 5:** SEM micrographs of the Cu deposit on CFRP (a): from the top view, (b): from the cross-section view

After cold spray deposition of Cu at various pressures, SEM micrographs of the coatings from the surface and cross-sectional views were obtained to study the microstructural features of the coatings on CFRPs (see Figures 3-6 to 3-8). From the surface morphology micrographs, it is observed that by increasing the pressure from 0.41 MPa to 0.46 MPa, no obvious morphological changes or severe plastic deformation of the powder particles were observed. This could be due to the small change in pressure. In addition, a few small pores and defects can be seen at the particle boundaries from the surface (see white arrows in Figures 3-6, 3-7 and 3-8).

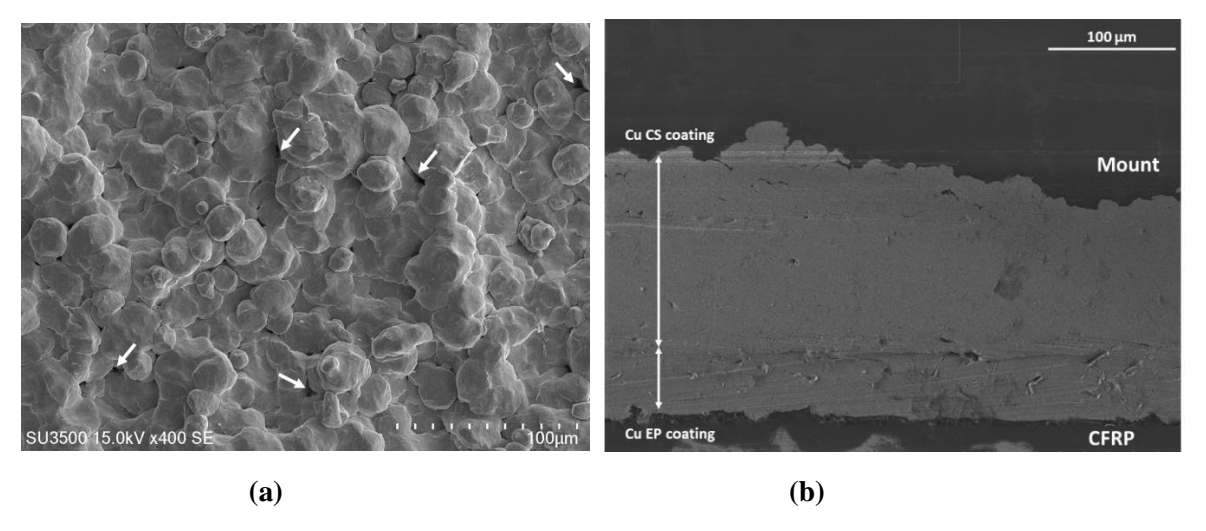
From the cross-sectional view, for all spray conditions, it was observed that continuous, uniform, compact and dense cold spray Cu coatings were formed on the electroplated copper interlayer. A thickness reduction of the interlayer from 100 µm to about 50 µm was also observed, indicating erosion of the electroplated layer by Cu particles during the cold spray process. Note that the mass loss corresponding to this approximately 50 µm thickness reduction of the electroplated layer was taken into account in the DE calculations in the following equation:

$$DE = \begin{bmatrix} \frac{M - M_0 + M_{\text{Cu Loss}}}{(d)(N)(f)} \\ V_{\text{gun}} \end{bmatrix} (100),$$
 Equation 4.

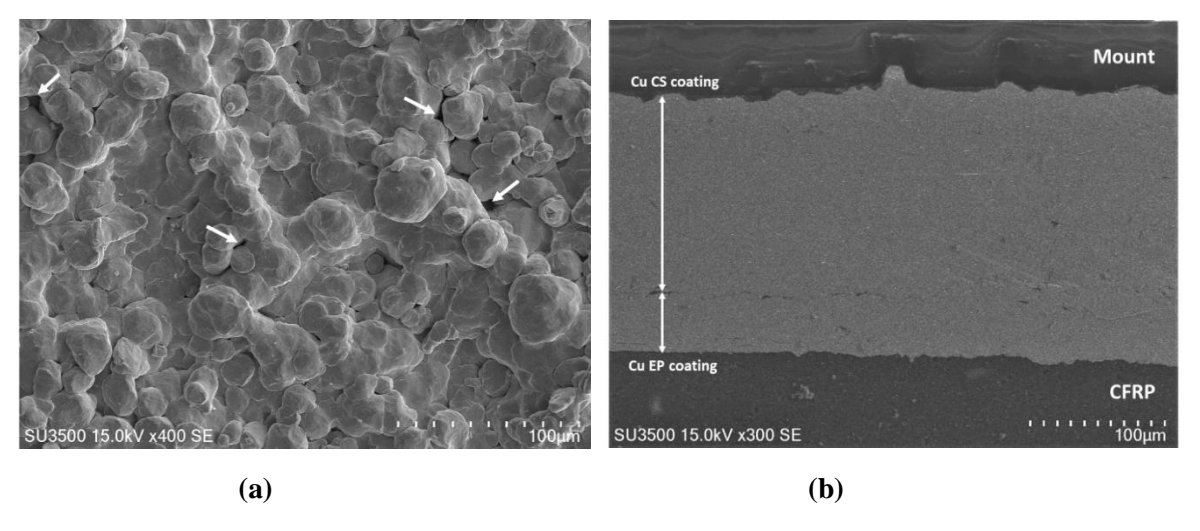
At a pressure of 0.41 MPa, around 90  $\mu$ m of copper cold spray coating was formed. A further increase in gas pressure to 0.45 MPa led to a coating thickness increase to 130  $\mu$ m and the overall deposition efficiency (DE) increased as well from 6.8 % to 9.85 %. A further increase in coating thickness to 145  $\mu$ m was achieved with an increase in pressure from 0.45 MPa to 0.46 MPa corresponding to an increase in DE from 9.85 % to 10 %.



**Figure 3- 6:** SEM top (a) and cross-sectional (b) images of the cold sprayed Cu coatings at P= 0.41 MPa on a Cu electroplated CFRP (white arrows show the presence of pores and inter-particle defects)

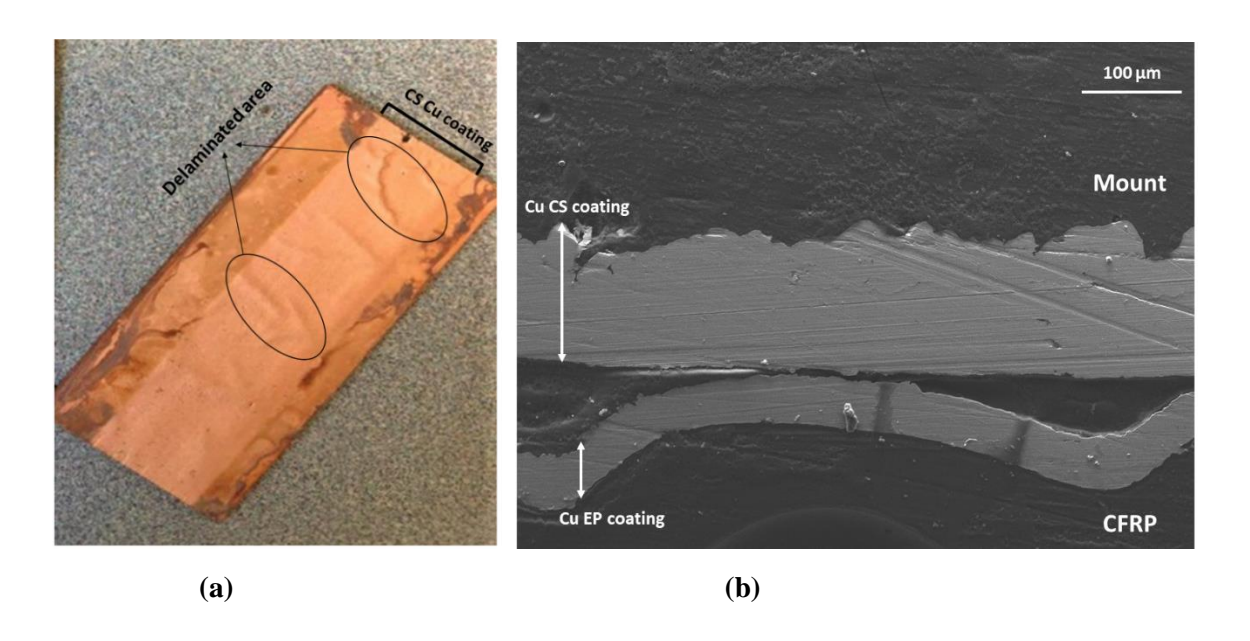


**Figure 3- 7:** SEM top (a) and cross-sectional (b) images of the cold sprayed Cu coatings at P= 0.45 MPa on a Cu electroplated CFRP (white arrows show the presence of pores and inter-particle defects)



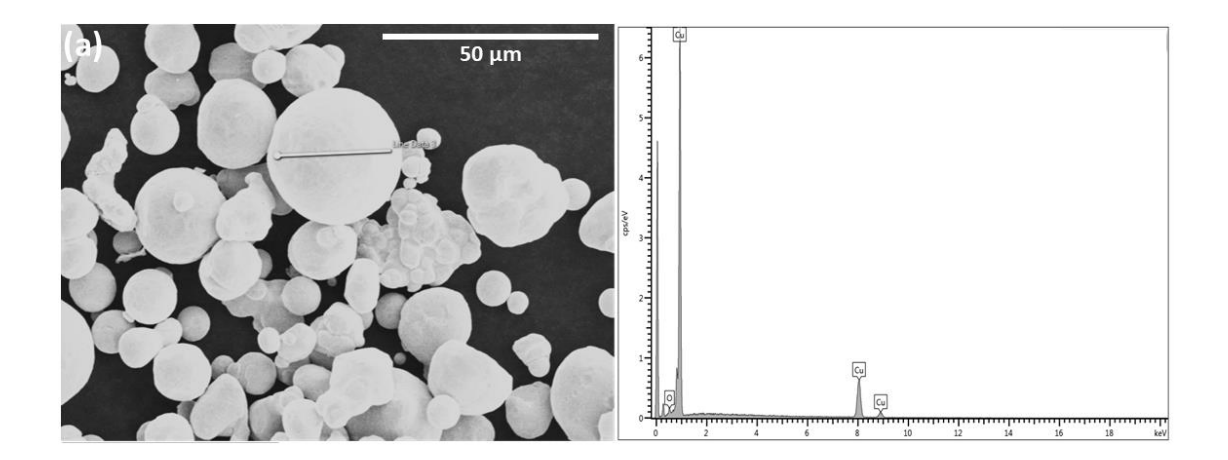
**Figure 3- 8:** SEM top (a) and cross-sectional (b) images of the cold sprayed Cu coatings at P= 0.46 MPa on a Cu electroplated CFRP (white arrows show the presence of pores and inter-particle defects)

At a pressure of 0.48 MPa, as shown in Figure 3-9, cold spraying resulted in the coating delamination. The increased gas pressure results in higher particle velocity, which might lead to residual stress and/or thermal expansion problems. It was reported in a study by Lupoi, *et al.* that a dense and hard powder particle such as copper will generate impact energy of about 0.02 mJ [46]. As a result, this order of magnitude of impact energy under this spray condition could have resulted in severe contact stresses and consequent delamination. Hence, the particle impact energy may have exceeded the adhesion energy at the interface, leading to rebounding of the coating from the substrate. Preheating the CFRP substrate was not performed in this work, since the degradation of the polymer could have occurred above 80 °C [6]. Therefore, delamination might also be due to the thermal expansion difference between the metallized coating and the CFRP.



**Figure 3- 9:** (a) Delaminated copper coating from the CFRP at a pressure of 0.48 MPa (b) SEM image of the delaminated coating

The EDS results of the electroplated copper coating, cold sprayed Cu coating deposited on CFRP, and the Cu powder particle are presented in Figure 3-10. Figure 3-11 also shows a comparison of the oxygen content evolution of the coatings and powder.



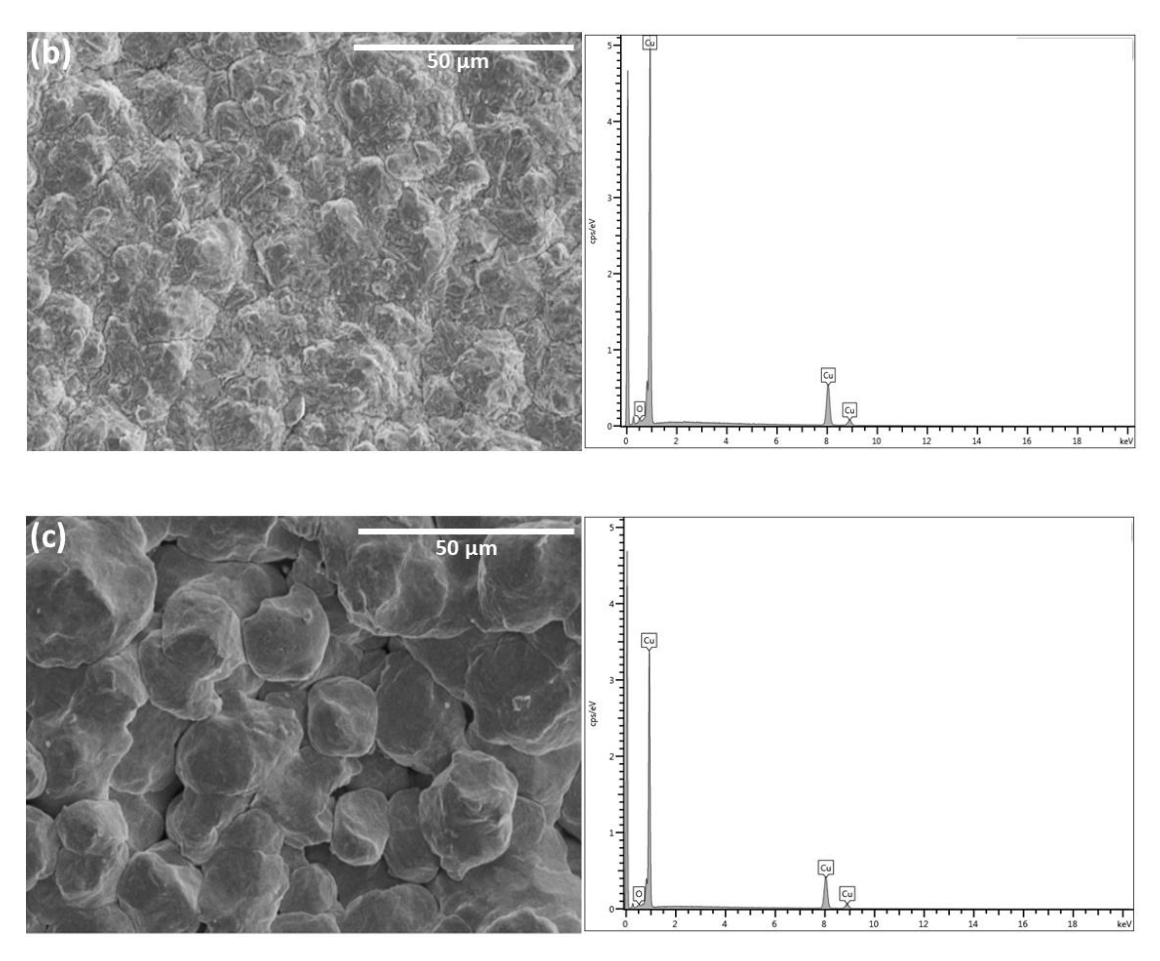


**Figure 3- 10:** EDS results of the (a) Cu powder, (b) electroplated Cu coating, and (c) cold-sprayed Cu coating at various pressures (0.41, 0.45, 0.46 MPa)

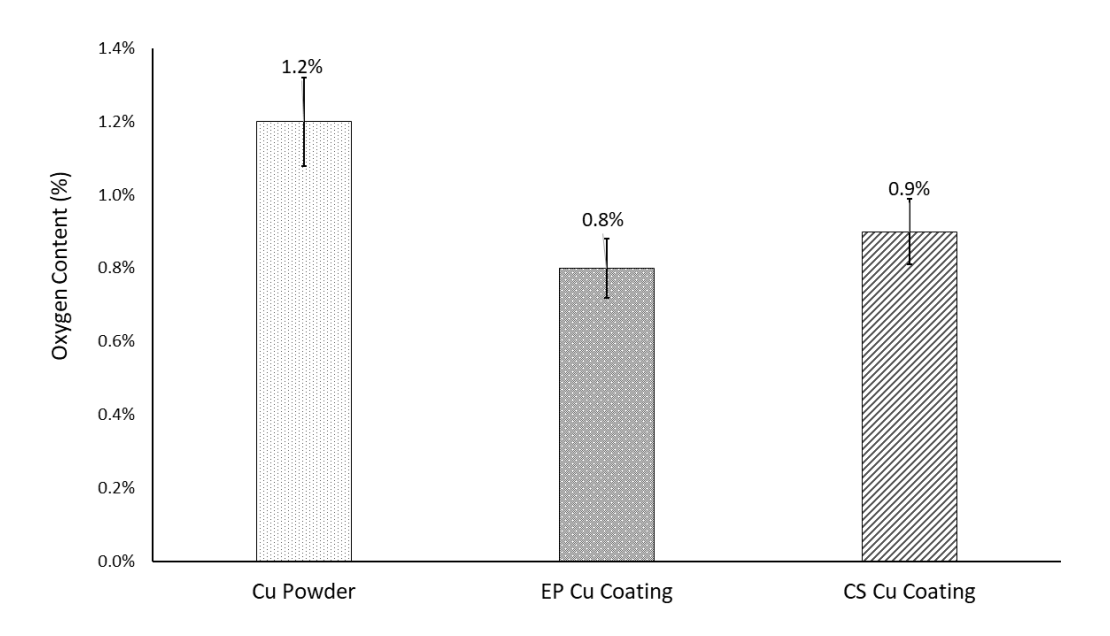


Figure 3- 11: Oxygen content in feedstock material and the coatings (EP Cu and CS Cu coatings)

It can be concluded that the amount of oxygen did not change significantly after cold spray deposition. This was likely due to the use of nitrogen as the carrier gas instead of the air, the low stand-off distance between the substrate and the nozzle that minimized the residence time of the particles in the carrier gas, and the low operating temperature of the cold spray process.

## 3.3.2 Comparison of cold spray on CFRP and Cu panel substrates

Figure 3-12 compares the DE of the Cu powder on the two different substrates; the gas temperature was fixed at the maximum of the Inovati system, 482 °C, and the gas pressure was varied from 0.41 MPa to 0.46 MPa. For the electroplated CFRP, deposition took place for pressures below 0.48 MPa, where the DE is approximately five times higher than that of Cu panel for all spray conditions. The maximum DE of the Cu powder on the electroplated CFRP was 10 %, which was obtained at a pressure of 0.46 MPa. A very slight increase (from 1.35% to 1.9%) in deposition efficiency was noticed for the Cu panels with the rise in gas pressure from 0.41 MPa to 0.46 MPa.

Limited cold sprayed deposition took place at pressures below 0.41 MPa. The reason might be because the particles do not exceed the critical velocity for deposition since the critical velocity of copper particles is relatively high and reported to be on the order of 500 m/s [38]. Similarly, Fukumoto *et al.* [82] cold-sprayed copper on stainless steel substrate for a gas pressure range of 1 MPa to 3 MPa at a gas temperature of 673 K. They confirmed that the deposition efficiency of the coating at a pressure of 1 MPa was very low (nearly to zero). It increased to approximately 40% at a pressure of 3 MPa due to the improved mechanical interlocking between the particle and the substrate.

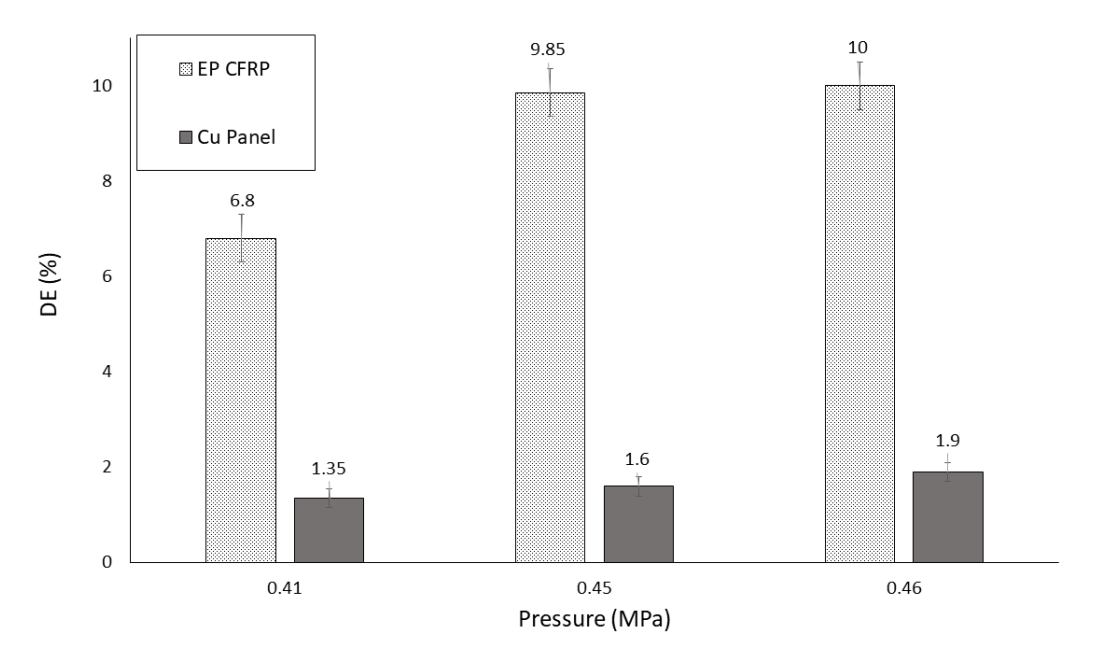


**Figure 3- 12:** Comparison of deposition efficiency of Cu at various pressures (0.41, 0.45, 0.46 MPa) for two different substrates (Cu electroplated CFRP and grit blasted Cu panel)

In this study, notable variation of DE for the two substrates are investigated through hardness and surface topology of the substrates as well as the thermal conductivity effect.

## 3.3.3 Hardness effect

In this study, the microhardness of feedstock powder, Cu electroplated CFRP, grit-blasted Cu panels and cold-sprayed Cu coatings are shown in Figure 3-13.

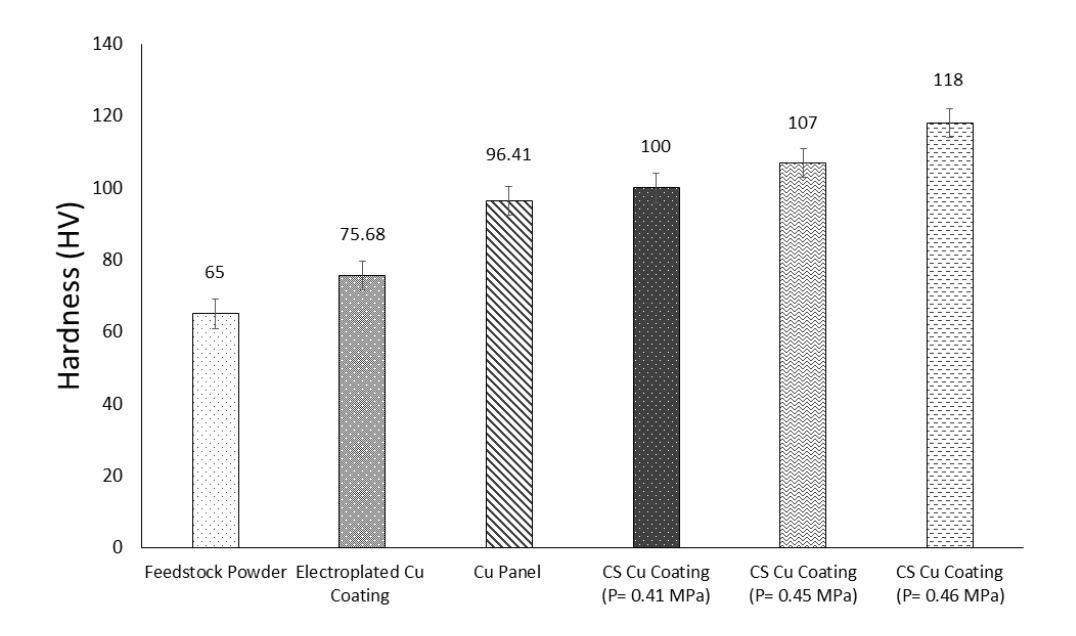


**Figure 3- 13:** Microhardness comparison of feedstock powder, electroplated Cu coating, Cu panel, and cold-sprayed Cu coatings at various pressures (0.41, 0.45, 0.46 MPa)

Previous studies [83, 84] showed that deposition behavior depends on the relative deformability of the particle to the substrate. In a system where the particles are more deformable than the substrate (i.e., soft particle/hard substrate), a higher degree of deformation happens in the particle, which results in flattening of the particle.

Christoulis *et al.* [85] studied the effect of substrate hardness on deposition behavior of the cold-sprayed Ti. They found that in the case of substrate (AISI304L) with the same hardness as the particle, deformation of both particle and the substrate occurred, and the initial spherical particle was changed to a parachute-like shape. However, in a case of a harder substrate (Ti-6Al-

4V), the Ti particles were plastically deformed upon impact, and the substrate maintained its initial geometry.

Yin et al. [86] experimentally and numerically studied the effect of substrate hardness on the particle deposition behavior. The sprayed particle was Ti and the substrates were Cu and SS. They found that in the case of Cu substrate, deformation of both particle and the substrate took place and metal jetting was achieved at the particle/substrate interface. As a result, metallurgical bonding occurred between the particle and the substrate due to the cleaning effect due to oxide breakdown. More intense deformation of the particle relative to the substrate was observed when the harder SS substrate was used. This was due to the transfer of kinetic energy from the impinging soft particle and the jetting of metal that occurred at the flattened particle interface and the formation of small craters on the substrate surface.

Similarly, in this work, in the case of Cu particle/Cu electroplated CFRP, plastic deformation of both materials may occur during the impact due to the similarity of the hardness values (see Figure 13). However, in the case of impacting copper particle on a harder substrate (i.e., copper panel), impacting particles may undergo a higher degree of deformation relative to the substrate, and a flattened particle can be formed on a slightly deformed substrate.

Consequently, the presence of softer copper interlayer as compared to the Cu panel, facilitated the penetration and impingement of particles, allowing for an improved mechanical interlocking between the particle and the substrate.

It can also be seen from Figure 3-13 that the microhardness of the cold-sprayed Cu coatings increased from 100 HV to 118 HV with an increase in gas pressure from 0.41 MPa to 0.46 MPa. The deposited Cu particle experienced greater plastic deformation by increasing the gas pressure

(higher particle velocity); therefore, higher microhardness of the cold-sprayed Cu coating was obtained due to the increased in work-hardening effect. No signs of cracking around the indentation were observed from the images of indents in Figure 3-14.

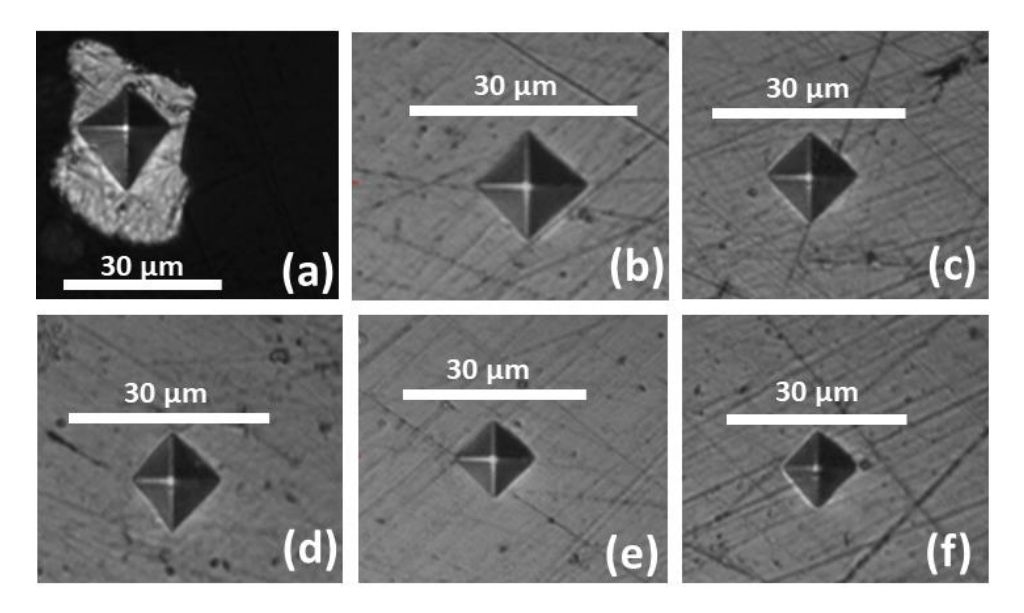


**Figure 3- 14:** Indentation micrographs of deformed zones of (a) Cu powder, (b) electroplated Cu coating, (c) Cu panel, and cold-sprayed Cu coatings at various pressures (d) P = 0.41 MPa, (e) P = 0.45 MPa, and (f) P = 0.46 MPa under 10 gf load for a penetration time of 15 seconds

# 3.3.4 Surface topology effect

In addition to the effect of relative hardness of particle/substrate on DE, surface topology of the substrate materials may also affect the deposition efficiency of the impacting particles. Therefore, surface topology and surface roughness of the substrates were studied before cold spray deposition.

Figure 3-15 shows the topologies of the electroplated CFRP and the grit-blasted copper panel, respectively. In Figure 3-15 (a), sharp asperities on the copper interlayer may function as the adhesion nucleation sites for the impacting particles by providing them with more contact area,

as compared to the grit-blasted copper panel. This statement can be verified by through the two measured parameters:  $S_{sk}$  and  $S_{ku}$ . Table 3-3 shows the results of the  $S_{sk}$  and  $S_{ku}$  for the two substrates.

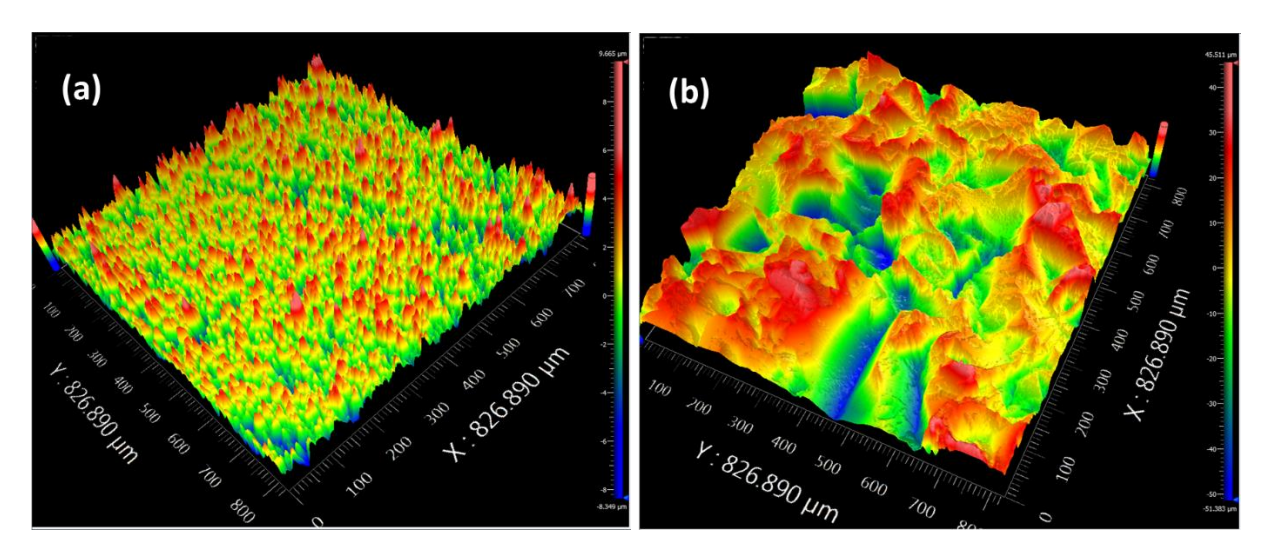


Figure 3-15: Surface topologies of (a) Cu electroplated interlayer, and (b) grit-blasted copper panel

Table 3- 3: Skewness and kurtosis of the electroplated CFRP and grit-blasted Cu panel substrates

Substrate	S <sub>sk</sub> (µm)	S <sub>ku</sub> (µm)
Electroplated CFRP	2.01	11.85
Grit-blasted Cu panel	-0.23	2.80

Larger  $S_{sk}$  values indicate isolated and steep peaks, while smaller  $S_{sk}$  suggests asperities with large plateaus, and also, as the  $S_{ku}$  becomes larger, the surface becomes rougher, developing the steep and sharp asperities [72]. The increase in  $S_{sk}$  and  $S_{ku}$ , increases the area of contact between the impacting particles and asperities, promoting particle adhesion to the substrate. In this present work, the electroplated CFRP has larger  $S_{sk}$  and  $S_{ku}$  as compared to the grit-blasted copper panel,

suggesting more interactions between the particles and the asperities, which contributed to the improved mechanical interlocking and higher DE on the electroplated CFRP.

## 3.3.5 Thermal conductivity effect

McDonald, *et al.* [87] studied the effect of substrate properties such as thermal conductivity on the surface temperature distribution. They showed that as the thermal conductivity of the material increases, a reduction in surface temperature is observed due to enhanced transfer of heat from the substrate surface to the environment. Fukumoto *et al.* [88] investigated the effect of substrate temperature on the deposition behavior of copper particles on AISI 304 substrates. They found that substrate temperature plays a significant role in deposition behavior of the impacting particles. A higher deposition efficiency (from around 0 to 55 %) was achieved and the number of craters was decreased by increasing the substrate temperature from 300 K to approximately 700 K while the gas temperature was kept at room temperature.

In this present study, since the thermal conductivity of CFRP (order of 0.4 W/m-K [89]) is much lower than that of copper (order of 400 W/m-K), the CFRP substrate beneath the copper interlayer acted as a heat insulator. It was more difficult for energy to transfer through the polymer, and conduction was greater through the copper. As a result, the CFRP substrate surface was warmer. Consequently, heat energy accumulation on the coated CFRP substrate during the cold spray deposition process likely allowed for softening of the electroplated interlayer, which improved mechanical anchoring between the particle and the substrate and resulted in increased DE.

## 3.3.6 Electrical characterization of cold-sprayed coatings

Electrical conductivity is an imperative feature of a coating for various applications requiring high electrical conductivity, such as lightning strike protection coating for polymer composite aircrafts.

Due to the high electrical resistivity of CFRP— in comparison to Al, the carbon fibers are almost 1000 times more resistive and epoxy resins are 1,000,000 more resistive [18]— copper coating was applied on CFRP to enhance its electrical property for conductive applications. Due to the presence of dense hybrid metallic coating, the electrical resistivity of the Cu cold sprayed coatings was approximately  $3.5 \pm 0.5 \mu\Omega$ -cm for all spray conditions, however; the electrical resistivity of the oxygen-free copper is reported to be 1.7  $\mu\Omega$ -cm [90]. In this present study, the electrical conductivity values of the cold sprayed Cu coating on CFRP substrates were 48% of that of bulk copper (58 MS/m [65]), which is also comparable to the value for Cu coating on metallic substrates [91]. It has been reported that high-pressure as-cold-sprayed coatings (80% IACS) have greater electrical conductivities than that of low-pressure as-cold-sprayed coatings (45% IACS) due to the formation of denser coatings that have limited oxide inclusions [92]. It should be noted that the electrical conductivity of Al is 61% of the bulk Cu [93], and this is also a metal being considered for lightning strike protection. Che et al. [6] has been successfully cold sprayed Sn onto CFRP and the electrical conductivity of the Sn coatings was measured 4.5 MS/m. They have shown that no failure was observed when currents up to 100 A were applied to the Sn coating during the lightning strike test.

From Figure 3-11, which shows the amount of oxygen in the feedstock material and the cold sprayed Cu coating, it can be concluded that the oxidation of the copper during cold spraying was

low and the higher electrical resistivity of the coatings, as compared to the oxygen-free copper, is likely due to microstructural defects, such as micro-pores at the interfaces of the particles.

Ganesan *et al.* [70] used dendritic copper particles for the coating formation on the PVC substrate with metallic interlayers of copper and tin, where the measured electrical resistivity of the coatings was  $11.39 \pm 1.6 \,\mu\Omega$ -cm and  $9.43 \pm 1 \,\mu\Omega$ -cm, respectively.

Figure 3-16 shows the comparison of the above-mentioned electrical resistivities for different materials.

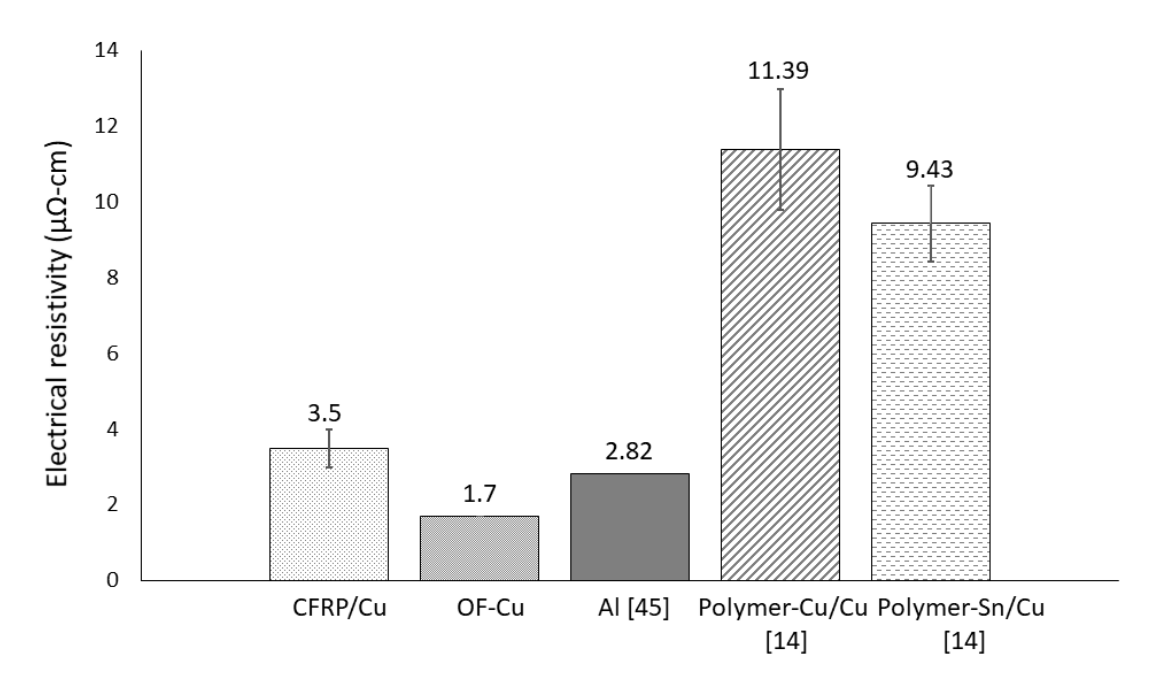


**Figure 3- 16:** Electrical resistivity comparison of Cu Cs CFRP, Oxygen-free copper, Al, PVC polymer cold sprayed by Cu with Sn and Cu as the interlayers

The present study shows that electrical resistivity of the cold spray copper coatings is lower than that obtained by Ganesan *et al*. They suggest that the trapped polymer debris in the copper coating resulted in high electrical resistivity. It is also important to note that the lack of similarity of the reported electrical resistivity values for the cold spray copper coatings may stem from the

difference in cold spray conditions as well as the properties of the feedstock powder particles, such as hardness, morphology, particle size and oxygen content.

#### 3.4 Conclusion

A continuous copper coating was successfully deposited by a low-pressure cold spray system on a CFRP substrate through a hybrid coating process that consisted of copper electroplating of an interlayer followed by cold spray deposition of copper particles. Erosion of the electroplated layer was accompanied by cold spray deposition and delamination occurred at higher gas pressures.

Both of these effects would limit DE. As compared to a Cu panel, around five times higher DE was achieved on the electroplated CFRP. This was explained by the surface characteristics of the two substrates. Based on the hardness effect on DE, it was found that the similarity of the hardness values of the particle and the substrate promoted plastic deformation at the interface by allowing particle and substrate to be deformed simultaneously.

Surface topology may also play a role in DE of copper particles on the two various substrates. In the case of electroplated CFRP, the presence of sharper asperities provided more area of contact with the impacting particles and hence resulted in an improved DE as compared to the Cu panel. In addition, the lower thermal conductivity of the CFRP as compared to the Cu panel might have resulted in heat accumulation on the copper interlayer, softening this layer and subsequently increasing the DE. Very low electrical resistivity of the coatings was achieved due to the presence of highly dense electroplated and cold sprayed coatings.

## 3.5 Acknowledgment

The authors would like to acknowledge the financial support of the Natural Sciences and Engineering Research Council of Canada (NSERC) through the Green Surface Engineering for Advanced Manufacturing (Green SEAM) Strategic Network [grant number NETGP 493955-16]. In addition, the industrial partner, Bombardier Aerospace, is gratefully acknowledged. We wish to thank the National Research Council Canada and Dr. Phuong Vo for assistance with the cold spray experiments.

# Chapter 4: Effect of Metallic Interlayer Hardness on Deposition Characteristics of Cold-sprayed Copper Particles on Carbon Fiber-Reinforced Polymers

#### Preface

After successful cold spray deposition of Cu on Cu-coated CFRP, this chapter is focused on the effect of various interlayer materials with different hardnesses on cold sprayability of the Cu particle. Single particle impact experiments were conducted to understand the correlation between the deposition and particle deformation behavior. Finite element simulation was also performed to deeply understand the particle retention behavior by examining various aspects of the particle/substrate contact, namely the strain energy, particle penetration depth, and average plastic equivalent strain of the particle.

## This chapter has been published as:

Panteha Fallah, Rohan Chakrabarty, Jun Song, André McDonald, Stephen Yue, "Effect of Metallic Interlayer Hardness on Deposition Characteristics of Cold-sprayed Copper Particles on Carbon Fiber-Reinforced Polymers", J. Therm. Spray Technol. 31 (2022), 559–573, https://doi.org/10.1007/s11666-021-01313-9. (Reprinted by permission from Springer Nature and licence to reuse in this thesis has been granted from Springer Nature)

#### **Abstract**

Copper (Cu) has been successfully cold spray deposited on carbon fiber-reinforced polymer (CFRP) by a hybrid fabrication process. In this present study, the feasibility of Cu coating buildup on a Cu electroplated CFRP under a process with two-step gas pressures was investigated numerically and experimentally. The deformation and deposition behavior of the Cu particles on CFRPs coated with tin (Sn), nickel (Ni), and Cu were studied by comparing the single particle impact with thick coating fabrication. The deposition efficiency (DE) of the cold-sprayed coatings was measured, and the microstructure and microhardness of the coatings were evaluated. The results showed that Cu coating build-up was possible with lower DE in the second spray pass of the cold spray system compared to that of the first fabricated cold-sprayed layer. This is due to the higher hardness of the previously cold-sprayed layer as compared to the electroplated Cu coating. Cold spray deposition of Cu on soft Sn and hard Ni interlayers was not feasible due to substrate erosion and insufficient plastic deformation of the substrate, respectively. From single particle impact deposition and thick coating fabrication, it was found that successful deposition in lowpressure cold spraying only takes place in the case of co-deformation phenomenon, where the substrate and the particle have nearly equal hardnesses. These results suggest that relative hardness of the substrate to the particle significantly affects the particle deformation behavior and DE of the cold sprayed coating.

**Keywords:** Carbon fiber-reinforced polymer; Deposition behavior; Deposition efficiency; Individual particle impact

#### 4.1 Introduction

Composite materials such as carbon fiber-reinforced polymers (CFRPs) are poor electrical conductors. Hence, they are susceptible to structural damage from lightning strikes [18]. To improve their electrical conductivity, applying metallic coatings to these materials has received increasing interest in the aerospace industry [4]. Amongst deposition methods, cold spray technology appears to be a suitable approach for metallizing the polymeric materials since it uses quite low-operating temperatures that limits the oxidation of metallic particles and damage of the heat-sensitive substrates [46, 47, 65, 94].

Cold spray is a solid-state deposition process, thus, the bonding mechanisms that may take place are metallurgical and/or mechanical bonding [95]. In metallurgical bonding, adiabatic shear instability (ASI) is assumed to be the main bonding mechanism [32]. Once a particle impacts a substrate with sufficiently high velocity, a plastic shear deformation takes place at the interface of the particle/substrate, leading to the formation of metal jetting [32, 96]. This fractures the surface oxide films on both particle and the substrate, generating a fresh and clean surface between the particle and the substrate for an intimate contact and metallurgical bonding. In mechanical interlocking, interfaces can bond through asperity-asperity interlocking or particles are embedded/penetrated into the substrates and a considerable fraction of the impact energy is transferred to the plastic deformation of the substrate [97, 98].

It has been reported that characteristics of the substrate material, including the substrate hardness, surface roughness, and substrate temperature, may affect particle deformation during cold spraying. The effect of these parameters on particle deformation behavior is widely studied [84, 99, 100]. Xiong *et al.* [101] investigated the impact and deposition characteristics of Ni particles on two substrates, Al alloy and Cu, through individual particle impact and full coating

deposition. It was observed that a very thin Ni coating was successfully deposited on the soft Al substrate, but no coating was achieved on the hard Cu substrate using 550 °C-29 bar nitrogen gas. Hassani *et al.* [102] showed that when the particle and the substrate materials are similar, codeformation of both materials occurs as a result of a similar degree of deformation [102]. As the spraying particle becomes denser, the possibility of mechanical bonding increases with an ultimate case being undeformed particle penetrating into a substrate. Different type of particle impact behaviours has been investigated and observed in the literature [103]. King *et al.* [104] have studied the effect of hardness of the aluminum substrate on Cu particle deformation behavior. They found that with increasing particle velocity, the relative deformation of the particles and the substrate altered, with deformation increasing at a higher rate in the substrate. Hence, higher deposition efficiencies were obtained at higher velocities due to the embedment of the particles to the substrate.

In a previous study by Fallah *et al.* [105], Cu was successfully cold sprayed onto CFRP through a hybrid coating process that involved electrochemical plating with Cu followed by cold spray. Maximum deposition efficiency of 10% (corresponding to a cold sprayed coating thickness of 145 µm) was achieved at the pressure of 68 psi and a temperature of 482 °C (900 °F) through one pass spraying; further increase in pressure resulted in coating delamination. It was found that deposition was possible due to the similar hardnesses of the particle and substrate. Nevertheless, the influence of the particle deformation behavior on deposition efficiency of the particle is not well-studied in the literature.

The objectives of this present study are to examine the effect of substrate hardness on DE and particle deformation behaviour, and to investigate the feasibility of coating build-up using two-pass schedules while spraying Cu-on-Cu electroplated CFRPs in low-pressure cold spraying.

# 4.2 Experimental procedure

# 4.2.1 Feedstock powders and the substrates

Near spherical copper (PG-PMP-1012, Plasma Giken Co., Ltd., Saitama, Japan) and tin (SST-S6001, CenterLine, SST, Windsor, ON, Canada) powders were used in this study to produce the final coating and to fabricate a metallic interlayer prior to cold spraying of Cu, respectively. The properties of the feedstock powders are presented in Table 4-1. The particle size of the feedstock powders was evaluated using a laser scattering particle size analyzer (LA-920, Horiba, Japan), and the distributions are presented in Fig 4-1. Scanning electron microscope (SEM, Hitachi SU 3500) images of the Cu and Sn powder particles are illustrated in Fig 4-2. The copper and tin powders were relatively spherical with the average particle size (D<sub>50</sub>) of 18.93μm and 12.03μm, respectively.

Microhardness of the substrates and as-polished powders were measured using a Clark CM-100AT Vickers Microhardness Tester (Sun-Tec, Novi, USA) for a penetration time of 15 s under a load of 10 gf according to the ASTM standard E384 [71]. Micro-Vickers hardness measurements were conducted on the polished cross-sections of the metallic interlayers to eliminate the influence of the soft CFRP substrate. This test method applied low forces (5-1000 gf), resulting in low penetration depth that is useful for a variety of applications such as testing thin films or small particles [106].

Table 4- 1: Properties of the feedstock powders used in this work

Powder	Morphology	Supplier	D <sub>avg</sub> , μm	Microhardness, HV
Cu	Relatively spherical	Plasma Giken	18.93	$65 \pm 9 \ (n=7)$
Sn	Relatively spherical	CenterLine, SST	12.03	$10 \pm 1 \ (n=7)$

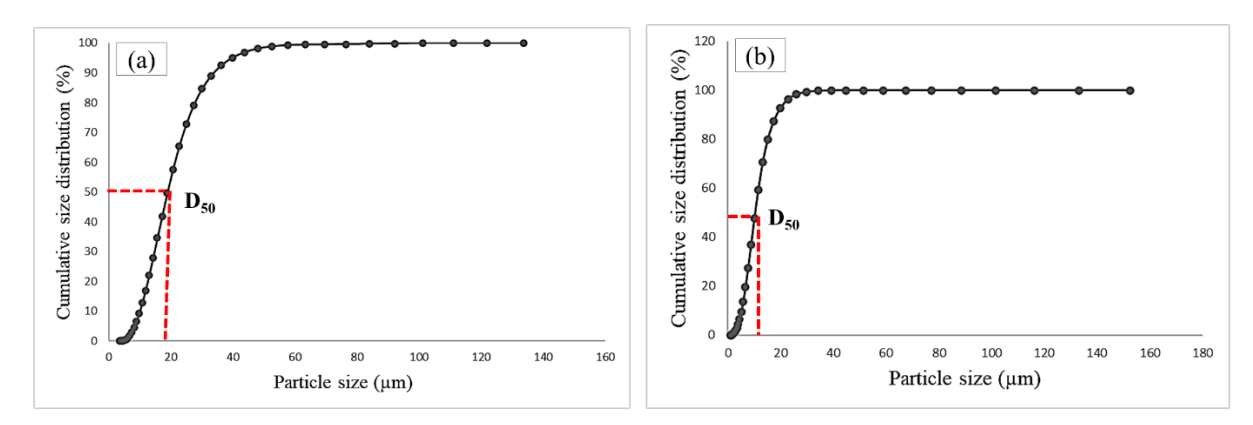


Figure 4-1: Particle size distribution of the (a) Cu and (b) Sn powders

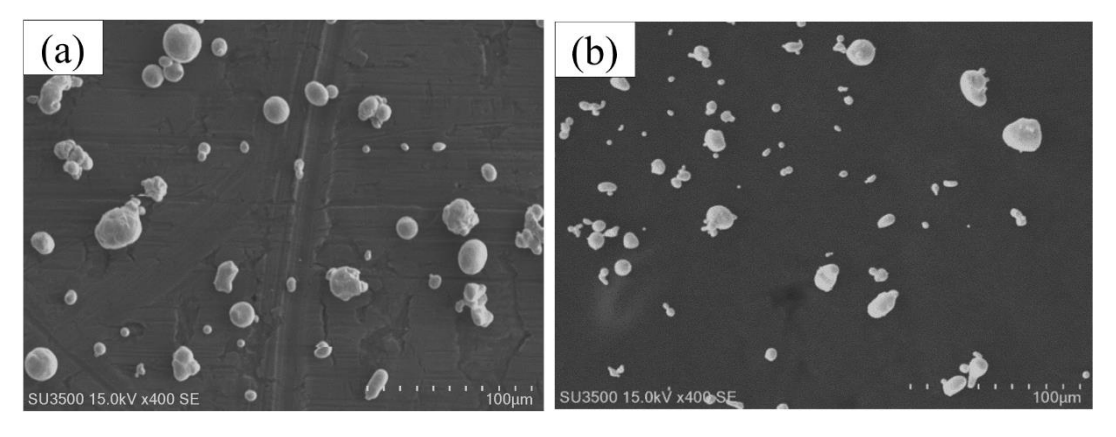


Figure 4- 2: SEM images of the feedstock powders: (a) Cu and (b) Sn

Four types of substrates were utilized in this study: CFRP coated with Sn, Ni and Cu, and 1020 mild-steel. The CFRPs manufactured by Bombardier Aerospace (Montreal, Canada) consisted of a thermosetting epoxy matrix with continuous carbon fiber reinforcements. The CFRP substrates were made of four plies of 5276-1/G30-500 epoxy carbon pre-preg ([0/90]2s). The CFRP substrates were 7 x 3 cm<sup>2</sup> with thickness of 1.7 mm and were degreased with methanol prior to coating. Mild-steel substrates of dimensions 7 x 7 cm<sup>2</sup> with thickness of 3 mm were used as a benchmark during cold spray experiments. Prior to cold spraying, the mild-steel plates were grit blasted with #24 alumina grit.

# 4.2.2 Fabrication of Sn, Ni, and Cu interlayers on CFRP substrates

Tin (Sn) interlayer was produced by cold spraying at low-pressure with a commercially available CenterLine SST system (Supersonic Spray Technologies, CenterLine Windsor Limited, Windsor, ON, Canada). This cold spray system allowed the use of the so-called "downstream injection" mode, where the particles are introduced in the gas flow after the throat of the nozzle to avoid the possibility of clogging while spraying low-melting point materials such as tin. The cold spray parameters are listed in Table 4-2. These parameters were selected according to previously successful Sn cold spray experiments [12]. The powder feed rate was 1 RPM that was measured three times during the cold spraying process. The average feeding rate was 11.5 ± 2.5 g/min. Only one spray pass was attempted with a step size of 1 mm (20 steps).

**Table 4- 2:** Cold spray parameters for the fabrication of Sn interlayers

Powder	Carrier gas	Gas temperature, °C	Gas pressure, psi	Stand-off distance, mm	Nozzle travel speed, mm/s
Sn	$N_2$	320	68	18	25

The Ni interlayer was fabricated through a two-step process; electroless Ni plating [105] followed by Ni electroplating to achieve a 100 μm Ni coating. The Ni electroplating process was performed in potentiostatic mode in a cell that contains 45 g/L H<sub>3</sub>BO<sub>3</sub>, 240 g/L NiSO<sub>4</sub>(H<sub>2</sub>O)<sub>6</sub>, 50 g/L NiCl<sub>2</sub>(H<sub>2</sub>O)<sub>6</sub> with two electrodes connected to the rectifier (XTS 7- 6 XANTREX, Canada) at room temperature [107]. The Ni coated CFRP was the working electrode, and a rectangular nickel sheet was used as the sacrificial anode. The applied voltage was -2.8 V and the corresponding deposition rate was 30 μm/h. Thus, 3 h of plating was needed to obtain nearly 100 μm Ni coating.

A 100 µm Cu interlayer was also produced with a similar procedure to the Ni interlayer that involved first electroless Ni plating followed by Cu electroplating [105]. Microhardness of the substrates is presented in Table 4-3. As is shown, Sn, Cu, and Ni interlayers have lower, nearly equal, and higher hardness values than the Cu particle, respectively.

**Table 4- 3:** Microhardness of the substrates

Substrate material	Microhardness, HV
Sn coated CFRP	$18 \pm 2 \ (n = 10)$
Cu electroplated CFRP	$75 \pm 4 \ (n = 10)$
Ni coated CFRP	$300 \pm 10 \ (n = 10)$
Mild-steel panel	$130 \pm 10 \ (n = 10)$

## 4.2.3 Cold spray deposition of Cu on various metallic interlayers

Low-pressure cold spray of Cu was conducted with a commercially available cold spray system (Inovati KM CDS 2.2, Santa Barbara, CA, USA). The cold spray process parameters for Sn and Ni coated CFRP substrates are listed in Table 4-4. Only one pass with a step size of 1 mm (20 steps) was sprayed for Sn and Ni coated CFRPs under the gas pressure of 68 psi. The cold spray parameters for Cu coated CFRPs are listed in Table 4-5. The powder feed rate was 1 RPM that was measured three times during the cold spraying process. The average feeding rate was 11.5  $\pm$  1.3 g/min. Pressures of 65 and 68 psi were selected as the first-pass gas pressure, since they led to the previously observed maximum one pass spraying DE of 9.85% and 10%, respectively, whilst avoiding delamination [105].

For all the spray conditions, the second pass pressures were selected to be at or below 68 psi to avoid possible coating delamination caused by higher particle velocity and/or differences in coefficients of thermal expansion. For two experiments, the gas pressure for the second pass was chosen to be the same as the first pass, which is the conventional way to implement multi-pass

spraying. The other two experiments used 60 psi for the second pass to explore the effect of hardness of the first pass on the deposition characteristics.

Deposition efficiency (DE) was measured as the weight of the deposited powder onto the substrate divided by the total weight of the powder sprayed while the nozzle was effectively over the substrate [105].

**Table 4- 4:** Cu cold spray parameters for Sn and Ni coated CFRP substrates

Powder	Carrier gas	Gas temperature, °C	Gas pressure, psi	Stand-off distance, mm	Nozzle travel speed, mm/s
Cu	$N_2$	482	68	35	25

 Table 4- 5: Cu cold spray parameters for Cu coated CFRP substrates

Powder	Carrier gas	Gas temperature, °C	Two-pass gas pressures, psi			
Cu	$N_2$	482	P1 65 68 65 68	P2 60 60 65 68	35	25
			08	08		

Single particle impact experiments were performed using a commercially available Inovati system. The process parameters were similar to that of Cu spraying onto Sn and Ni coated CFRPs

except for the nozzle travel speed, which was set 1000 mm/s to obtain a single particle impact using only one line of powder.

## 4.2.4 Characterizations of coating and cold spray process

After electroplating the CFRP substrates, cold sprayed coating deposits and single particle impact deposit, a scanning electron microscope (SEM) was used to characterize samples for top view observation. For cross-sectional images, Cu cold-sprayed samples were cut with a manual abrasive cutter (ISOMET 5000, Buehler, Lake Bluff, Illinois, USA). The specimens were then metallurgically mounted in epoxy resin and cured at room temperature. Subsequently, the samples were ground using #800 and #1000 grit SiC polishing papers and eventually polished with 3 μm diamond suspension. Compositional analysis of the Sn coated CFRP after cold spraying was performed using Energy-Dispersive X- ray Spectroscopy (EDS) in the SEM.

The particle in-flight velocity at different pressure conditions was measured by using a cold spray meter (Tecnar Automation, St-Bruno, QC, Canada). No substrates were placed in front of the nozzle and the measurements were performed at the same location where the substrates were placed during cold spray. A FLIR SC620 infrared high-speed camera was used to monitor the surface temperature of tin-coated CFRP substrates during cold spraying of Cu.

## 4.2.5 Finite element simulations

To analyse the splat rebounding behavior during impact, a 3D Lagrangian model was developed using finite element (FE) analysis software, Abaqus/Explicit [108]. The copper particle size in the simulations was set as 19 µm similar to that listed in Table 4-1. To eliminate any possible boundary effects, the dimensions of the substrate were kept significantly larger than the particle diameter, as shown in Fig. 4-3a. The particle and substrate were meshed with C3D8R linear brick

element, with reduced integration. A meshing resolution of  $1/32d_p$  was used for the particle and in the contact region of the substrate, which has also been used in earlier studies [109, 110]. A fixed boundary condition was applied to the substrate bottom, while symmetry boundary conditions were applied to the sides. The material deformation behaviors of both the particle and substrate were prescribed by the Johnson-Cook plasticity model [111], which accounts for strain and strain rate hardening, as well as thermal softening. In this model, the flow stress is given by Eq. 1 as

$$\sigma = [A + B\varepsilon^n][1 + C \ln \dot{\varepsilon}^*][1 - T^{*m}],\tag{1}$$

where A is the quasi-static yield strength of the materials, n the strain hardening exponent, and B, C, m are other material-dependent constants.  $\varepsilon$  is the equivalent plastic strain,  $\dot{\varepsilon}^*$  is the equivalent plastic strain rate normalized by a reference strain rate.  $T^{*m}$  is the homologous temperature given by  $(T-T_{ref})/(T_m-T_{ref})$  where,  $T_{ref}$  is the reference temperature and  $T_m$  denotes the melting temperature of the material. The deformation process has been considered as adiabatic and based on the relationship between gas temperatures and particle temperatures [33], the initial temperature of the particle was set to be 473K while the substrate was set to be at room temperature (298K).

To incorporate the hardness of the substrate material in Eq. 1, the parameter 'A' (quasi-static yield strength) was modified according to the relationship proposed by Cahoon *et al.* [112] in Eq. 2 as

$$A = \frac{H}{3}(0.1)^n. (2)$$

Here, *H* is the Vickers hardness in MPa and *n* the strain hardening exponent shown in Table 4-7.

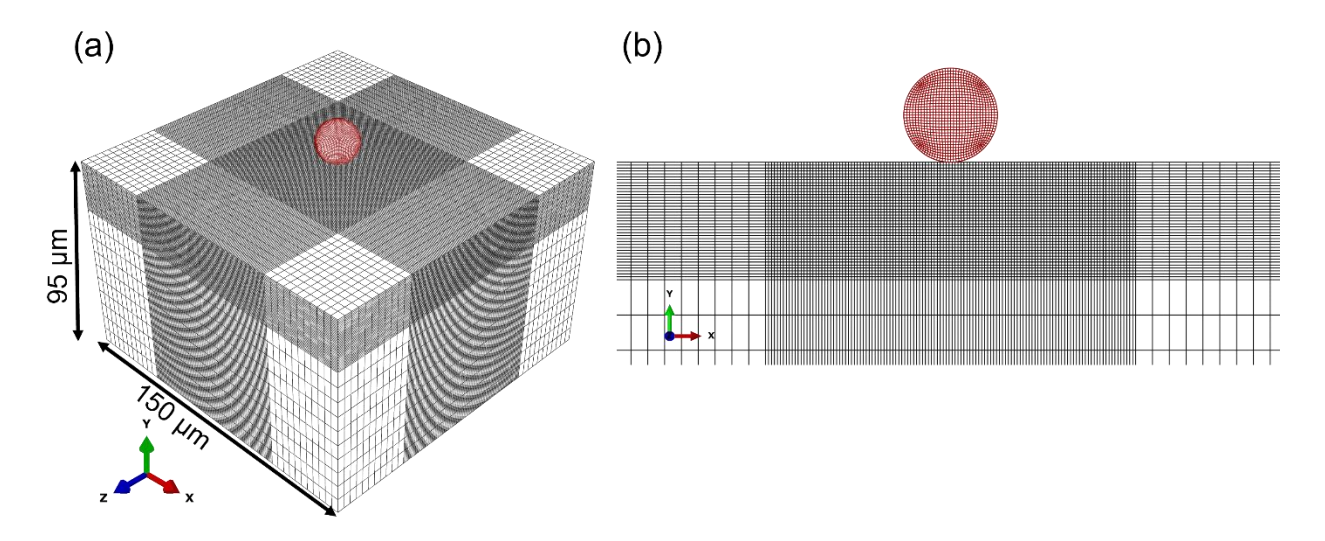


**Figure 4- 3:** (a) Schematic diagram of the meshed model with the substrate dimensions (b) Magnified view of the meshing

## 4.3 Results and discussion

# 4.3.1 Cold-sprayed coatings and deposition characteristics

## Cu-on-Sn interlayer

No deposition was possible, in fact, severe substrate erosion took place after spraying, leading to a negative DE (-30%); negative DE has been observed by other investigators and have been attributed to severe erosion of the substrate [12]. The approximate thickness of Sn interlayer before cold spraying Cu was  $250 \pm 15 \mu m$ . Figure 4-4 shows the morphology of the Sn interlayer before and after spraying with Cu particles. The EDS result (Fig 4-4 (c)) indicates that 100 wt% Sn was observed after spraying with the Cu (i.e., no Cu was deposited on the Sn).

The maximum surface temperature during cold spraying was 164.8 °C for the 68 psi pressure, which is well-below the melting point of Sn (232 °C). Therefore, no melting was expected as a result of cold spraying Cu at 482 °C. Ganesan *et al.* [13], successfully cold sprayed Cu particles onto thermoset epoxy polymers using cold spraying of Sn prior to Cu deposition with different cold spray parameters. Further studies and experiments need to be conducted to be able to successfully cold spray Cu on CFRPs coated with Sn.

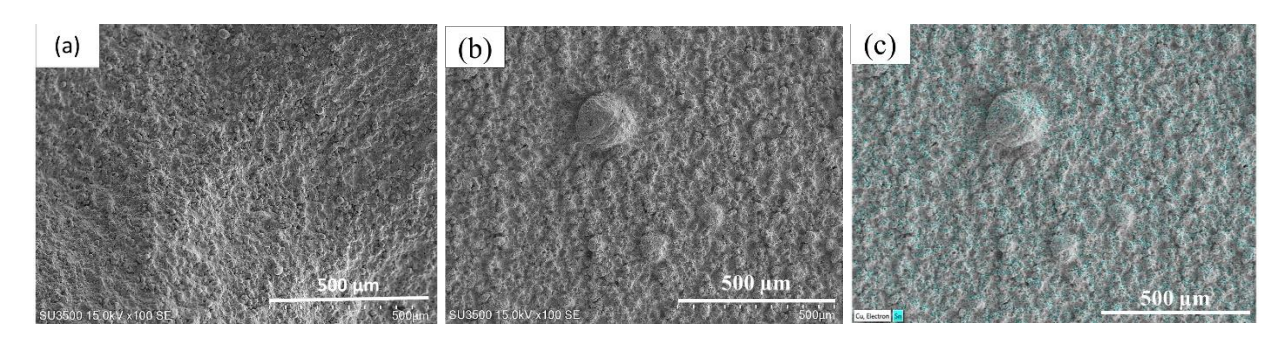


**Figure 4- 4:** SEM micrographs of the Sn interlayer (a) before and (b) after cold spraying Cu (c) EDS map analysis result of the Sn interlayer after cold spraying Cu

#### Cu-on-Cu interlayer

Here, Cu can be deposited by probably a mixture of metallurgical bonding and physical interlocking even though there is some erosion of the Cu interlayer [105]. Figure 4-5 exhibits the deposition efficiency of the Cu for the various conditions described in Table 4-5. It can be seen that the overall DE of the Cu coatings was reduced for the two-pass schedules as compared to the single spray pass schedule. This is clearly due to the DE of the second pass being lower than that of the first pass for the experiments. This can be explained by a change in the 'substrate' characteristics.

In the first pass, the particles impact onto the electroplated CFRP substrate, which gives the DE measured. In the second pass, the particles impact on the previously deposited layer, which

has less favourable deposition properties. According to the previous study [105], the hardnesses of the first cold-sprayed layers are 107 HV and 118 HV at 65 psi and 68 psi, respectively, which are greater than that of the electroplated Cu interlayer (75 HV). The decreases in DE of the second pass are 50% and 48% for the 68 psi and 65 psi experiments, respectively. These values are probably not statistically different, but the expectation is that the harder the substrate the lower the DE, which seems to be supported by these initial results.

In the two-pass pressures of 68-60 psi and 65-60 psi, the deposition efficiency of the second passes were 3.6% and 4%, respectively. This difference resulted from the increasing hardness of the first pass layer going from 65 psi to 68 psi. Consequently, it is concluded that the substrate hardness relative to the particle exhibits significant effect on the deposition efficiency of the Cu particle. A similar trend was also noticed for the steel substrate when compared with electroplated CFRP substrates. The hardness of the steel (130 HV) is higher than that of the cold sprayed Cu layer, leading to much lower deposition efficiencies compared to the corresponding two-pass schedules on the electroplated substrates and lower DE was obtained for P1-P2 (MS) than that of P1 (MS). In fact, the overall DE of the mild steel coatings is more or less the same as the DE of pass 2 in the electroplated substrates. These results suggest that the second pass has a very low DE compared to the DE of pass 2 schedule in electroplated CFRP substrate.

Response of the DE on the relative hardness of the particle and the substrate has been thus explored further using finite element simulations in Section 4.3.2 of this study.

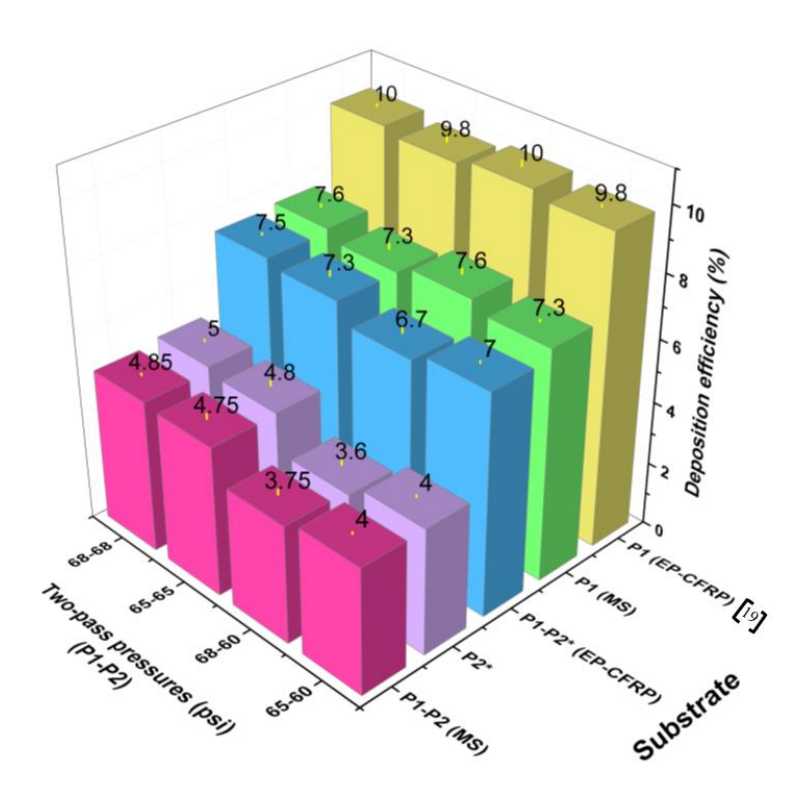


**Figure 4- 5:** Comparison of deposition efficiency of the Cu particle sprayed on the electroplated CFRP substrates and mild-steel panels (MS) at various pressures (Substrate refers to: Mild-steel for P1-P2 (MS) and P1 (MS), first cold-sprayed layer for P2\*, Cu electroplated CFRP for P1-P2\* (EP-CFRP) and P1 (EP-CFRP)). (Note: Standard deviations are indicated in yellow vertical lines (SD = 0.1 to 0.2 for n = 3))

Figure 4-6 shows the SEM top and cross-sectional micrographs of the cold-sprayed Cu coatings. From the top surface micrographs (Fig. 4-6 (a-c)), it can be seen that by increasing the pass 2 pressure from 60 psi to 65 psi, no obvious morphological changes were observed due to the small change in pressure. From the polished cross-sectional view (Fig 4-6 (d-f)), the particles cannot be delineated, but the coating is continuous and dense. As the DEs of the two pass schedules are very close, the thickness values of the cold-sprayed coatings are very close to each other and are approximately 240 µm (given specific fields of view in the cross-sections). A slight separation between the cold sprayed coating and the electroplated coating can be observed, which may have

been due to cutting, grinding, and polishing of the samples. The adhesion strength of the hybrid Cu coatings will be studied in future work.

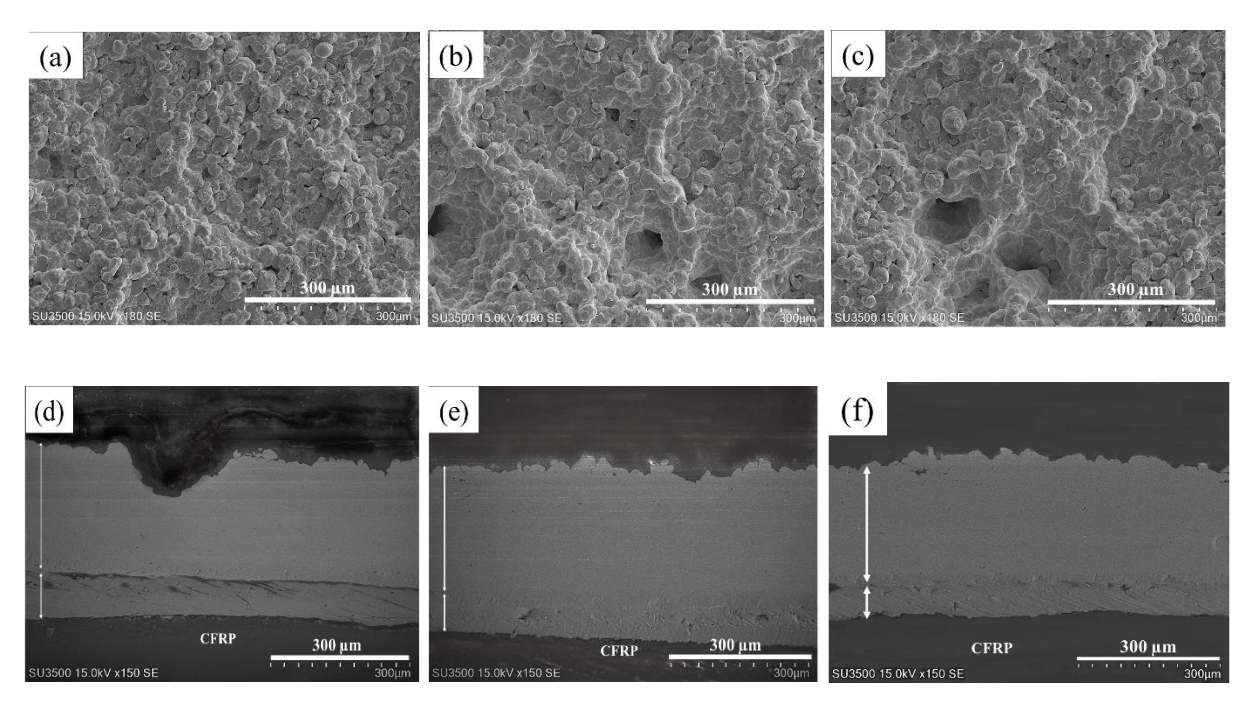


**Figure 4- 6:** SEM micrographs of the Cu cold sprayed coatings after two-pass pressures of (a and d) 65-60 psi, (b and e) 68-60 psi, (c and f) 65-65 psi from top and cross-sectional observations

## Cu-on-Ni interlayer

As can be seen from the SEM micrographs of the Ni interlayer after cold spraying (Fig 4-7 (a and b)), it was not possible to form good coating of Cu, although there were random regions of Cu particle deposition, but this only led to a deposition efficiency close to 1%. These regions were poorly adhered to the substrate and caused the substrate to be moderately deformed as it is clearly observed in Fig 4-7 (a). The negligible deposition was likely due to the significant hardness difference (300 HV versus 65 HV) between the substrate and the particle that prevented the substrate from sufficient deformation, thus preventing the formation of metallurgical bonds or

physical interlocking. As is shown in Fig 4-7 (c), the backing surfaces of the sprayed particles were flattened, indicating the occurrence of the particle plastic deformation during cold spraying.

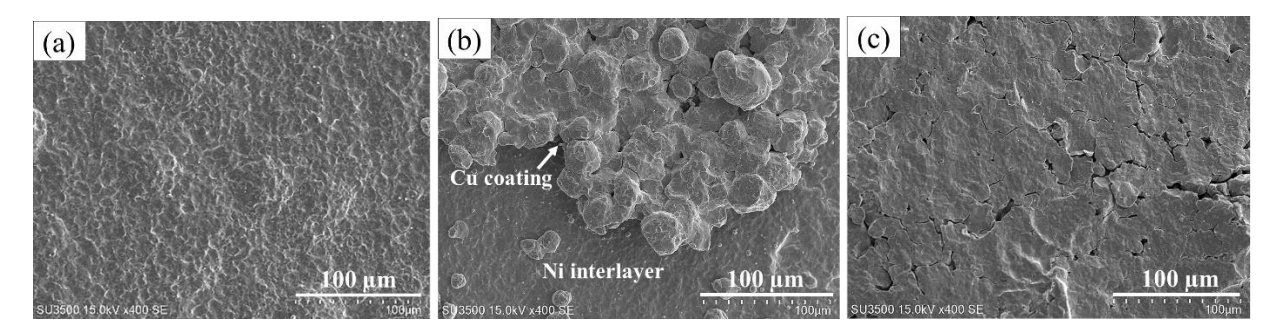


**Figure 4- 7:** SEM micrographs of (a) the Ni interlayer after cold spraying (b) the Cu coating formed on the Ni interlayer and (c) backside view of the randomly fabricated Cu coating

## 4.3.2 Modeling results

The lower overall DE after the second layer deposition that was observed in this study was attributed to the increased hardness of the first cold sprayed layer compared to the electroplated Cu coating. To investigate this further, FE simulations were conducted considering four cases described in Table 4-6. The varying substrate hardness was incorporated in the Johnson-Cook model by modifying the parameter 'A' (quasi-static yield strength) according to Eq. 2. For the first case, the impact behavior of Cu particles with hardness of 65 HV on the electroplated Cu substrate with hardness of 75 HV was considered. This corresponds to the first layer deposition explored in a previous study [105]. While for the second, third, and fourth cases, the impact behavior of Cu particles with a hardness of 65 HV on the first deposited layers was examined. In our previous study [105], the hardness of the first deposited layer at different pressures (107 HV at 65 psi and HV 118 at 68 psi) were determined. Some particles on the top surface of the first cold-sprayed layers seem to be partially deformed and/or retain their shape from the top surface observations [105]. Therefore, the hardness of the first cold-sprayed coating layer was measured in the coating

from the interface to the very top layers of the particles and the average was reported for ten measurements on each condition (n = 10). The standard deviation of the hardness measurements for the first cold sprayed layer has been reported to be relatively low (about 5  $\mu$ m) [105]. Therefore, the effect of hardness variation within the coating was considered to be negligible.

Using Eq. 2 and the hardness values from the experiments, the particle and substrate material properties were modified for the simulations and are shown in Table 4-7. It should be noted that with the exception of parameter A, all other material parameters are the same in Cu particle and the Cu substrates. The particle impact velocities outlined in Table 4-8 are used in the simulation.

**Table 4- 6:** Descriptions of the simulations

Case 1.	Cu powder (HV65) on Cu Substrate (HV75), Particle Velocity = 455 m/s
Case 2.	Cu powder (HV65) on Cu Substrate (HV107), Particle Velocity = 455 m/s
Case 3.	Cu powder (HV65) on Cu Substrate (HV107), Particle Velocity = 443 m/s
Case 4.	Cu powder (HV65) on Cu Substrate (HV118), Particle Velocity = 443 m/s

**Table 4- 7:** Material parameters for copper particles and the substrates of different hardness values. (\* refers to experimental hardness values determined for the particle and first deposited layers. \*\* signifies the modified values of A according to Eq. 2)

		Cu		Cu	Ni	Sn
Parameter/material	Cu (Particle)	(Electroplated)	Cu (65psi)	(68psi)		
Density (g/cc)	8.96	-	-	-	8.89	7.28
Young's modulus						
(GPa)	124	-	-	-	207	45
Poisson's ratio	0.34	-	-	-	0.31	0.299
Heat capacity						
(J/Kg·K)	383	-	-	-	456	220
Melting temperature						
$T_m(K)$	1356	-	-	-	1726	501
HV (Kg/mm <sup>2</sup> )*	65	75	107	118	300	18
A modified						
(MPa)**	104.1	120.1	171.3	188.9	458.7	11.7
B (MPa)	292	-	-	-	648	243
n	0.31	-	-	-	0.33	0.703
С	0.025	-	-	-	0.006	0.096
m	1.09	-	-	-	1.44	0.08

Reference temp $T_{ref}$						
(K)	298	-	-	-	298	298
Reference strain rate						
(1/s)	1	-	-	-	1	1

**Table 4- 8:** Copper particle velocity measurements at 482 °C for different pressures

Gas	Gas	Particle
pressure,	temperature,	velocity,
psi	°C	m/s
60	482	443
65	482	455
68	482	459

Velocities corresponding to the pressures of 65 psi for the first layer deposition (Case 1), and 65 psi, 60 psi and 60 psi for the second layer deposition (Case 2, Case 3 and Case 4, respectively) were employed.

To analyze the retention behaviors of the Cu particle for the substrates with varying hardness, three aspects of the particle/substrate contact were examined, namely (i) the strain energy of the model (i.e. the recoverable strain energy) both at the end of the simulations and the area under the temporal evolution curve (ii) the penetration depth of the particle into the substrate (i.e., crater depth) and (iii) the average plastic equivalent strain of the particle given by the  $\overline{PEEQ}$  at the end of the simulation.

In their evaluation of the deposition behavior of cold sprayed powders onto similar and dissimilar materials, Bae et al. [84] and Manap et al. [113] attributed lower recoverable strain energy (RSE) to lower rebound energy. The recoverable strain energy representing the stored elastic strain energy to facilitate the rebounding of the particle is shown in Fig 4-8 (a). The curve indicates the evolution of the stored elastic strain energy from the start of simulation and till the end. The curve increases as the kinetic energy of the particle is being stored in the model as strain energy. After reaching the peak, a part of the stored energy is being utilized by the substrate to relax and the particle to bounce back (rebounding). Once the particle completely leaves the substrate, as there is no further interaction or deformation involved, there is no significant change in strain energy in the system, resulting in constant values. The final time (60 ns) corresponds to the simulation end time. Comparing the final RSE at the end of the simulation, it can be observed that Case 1 shows significantly lower recoverable strain energy than the other three cases, indicating a higher retention possibility of the Cu particles in Case 1 than in Cases 2 - 4. This correlates to the lower second layer DE described earlier in Fig 4-5. Additionally, the area under the curves can be used determine the total strain energy over the entire time and a higher value will indicate greater probability to rebounding. The area under the curves in Fig 4-8 (a) were Case  $1 = 3.08 \times 10^{-7} \text{ J.sec}$ , Case  $2 = 3.53 \times 10^{-7} \text{ J.sec}$ , Case  $3 = 3.33 \times 10^{-7} \text{ J.sec}$ , Case  $4 = 3.46 \times 10^{-7} \text{ J.sec}$ . This also showed that increased hardness of the substrate resulted in higher total strain energy of the model.

Comparing Case 1 with Cases 2-4 in Fig. 4-8 (b-c), Case 1 exhibited a higher crater depth and a comparative  $\overline{PEEQ}$  of 5.8 µm and 0.83, respectively, indicating a more shared plastic deformation at the interface. The harder substrate (Cases 2-4) showed significantly lower crater depths (cf. Fig. 4-8 (b)) indicating lower deformation of the substrate. However, from Fig. 4-8 (c),

it can be observed that the particle experienced higher overall plastic deformation ( $\overline{PEEQ}$ ) for the harder substrates than the softer electroplated Cu substrate in Case 1, thereby facilitating the particle deposition. A higher particle deformation was also observed by Yin *et al.* [114] during the deposition of a Cu particle on the harder substrate materials with a thin (less than particle diameter) Cu coating. Similar to our observation, Yin *et al.* also reported lower crater depths with increased substrate hardness. However, the simulation results together with the measured deposition efficiencies suggest that a higher shared deformation between the particle and the substrate results in enhanced mechanical/metallurgical bondings as indicated by the higher DE for Case 1. While lower DE and lower shared deformation for the other cases demonstrate the negative influence of substrate hardness on the DE.

Finally, the temperature profile of the particles did not show a significant difference between the four cases due to the moderate differences between the particle deformation behavior (Fig. 4-8 (d)).

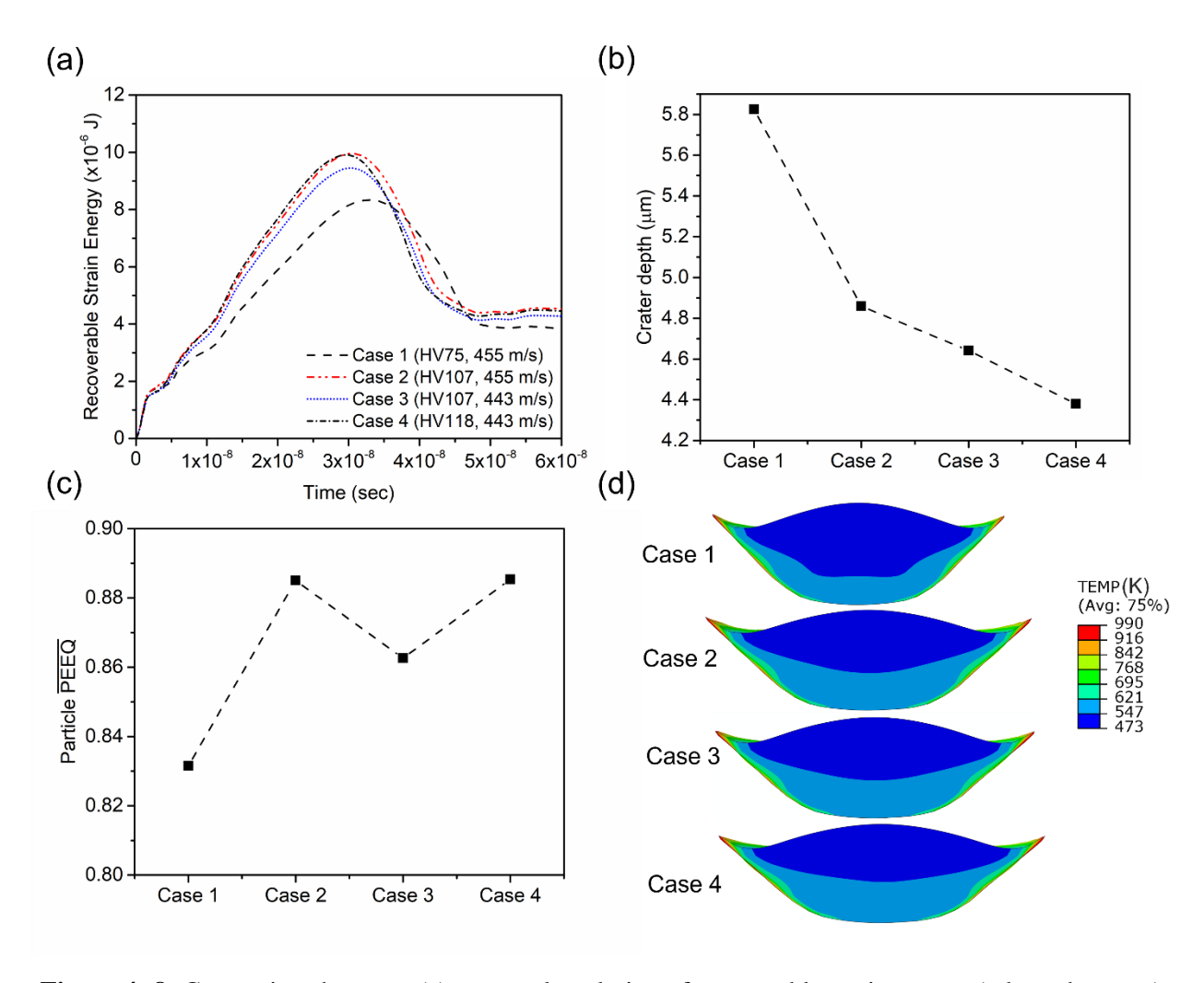


**Figure 4- 8:** Comparison between (a) temporal evolution of recoverable strain energy (rebound energy) of the entire model (the substrate hardness and particle velocities for different cases have been provided in the legend), (b) the particle crater depth and the (c) particle  $\overline{PEEQ}$  at t = 60 ns for the different cases (d) the temperature profile of the particle

To further investigate the substrate hardness effect on the particle deposition behavior, Cu particle impacts were also carried out on nickel and tin substrates with hardness HV300 and HV18, respectively. For comparing with the Cu substrate, the particle velocities were kept similar to Case 1 (Cu substrate HV75, 455 m/s). The nickel and tin substrate properties are shown in Table 4-7. The simulation results are shown in Fig 4-9. Contradictory to the previous case, the final RSE at 60ns was higher for softer Cu substrate than for the harder nickel substrate. However, Fig 4-9 (a)

shows that the RSE peak for nickel substrate was achieved at an earlier time than for Cu and Sn substrates indicating lower rebounding times. Also, considering the higher modulus and yield strength of nickel substrate, a higher share of the kinetic energy of the particle was being stored in the model as elastic strain energy. While, for tin substrate, excessive deformation resulted in a gradual increase of the RSE and the peak energy was not reached during the 60ns simulation time. Comparing the area under the curves in Fig 4-9 (a), Case 1 (3.08x10<sup>-7</sup> J.sec) and tin substrate (1.5 x10<sup>-7</sup> J.sec) had lower total strain energy than nickel substrate (3.21 x10<sup>-7</sup> J.sec).

Comparing Case 1 with nickel and tin substrates in Fig 4-9 (b-d), Case 1 and tin exhibited a significantly higher crater depth than harder nickel substrate, while particle  $\overline{PEEQ}$  and particle temperature was larger in the latter case. As discussed earlier, the degree of shared particle and substrate deformation is important to determine deposition success. As such, the significantly lower crater depth of nickel substrate might result in lower deposition efficiencies. Additionally, impact on softer tin substrate showed particle embedding, excessive substrate deformation (Fig 4-9 (d)) and minimal particle  $\overline{PEEQ}$ , indicating mechanical interlocking to be the dominant bonding mechanism in this case. It should be noted that in this present study, only the effect of substrate hardness on deposition characteristics was studied and some parameters such as the influence of underlying CFRP and surface roughness of the substrate were neglected.

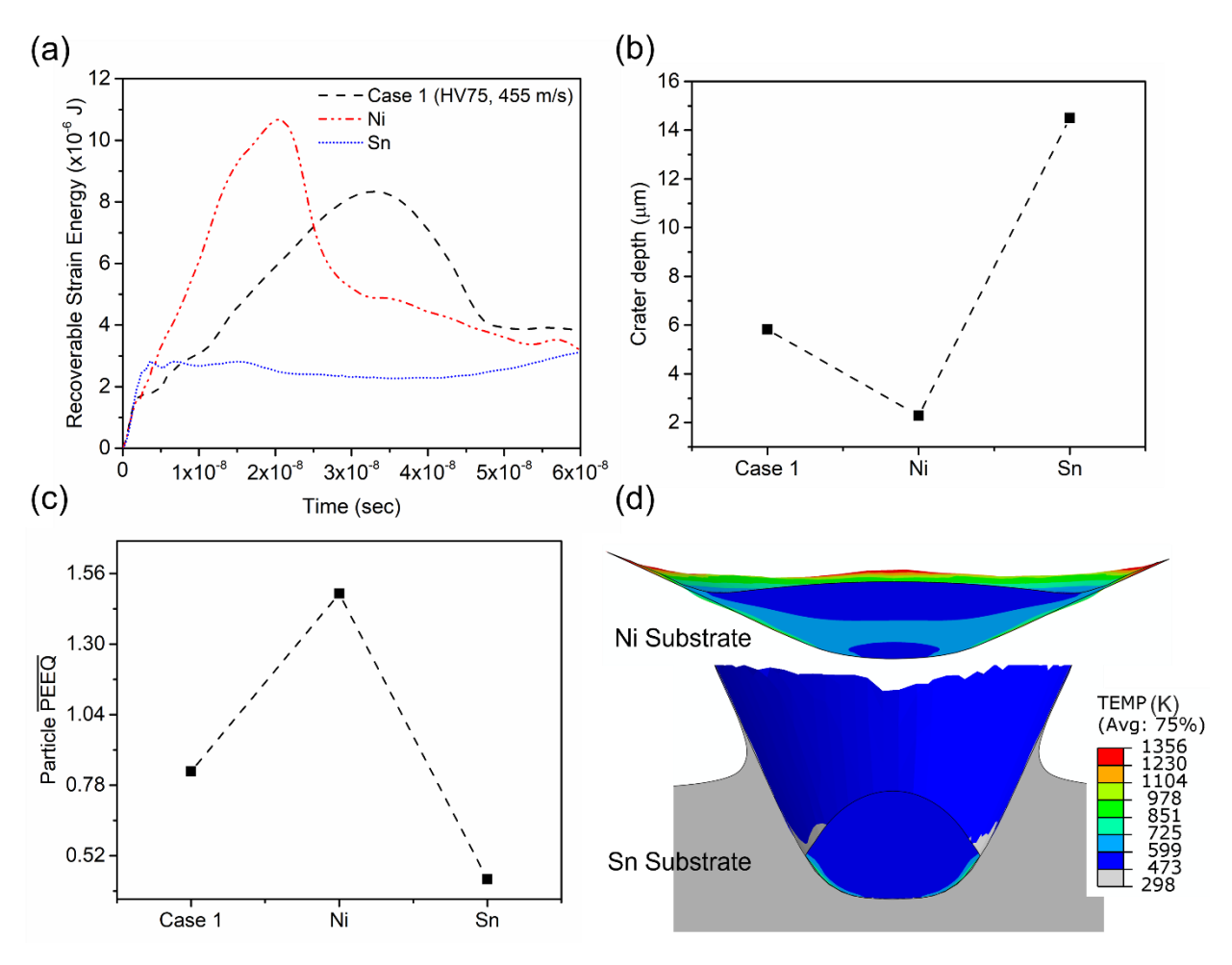


**Figure 4- 9:** Comparison between (a) temporal evolution of recoverable strain energy (rebound energy) of the entire model for different substrate materials, (b) the particle crater depth and the (c) particle  $\overline{PEEQ}$  at t = 60 ns for the different substrate materials (d) the temperature profile of the copper particle and deformed tin substrate

## 4.3.3. Single particle impact

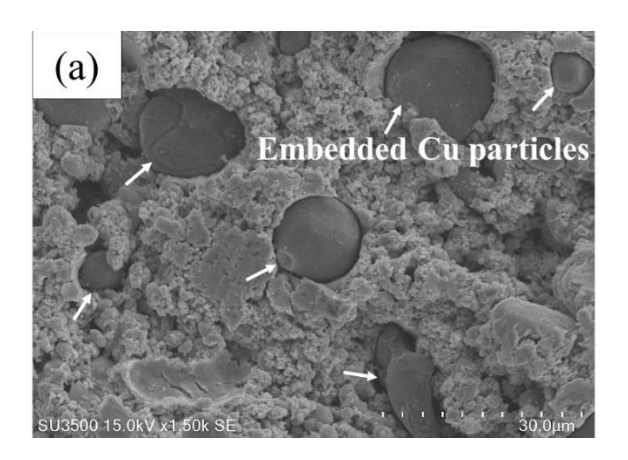
Figures 4-10 and 4-11 show the micrographs of the Cu particles cold sprayed onto Sn coated CFRP, Cu coated CFRP, and Ni coated CFRP substrates through a single particle impact. It can be seen that different deformation behaviours may take place, depending on the substrate material. Copper particles (indicated by white arrows) were deeply embedded into the Sn interlayer and did not appear to exhibit plastic deformation from observations of the upper surfaces. However,

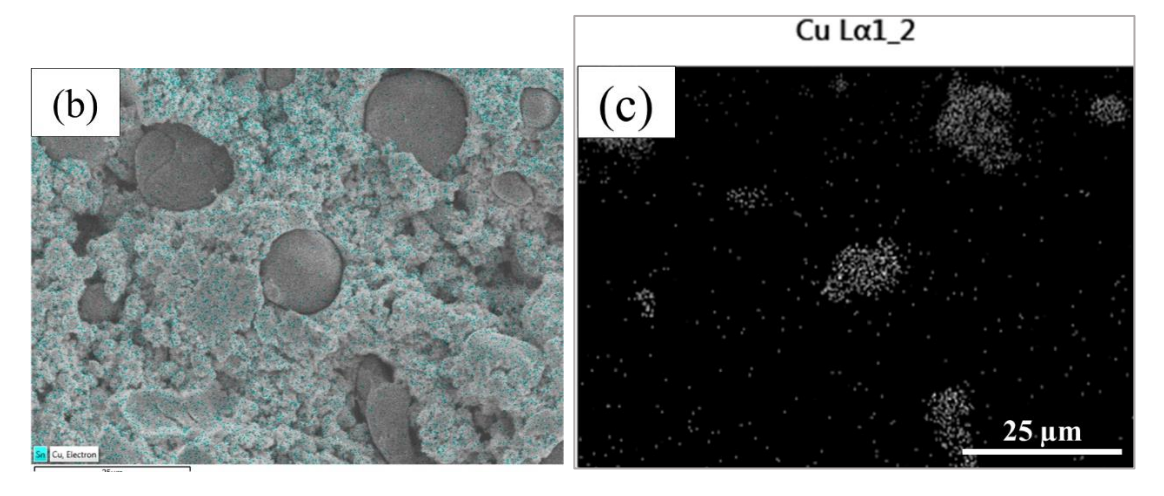
significant deformation took place in the Sn interlayer, and this is due to the substantial difference (about 47 HV) between the microhardness of the Cu particle and the Sn interlayer. Hence, most of the particle impact energy was transferred to the deformation of the soft component (i.e., Sn interlayer).

The EDS results of the Sn interlayer after single particle spraying (Fig 4-10 (b) and (c)) confirmed the presence of the penetrated Cu particles into the Sn interlayer. The higher nozzle travel speed during the single particle impact experiment (1000 vs. 25 mm/s), possibly allowed for the embedment of a few Cu particles in the Sn interlayer. Insignificant thermal softening of Sn has possibly occurred, and a smaller number of Cu particles impacted the Sn interlayer. As a result, less impact energy was generated, allowing Cu particle penetration into the Sn interlayer. However, strong Sn interlayer erosion took place at a nozzle travel speed of 25 mm/s and no Cu particles were observed on the Sn interlayer. In this case, more Cu particles impacted the Sn interlayer, and a greater amount of impact energy was generated as compared to that of 1000 mm/s, leading to Sn interlayer erosion. In addition, greater thermal softening of Sn interlayer at a nozzle travel speed of 25 mm/s may have facilitated the erosion of the Sn interlayer.

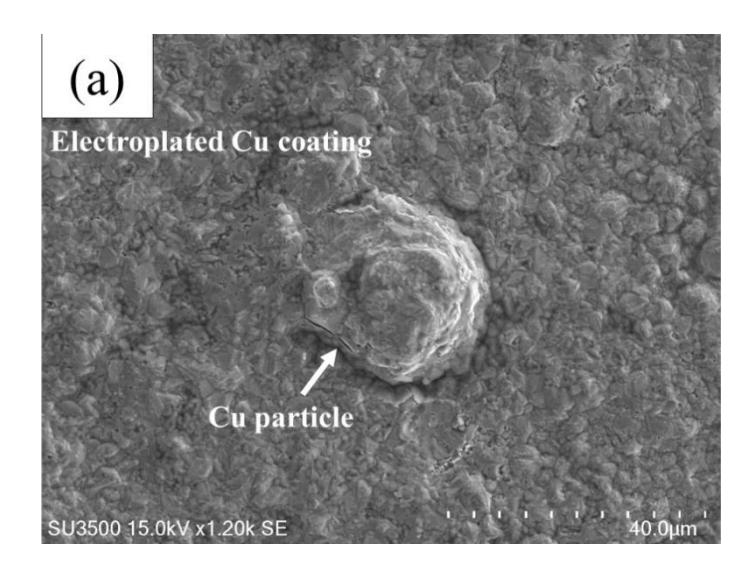
In the case of spraying Cu particle on a Cu interlayer (Fig 4-11 (a)), particle penetration was not observed, and the particle appeared to be successfully adhered and co-deformed with the substrate. However, metal jetting was not observed due to the relatively low particle velocity. These results show that a transition from penetration to co-deformation mechanisms takes place as the hardness difference between the particle and the substrate decreases. Hassani *et al.* [102] found that when the particle and the substrate materials are similar, co-deformation of both materials occurs as a result of a similar degree of deformation. Figure 4-11 (b) indicates that the Cu particles in the field of view, experienced severe plastic deformation/flattening and did not

penetrate into the Ni substrate. This is due to the very large difference between the hardnesses of the Ni substrate and the Cu particle (about 280 HV), preventing the mutual plastic deformation. In Fig. 4-11 (c), it can also be observed that craters were generated on the Ni interlayer as the particles were rebounded off from the Ni interlayer. These results suggest that particle impact energy was transferred to the extreme and moderate levels of plastic deformation in the particle and the substrate, respectively.





**Figure 4- 10:** (a) SEM micrograph of Cu deposit on Sn interlayer by individual particle impact (b) and (c): EDS mapping SEM micrographs of the Sn interlayer after single particle impact cold spray



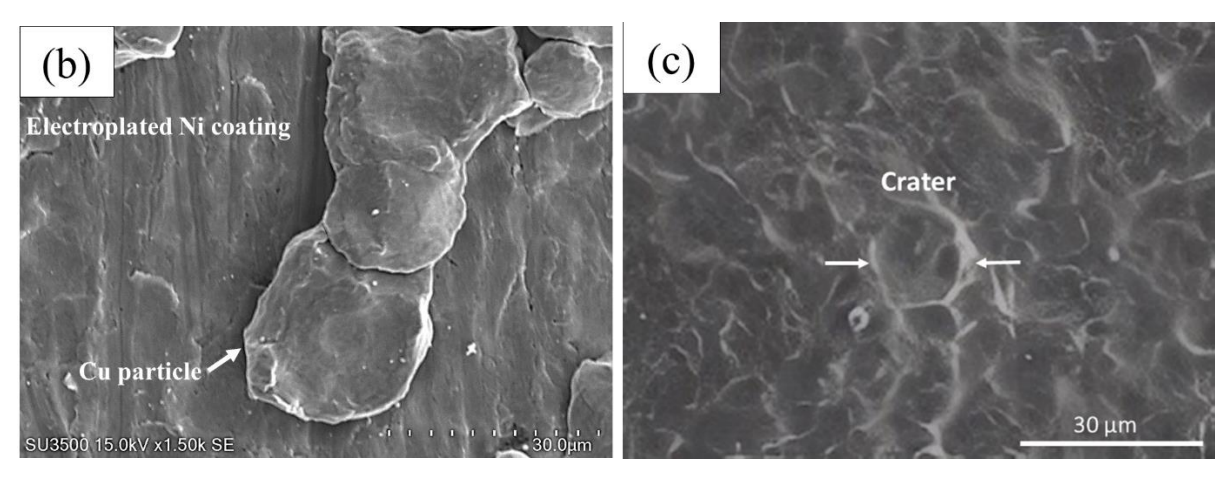


**Figure 4- 11:** SEM micrographs of the Cu deposits on (a) electroplated Cu interlayer and (b) electroplated Ni interlayer by an individual particle impact (c), and craters on the Ni interlayer surface

## 4.4 Discussion on the deposition behavior

In this study, it appeared that the Cu particles were penetrated into the Sn interlayer and did not experience significant plastic deformation (Fig 4-10). Interlayer erosion took place (Fig 4-4) as a result of the poor erosion resistant of tin. This indicates that adiabatic shear instability mechanism was not applicable when forming a coating on a Sn interlayer. Therefore, other mechanical properties such as substrate susceptibility to erosion, may also control and affect the deposition process. For the Cu interlayer, deposition was possible through the co-deformation

mechanism (Fig 4-11 (a)). This was due to the Cu interlayer having similar hardness as the Cu particle, allowing for metallurgical/mechanical bonding. This signifies that a successful bonding can only be achieved if both particle and the substrate deform simultaneously.

Development of the second deposition layer was also possible, but with lower deposition efficiency when compared to the first layer. It was observed that the presence of the harder first deposited layer as compared to the Cu electroplated interlayer (nearly 45% harder), led to a decrease in DE from approximately 10% to 7% (30% lower DE). From the experimental results, it can be noticed that a greater number of impacting particles was likely rebounded off from the first cold sprayed layer, and fewer particles were available with sufficient kinetic energy to plastically deform upon impact. Hence, the DE decreased by approximately 30% after applying the second pass as compared to the first pass due to the increased hardness of the interlayer. In addition, there were no significant changes in DE with changes in pressure, i.e., the increase in pressure from 60 psi to 68 psi while spraying the second pass, would not have a significant effect on its DE.

For the Ni interlayer, as was observed in the single particle impact experiment (Fig 4-11 (b) and (c)), particle impact energy was mostly transferred to the deformation of the particle and slightly to the deformation of the substrate, generating craters on the Ni interlayer. The fabricated Cu coating was not well-adhered to the Ni surface, suggesting insufficient substrate deformation for bonding. Cold spray of metal on bulk metal substrate seems to be different from cold spray of metal on metallized CFRP substrates, since a higher DE was obtained on the Cu interlayer than that of steel substrates.

Apart from the hardness effect, another major difference is the effect of thermal conductivity. The CFRP substrate underneath the Cu interlayer functioned as a heat insulator due to its lower thermal conductivity than that of the steel substrate [89]. Therefore, softening of the electroplated Cu interlayer allowed for improving mechanical anchoring between the particle and the substrate and resulted in a greater DE. Finally, it is worth saying that relative hardness of the particle to the substrate is not the only influencing parameter in determining the DE and deposition behavior. Surface roughness, substrate erosion, interlayer thickness, and thermal conductivity property may also play a role and their contribution to the deposition characteristics needs to be further studied.

#### 4.5 Conclusion

Copper powder was cold sprayed onto various metallic interlayers such as Sn, Cu, and Ni through the individual particle impact and full coating fabrication. It was observed that cold spraying Cu on a Sn interlayer, resulted in particle penetration and coating fabrication was not possible due to the interlayer erosion. A thick and dense coating was successfully deposited onto a Cu coated CFRP under a two-pass gas pressures. However, the overall DE of the cold sprayed coatings was lower than that of the first deposited layer. In the second layer of deposition, particles impacted a harder substrate (i.e., first cold sprayed layer) as compared to the electroplated Cu coating.

FE simulations indicated that the increased hardness of the first cold sprayed layer resulted in higher strain energy and lower substrate penetration thereby hindering particle retention. Codeformation of the material couples was found to be the impact behavior of the Cu particle, allowing for the deposition to successfully take place during the first spray layer. Insignificant deposition (1% DE) was randomly obtained on the Ni interlayer, leaving craters on the substrate

surface. The presence of a very hard substrate relative to the particle led to the insufficient plastic deformation of the Ni interlayer and consequently poor adhesion of the coating to the substrate.

In the case of single particle impact, Cu particles were plastically deformed/flattened, and craters were also generated on Ni interlayer. In low-pressure cold spraying, coating formation is highly dependant on the relative deformability of the impacting particle and the substrate. As the hardness gradient of the material couples decreases, the possibility of the successful coating formation increases in low-pressure cold spraying.

## 4.6 Acknowledgements

The authors wish to acknowledge the financial support of the Natural Sciences and Engineering Research Council of Canada (NSERC) through the Green Surface Engineering for Advanced Manufacturing (Green SEAM) Strategic Network [grant number NETGP 493955-16]. In addition, the industrial partners, Bombardier Aerospace, is gratefully acknowledged. Dr. Phuong Vo from National Research Council Canada is acknowledged for his contribution to the cold spray experiments.

Chapter 5: Properties of Multilayered Metallic Coatings Deposited on Carbon Fiber-Reinforced Polymers (CFRPs) through Electrochemical and Cold Spray Processes

#### Preface

The previous chapters focused on the cold spray deposition of Cu particle onto an epoxy-CFRP and the effect of various interlayers on the deposition process. Successful deposition was obtained in case of a Cu interlayer due to the hardness similarity of the particle to the underlying Cu interlayer. Apart from the deposition that is required to obtain coating on a substrate, it is also necessary to study the properties of these multilayered metallic coatings. Thus, in this chapter, adhesion properties and microstructure of these coatings have been assessed.

# This chapter has been published as:

Panteha Fallah, Sima A. Alidokht, Phuong Vo, Richard R. Chromik, André McDonald, Stephen Yue, "Properties of Multilayered Metallic Coatings Deposited on Carbon Fiber-Reinforced Polymers (CFRPs) through Electrochemical and Cold Spray Processes", J. Therm. Spray Technol. (2022), https://doi.org/10.1007/s11666-022-01475-0. (Reprinted by permission from Springer Nature and licence to reuse in this thesis has been granted from Springer Nature)

#### **Abstract**

Previous studies have shown that copper (Cu) may be cold spray deposited on epoxy carbon fiber-reinforced polymers (CFRPs) if an interlayer Cu of electroplated on an electroless nickel (Ni)

coating is present prior to cold spraying. In this present study, the tensile adhesion bond strength of these multilayered metallic coatings was measured in accordance with ASTM Standard C-633-13. Fractured surfaces after tensile adhesion testing were examined by scanning electron microscopy (SEM) and optical microscopy (OM). Scratch adhesion testing from the polished cross-sections of the multilayered coatings was also performed to compare the results with those obtained from the tensile adhesion testing. The microstructure of the cold-sprayed and electroplated Cu coatings was analyzed by electron channeling contrast imaging (ECCI), and its correlation with hardness values was studied. Adhesive failure at the Ni coating/CFRP interface was observed in the absence of a cold-sprayed Cu coating. Enhanced bonding between electroless Ni coating and exposed carbon fiber areas was observed relative to the epoxy regions. This enhanced bonding was attributed to the increased roughness of the carbon fiber regions relative to the epoxy areas. However, after cold spraying with Cu, cohesive failure of the cold sprayed Cu coating occurred, which was likely due to insufficient plastic deformation of the particles cold sprayed close to the critical velocity of Cu. Electron channeling contrast imaging analysis from the cross-sections revealed uniform and inhomogeneous microstructures within the electroplated and cold-sprayed Cu coatings, respectively.

**Keywords:** Adhesive failure; Cohesive failure; Grain size; Microstructure; Scratch adhesion testing; Tensile adhesion bond strength

#### **5.1 Introduction**

Metallization of polymeric substrates such as carbon fiber-reinforced polymers (CFRPs) has gained significant interest in the aerospace industry over the past few decades. Carbon fiber-reinforced polymers are advantageous due to their high specific strength; however, they are more

electrically resistive than aluminum, limiting their applications [18]. Different coating methods are available for metalizing polymers, including physical vapor deposition (PVD) and chemical vapor deposition (CVD), but, with these techniques, only very thin films (below 100 µm) can be deposited on the substrates [63, 64, 115]. High-temperature thermal spray technologies, including wire arc spray, flame spray, and air plasma spray can be used to achieve thick coatings. However, thermal degradation of the polymeric structures and oxidation of metallic powders may take place during thermal spray processes [1, 8, 66, 67].

Cold spraying uses relatively lower temperatures (below the melting point of the sprayed material) as compared to other thermal spray techniques [116]. As a result, oxidation of metallic powders, accumulation of tensile residual stress and damage to the heat-sensitive materials, such as polymeric substrates, are minimized [65]. In this solid-state deposition process, particles are accelerated to a high velocity (ranging from 500-1200 m/s) through a converging-diverging nozzle onto a substrate to form a dense metallic coating [26].

In cold spraying metallic powders onto metallic substrates, bonding between the particles and the substrate occurs through metallurgical bonding and/or mechanical interlocking [117]. However, cold spraying metallic powders onto polymeric substrates and polymer-based composites is challenging due to their poor erosion resistance, limiting coating formation and growth on these substrates [12]. Thermoplastic substrates are more amenable to cold spraying as they have better ductility than brittle thermosets, allowing for particle embedding (mechanical interlocking) as opposed to the brittle fracture and erosion of the thermosetting substrates [13]. Thus, bonding between metallic powders and the polymeric substrate is achieved by mechanical interlocking.

Polymeric substrates and polymer-based composites have been successfully cold sprayed with a variety of metallic powders such as tin (Sn) [12], iron [60], aluminum [118], copper [119] and 316L stainless steel [120]. However, these coatings showed some issues related to the delamination/insufficient coating adhesion [119], low deposition efficiency (DE) and substrate damage and erosion that have limited further coating growth [69].

In previous studies [4, 13, 70, 121], the adhesion/cohesion properties of the cold-sprayed coatings deposited on a polymeric substrate were found to be relatively low (below 30 MPa) when compared with a coating cold-sprayed on metallic substrates. It was reported that soft metallic powders such as Sn can be cold-sprayed on thermosetting epoxy-CFRP through the "crack filling" mechanism. It was hypothesized that partially melted or thermally softened particles impact the substrate, and the solid core of the particle generates microcracks which were subsequently filled by the molten part of the Sn particle, allowing for mechanical interlocking [12]. However, Che et al. [13] and Liberati et al. [122, 123] reported low adhesion/cohesion bond strength of tin (Sn) and Sn mixed with different secondary metallic powders cold-sprayed onto a variety of CFRP substrates with different surface finishes (bond strength was varied from 2 MPa to 20 MPa). They observed the full range of failure types (adhesive, cohesive and a mixture of adhesive-cohesive) depending on the sprayed material, spray condition, and the CFRP surface characteristics. Ganesan et al. [70] obtained shear adhesion strengths below 3 MPa when cold spraying Cu onto a polyvinyl chloride (PVC) substrate. Małachowska et al. [14] achieved an adhesion strength of only 3.6 MPa for cold-sprayed Cu coating deposited onto polyamide 6 substrates at a gas pressure of 0.9 MPa. Rezzoug et al. [124] modified the CFRP surface with various interlayers (aluminum mesh layer) and fillers (pure copper and a mixture of copper and stainless-steel powders) before spraying zinc via the wire-arc spray technique. They found that surface modification greatly affected adhesion

bonding between the coating and the modified substrate. In the case of pure Cu filler, adhesion strength was not improved due to the smooth topography of the substrate after applying the Cu powder filler which was measured to be 2.7 MPa. Stainless-steel powders mixed with Cu powder led to the generation of a rougher surface finish as compared to that of pure Cu powder filler due to the irregular morphology of stainless-steel powder. As a result, mechanical interlocking was enhanced, and adhesion strength was 5.1 MPa. In the case of the aluminum mesh layer, the highest adhesion was achieved and found to be 6.5 MPa.

There are two distinct deposition steps when cold spraying onto polymeric substrates: 1) first-layer deposition that occurs between the impinged metallic particles and the polymeric substrate, and 2) build-up that occurs between the metallic powders and the previously deposited particles [60]. Coating thickness growth is challenging in each deposition step due to the completely different properties of the substrates (polymeric surface vs. the first layer of metallic coating). Barletta *et al.* [69] successfully cold-sprayed Cu onto a thermoplastic (PA66) substrate for various cold spray exposure times. They found rapid coating growth initially (from 0 to 6s) through the embedding of the Cu particles into the polymeric substrate. However, coating deposition slowed down after fabrication of the very first metallic layer, because Cu particles impacted on a much harder substrate (Cu coating) as compared to the soft polymeric substrate, preventing further coating growth.

Fabrication of metallic interlayers onto an epoxy-CFRP substrate prior to cold spraying Cu was proposed recently to avoid substrate damage, increase DE and enhance bonding formation [105]. The presence of a Cu interlayer with an almost similar hardness as the Cu powder permitted mutual plastic deformation of both material couples, likely allowing for successful cold spray deposition [125]. This study aims to evaluate and understand the adhesion/cohesion properties and

microstructure of the multilayered metallic coatings fabricated in a previous study [105] onto a CFRP substrate through tensile and scratch adhesion testing and electron channeling contrast imaging (ECCI), respectively. The CFRP substrate was first metallized with an electroless Ni (EN) coating to enable the fabrication of a subsequent interlayer through electroplating of a 100 µm Cu coating followed by cold spraying Cu at various gas pressures of 60 to 68 psi. Top and cross-sectional SEM images of the cold sprayed Cu coatings have been presented elsewhere [105]. The configuration of multilayered metallic coatings is abbreviated as EN-Cu<sub>1</sub>-Cu<sub>2</sub>, where EN refers to the electroless Ni coating, Cu<sub>1</sub> is the electroplated Cu coating, and Cu<sub>2</sub> is the cold-sprayed Cu coating.

# **5.2 Experimental Methodology**

# 5.2.1 Materials, Metallization Steps, and Conditions

Oxygen-free Cu powder (PG-PMP-1012, Plasma Giken Co., Ltd., Saitama, Japan) was used as the feedstock powder. Its characteristics were examined previously [105] and are summarized in Table 5-1. The particle size of the Cu powder was assessed using a laser scattering particle size analyzer (LA-920, Horiba, Japan), and the distribution has been presented elsewhere [105]. A scanning electron microscope (SU 3500, Hitachi, Japan) was used to obtain images of the Cu powder particles from the top and cross-section views (see Fig 5-1). The Cu powder was nearly spherical, and its average particle size ( $D_{50}$ ) was 18.9  $\mu$ m, where 50% of the particles were smaller than 18.9  $\mu$ m.

**Table 5-1:** Properties of the feedstock Cu powder

Powder	Morphology	Supplier	D <sub>50</sub> , μm	Microhardness, HV <sub>0.01</sub>
Cu	Nearly spherical	Plasma Giken	18.9	$65 \pm 8 \ (n=7)$

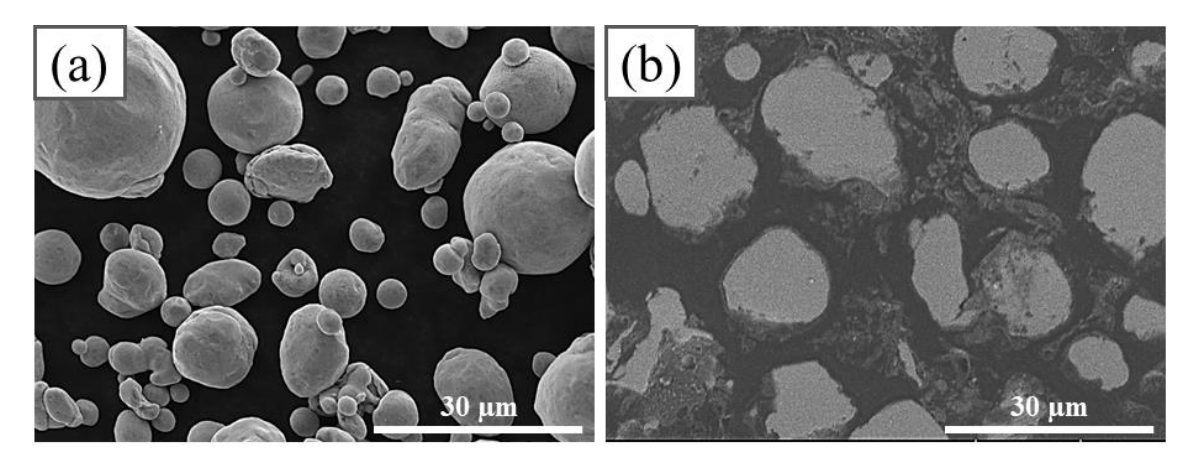


Figure 5- 1: SEM images of the feedstock Cu powder from (a) top and (b) polished cross-section views

The substrate materials used in this study were epoxy-CFRPs, fabricated by Bombardier Aerospace (Montreal, Canada), consisting of a thermosetting epoxy matrix with continuous carbon fiber reinforcements. The CFRP panels were made of four plies of 5276-1/G30-500 epoxy carbon prepreg ([0/90]2s). The CFRP substrates were 1.7 x 1.7cm<sup>2</sup> with a thickness of 1.7 mm and were degreased with methanol prior to coating.

CFRP substrates were first activated by palladium (Pd) particles to accelerate the chemical reactions occurring in the subsequent EN deposition. A Ni-coated CFRP with 5  $\mu$ m coating thickness was then electrodeposited with Cu to achieve a 100  $\mu$ m Cu coating. The metallization process has been extensively described in a previous study [105].

Cold spray of Cu at low pressure was conducted with a commercially available cold spray system (KM CDS 2.2, Inovati, Santa Barbara, CA, USA). The cold spray process parameters for

Cu-coated CFRP substrates are listed in Table 5-2. Only one pass was sprayed at each gas pressure, which ranged from 60 to 68 psi. A step size of 1 mm (20 steps) was selected, and the feeding rate was measured to be  $10 \pm 2$  g/min for three measurements. The cold spray parameters were chosen based on the previously successful cold spay experiments with Cu-on-Cu interlayer [105, 125].

Single pass cold spray experiments were conducted three times for each gas pressure (n = 3) and the corresponding standard deviations were reported to be relatively small (i.e., approximately 1%) [105].

Table 5- 2: Cu cold spray parameters for Cu coated CFRP substrates

Powder	Corrier and	Gas temperature,	Gas pressure, psi	Stand-off	Nozzle travel
rowdei	Carrier gas	°C	(MPa)	distance, mm	speed, mm/s
Cu	$N_2$	482	60 (0.41), 65 (0.45),	35	25
Cu	1N2	462	68 (0.46)	33	23

# 5.2.2 Coating Properties and Characterization

The coating adhesion/cohesion bond strength was evaluated by means of a tensile adhesion (i.e., "pull-off") test performed on coated CFRP samples after each metallization step, according to ASTM standard C-633-13 [126]. The modified testing required sectioning (Delta Abrasimet, Buehler, Illinois, USA) of the CFRP samples into square specimens of 1.7 x 1.7 cm². In this modified testing standard, the square specimens covered most of the circular surface area, thus leading to a nominal stress distribution difference with that of the circular test. A similar modification to ASTM standard C-633-13 has been made by other researchers for various cold-sprayed coatings on CFRP substrates [12, 121, 122]. Although the ASTM standard C-633-13 is applicable for coatings with thickness greater than 380 μm, thin layers of "dense" coating can be

tested satisfactorily. Observations from the cross-sections of all the coatings suggested the formation of dense and uniform coatings [105]. Therefore, this adhesion method has been used for testing thin coatings in this study.

The coating surfaces were then ground using #2000 grit SiC polishing papers to remove any loose particles that remained from the cold spray process.

A room temperature curing epoxy adhesive (J-B weld original cold weld, USA) was used to bond the coated specimens between two steel cubic blocks of 1.7 x 1.7 cm<sup>2</sup> with a height of 1cm, which was machined on a 2.54 cm cylindrical steel blocks (see Fig 5-2). A 'room temperature' curing adhesive was selected to avoid the occurrence of any possible thermal degradation to the heat-sensitive epoxy-CFRP substrate. The modified design of the counter blocks allowed for more accurate measurements as falling glue from the sample sides can be controlled. When the epoxy adhesive was completely cured, the coating was pulled off using an MTS servo-hydraulic pressure machine at a constant crosshead speed of 1.0 mm/min. The strength of the adhesive, that is the strength at which the adhesive fails, was measured by performing an adhesion strength test on the two steel blocks joined with the cured glue.

The fractured surfaces were then characterized with a digital microscope (VHX-5000, Keyence, Japan) and an SEM. For each coating condition, three measurements were performed, and the average strength was reported.

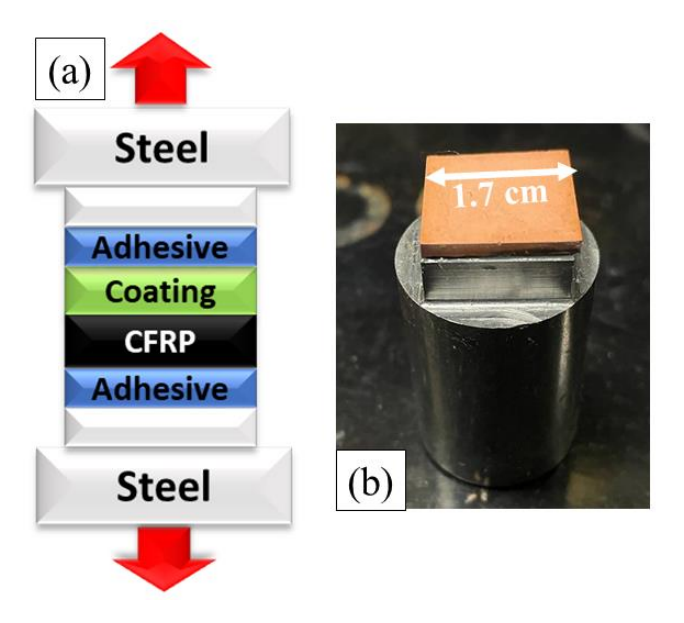


Figure 5- 2: (a) Adhesion strength testing setup and (b) machined steel block

Scratch adhesion testing was performed according to ISO 27307 [127] to qualitatively characterize the bond strength of the multilayered metallic coatings using a scratch tester (Micro-Combi, Anton Paar, Switzerland). In this test, a Rockwell diamond stylus was drawn across the polished cross-section of the coatings, starting in the substrate and ending in the cured resin. The applied normal load, speed and scratch length were 0.2 N, 3.5 mm/min, and 0.5 mm, respectively. The scratch parameters were chosen based on the previously scratch testing for Cu coating [128]. Scratches were then examined by SEM to identify the failure mechanism and possible inter-splat decohesion. A qualitative-quantitative comparison was then made from both tensile and scratch adhesion testing.

A cold field emission SEM (SU 8230, Hitachi, Japan) with a photodiode backscattered electron (BSE) detector was used to analyze the CFRP surface after Pd activation to obtain a correlation between the distribution of the dispersed Pd nanoparticles onto a CFRP substrate, CFRP surface topology, and adhesion behavior of the EN coating to the CFRP. Compositional

analysis of the CFRP after Pd activation was conducted using Energy-Dispersive X-ray Spectroscopy (EDS) in the SEM. A 3D optical surface profiler (ZYGO, Connecticut, USA) was used to determine the surface roughness and topology of the CFRP substrate before activation treatment to study the effect of CFRP surface topography on the dispersion behavior of the Pd particles over the entire CFRP surface.

Microstructural observations were performed on the polished cross-sections of the coatings to reveal the grains and deformed structures of the coatings. Cross-sections of the coatings were cold mounted, mechanically grounded, and polished using 9, 3, and 1 µm diamond pastes followed by 0.05 µm colloidal silica. The morphology and microstructure of the initial Cu powder, deposited and cold sprayed Cu coatings were revealed by Electron Channeling Contrast Imaging (ECCI) using a cold field emission SEM (SU-8230, Hitachi, Japan) with a photodiode backscattered electron (BSE) detector. The accelerating voltage was in the range of 5-10 keV, and the working distance varied from 8 to 10 mm. A correlation between the microstructure and the measured hardness of the coatings was then explored. An image analysis software (ImageJ) was used to measure the grain and particle sizes.

## **5.3 Results**

## 5.3.1 Tensile Adhesion/Cohesion Bond Strengths

The adhesion strength results of the deposited coatings after each metallization step are shown in Fig 5-3. Electroless Ni coating, electroplated and cold-sprayed Cu coatings fabricated on CFRP substrate are abbreviated as EN, Cu<sub>1</sub>, and Cu<sub>2</sub>, respectively. From the cross-sectional SEM images of the multilayered coatings [105], the thickness of the cold sprayed Cu coatings increased

from approximately 90  $\mu$ m to 145  $\mu$ m by increasing the gas pressure from 60 to 68 psi [105]. The glue adhesion strength was determined to be 13 MPa.

In the adhesion strength test, the EN and EN-Cu<sub>1</sub> coatings failed at the EN/CFRP interface, indicating adhesive failure. No significant change in the adhesion bond strength of the EN and EN-Cu<sub>1</sub> coatings to the CFRP substrate was observed and their adhesion bond strengths were measured to be 6.85 psi and 6.38 MPa, respectively. The almost similar bond strengths were possibly due to the electroplating being performed at low 'intensity' process conditions of room temperature and a very low applied current.

After cold spraying Cu on the EN-Cu<sub>1</sub> layer, the adhesion strength test led to the failure of the cold-sprayed Cu coatings, indicating cohesive failure. The cohesion bond strength of the cold-sprayed Cu coatings slightly increased from 1.45 MPa to 2.45 MPa by increasing the gas pressure from 60 to 68 psi.

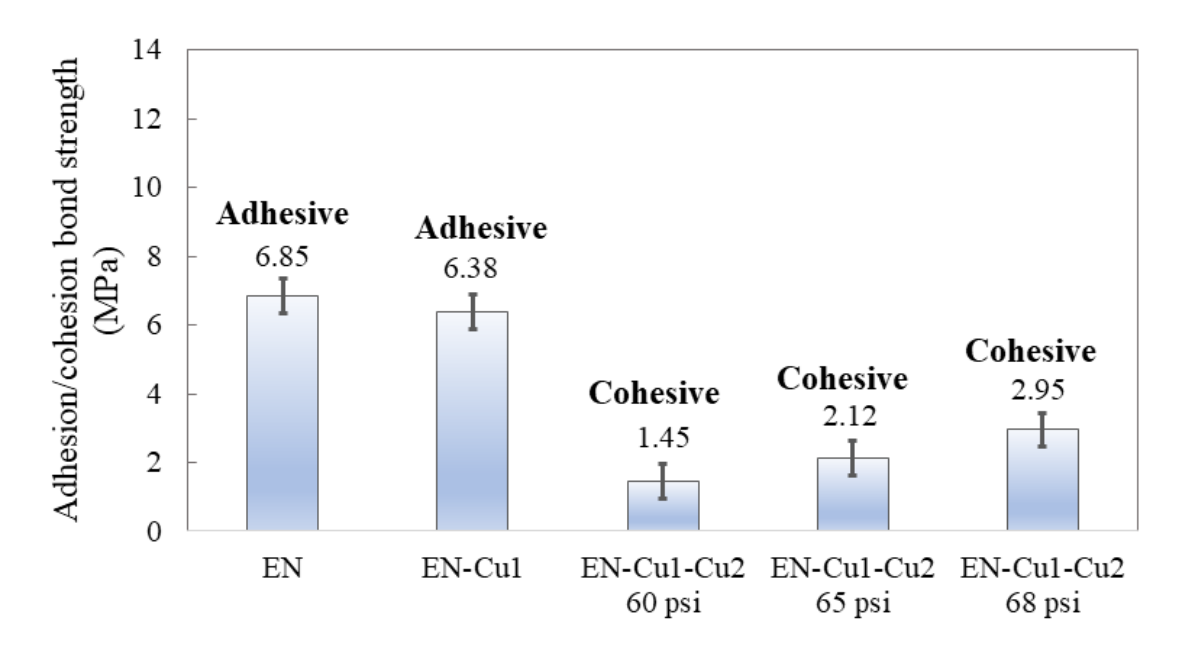


**Figure 5- 3:** Adhesion/cohesion bond strength of the coatings obtained after electroless Ni deposition (EN), Cu electrodeposition (EN-Cu<sub>1</sub>), and Cu cold spraying (EN-Cu<sub>1</sub>-Cu<sub>2</sub>) at three different gas pressures of 60, 65, and 68 psi

# 5.3.2 Characterization of fractured surfaces in the EN and EN-Cu<sub>1</sub> coating configurations

Figures 5-4 (a) and (b) show the OM images of the fractured surfaces in the EN and EN-Cu<sub>1</sub> coating systems where adhesive failure at the EN/CFRP interface occurred. It can be seen in Fig 5-4 (a) that damage to the epoxy took place in areas where the carbon fibers were exposed and a degree of roughening in these areas is noticeable. Figure 5-4 (b) shows the corresponding surface of the peeled EN coating, revealing the pattern of the underlying carbon fiber region.

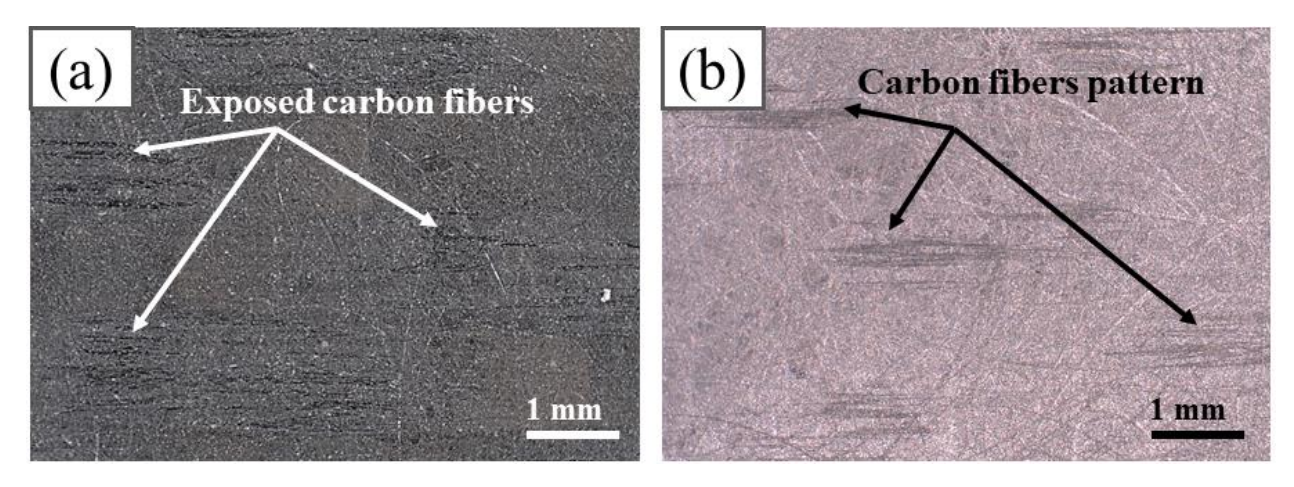


**Figure 5- 4:** Keyence digital microscope images of the (a) CFRP substrate and (b) backing surface of the EN coating after performing the adhesion strength test

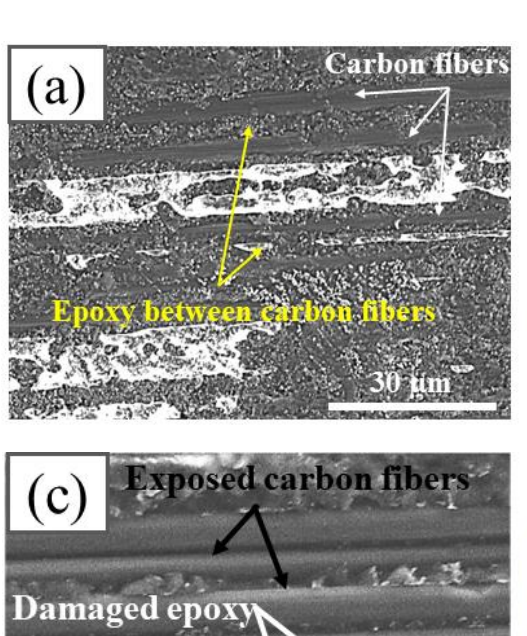
Figures 5-5 (a) and (b) show the top and cross-section views of the as-received CFRP, respectively. It can be seen in Fig 5-5 (a) that carbon fibers (shown by white arrows) are separated by epoxy regions (shown by yellow arrows) and from the cross-sectional OM image (Fig 5-5 (b)), areas rich in carbon fibers close to the top surface and others rich in epoxy polymer can be observed.

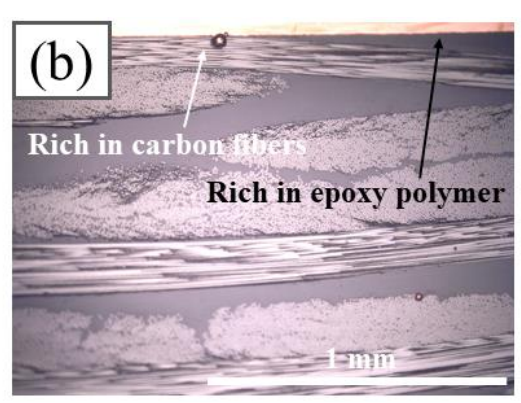
Further SEM characterization of the exposed carbon fiber areas was conducted after performing the adhesion test, and the corresponding SEM images of the fracture surfaces can be seen in Fig 5-5 (c-g). In Fig 5-5 (c), damaged epoxy in the carbon fiber regions was observed

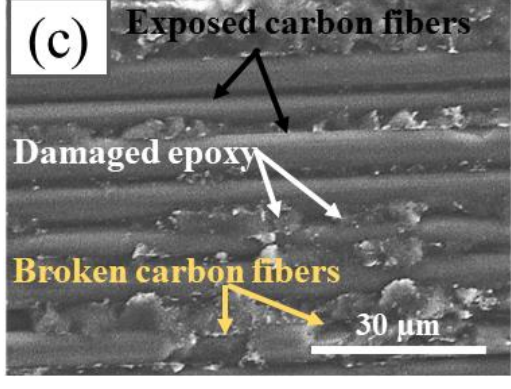
(shown by white arrows), leading to more visible exposed carbon fibers (shown by black arrows). A degree of discontinuity along the carbon fiber (i.e., broken carbon fiber) was also noticed, which is shown by the yellow arrows. Figures 5-5 (d) and (e) show the EDS map of the same area and the corresponding EDS results, respectively, confirming the presence of 96.1 wt% carbon and 2.6 wt% nickel. According to the EDS results, the bright spots in Fig 5-5 (c) are possibly the traces of the residual nickel, which is mostly observed in the grooves between the carbon fibers.

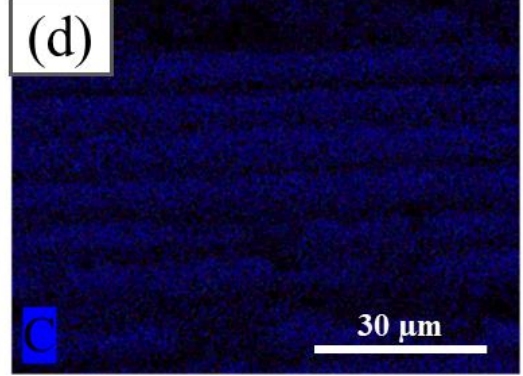
Figure 5-5 (f) shows the backside of the peeled EN coating which is complementary and corresponds to the pattern of the carbon fiber regions in Fig 5-5 (c). As shown in Fig 5-5 (f), linear smooth structures are the traces of the carbon fibers, and the rough area are the damaged EN coating. This result could suggest that EN coating has been mechanically interlocked in the grooves between carbon fibers where epoxy is present.

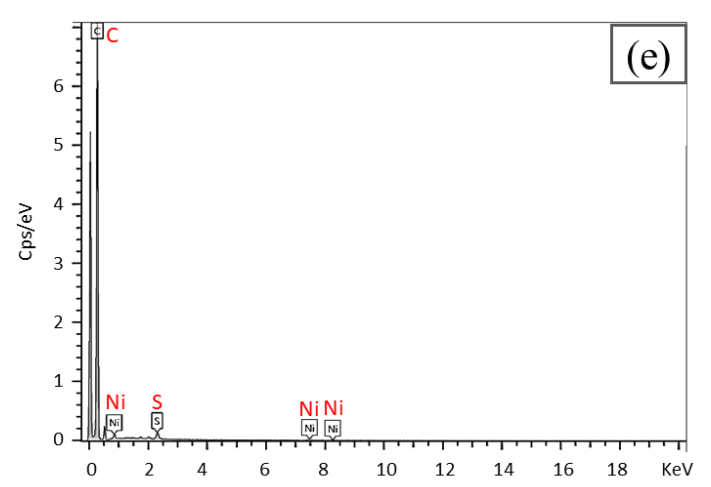
Figure 5-5 (g) shows the polished cross-section of the EN-Cu<sub>1</sub> coating deposited on the carbon fiber area of the CFRP substrate. Carbon fiber regions consisted of exposed carbon fibers and epoxy polymer between them. As shown, the EN-Cu<sub>1</sub> coating followed the surface profile of the CFRP substrate. A unique characteristic of the electroless deposition is that a uniform coating that follows the substrate surface topography can be achieved [56, 129]. Possible mechanisms affecting the adhesion properties of the EN coating to the epoxy-CFRP are explained in the following section 5.3.3.











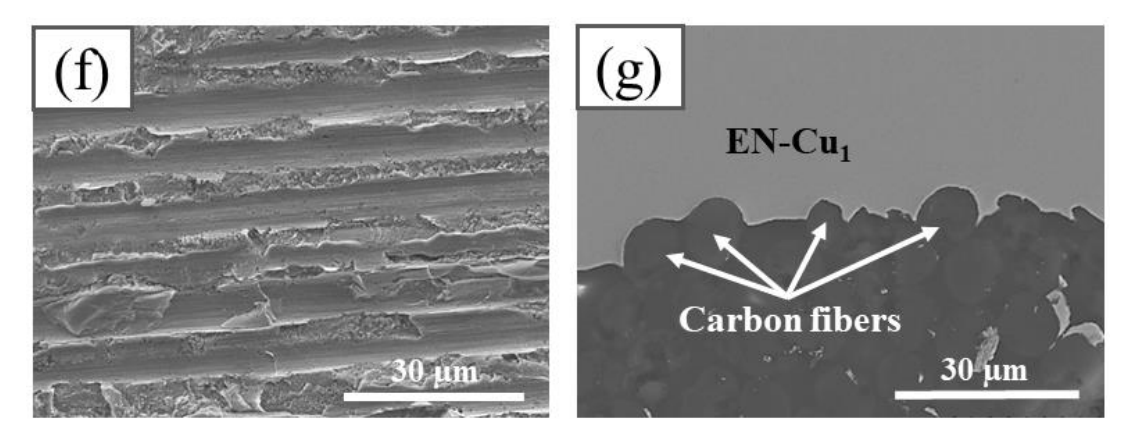


**Figure 5- 5:** (a) top and (b) cross-section views of as-received CFRP, (c) SEM image, (d) EDS map and (e) EDS results of the CFRP surface after the adhesion strength test. SEM images of the (f) peeled EN coating and (g) polished cross-section of the carbon fiber region of CFRP

# 5.3.3 Effect of CFRP surface characteristics on EN coating formation mechanisms

In the EN coating deposition of non-conductive surfaces (i.e., epoxy regions which constituted the majority of the CFRP surface), the first step after surface cleaning is surface catalysis by reducing Pd ions to Pd atoms from a colloidal solution containing PdCl<sub>2</sub> and SnCl<sub>2</sub> [78, 130, 131]. In this study, Pd particles were electrochemically activated on the heterogeneous surface features of the CFRP, containing regions of epoxy and carbon fibers. Figure 5-6 shows the SEM images of the CFRP surface after the Pd activation and the corresponding EDS results. As shown, Pd nanoparticles (bright spots) with an average particle size of  $45 \pm 5$  nm were distributed over the entire surface of CFRP, but with greater accumulation on exposed carbon fiber areas. The volume fraction of Pd particles was measured to be 15%. Catalytically active Pd nanoparticles act as nucleation seeds to initiate subsequent autocatalytic (self-reduction) chemical reactions occurring during electroless deposition. The catalysis, activation, and electroless deposition processes have been described previously [105].

Figures 5-6 (a) and (b) show the SEM images of the CFRP surface for two distinct regions of epoxy and carbon fibers, respectively. As shown, fewer Pd nanoparticles (indicated by the red arrows) are dispersed in the epoxy region as compared to the area with exposed carbon fibers. According to Fig 5-6 (b), Pd particles accumulate on both carbon fibers and the epoxy areas in between these carbon fibers. The preferential dispersion of the Pd nanoparticles on the carbon fiber regions might be attributed to the physical and chemical properties of carbon fibers and the inhomogeneous surface profile of the CFRP. It has been reported in the literature that carbon materials such as graphite, activated carbon, carbon fibers, and carbon nanotubes are common and suitable catalyst support materials for various chemical reactions. Carbon fibers have been found to be a promising support for the catalysis of noble metals such as Pd and Pt due to their large specific surface area, high porosity, excellent electron conductivity and chemical inertness [132]. The specific surface area of carbon fibers has been reported to be high, 1000-3000 (m²/g), which provides a high available surface area for accumulation of the active Pd metal atoms [133, 134].

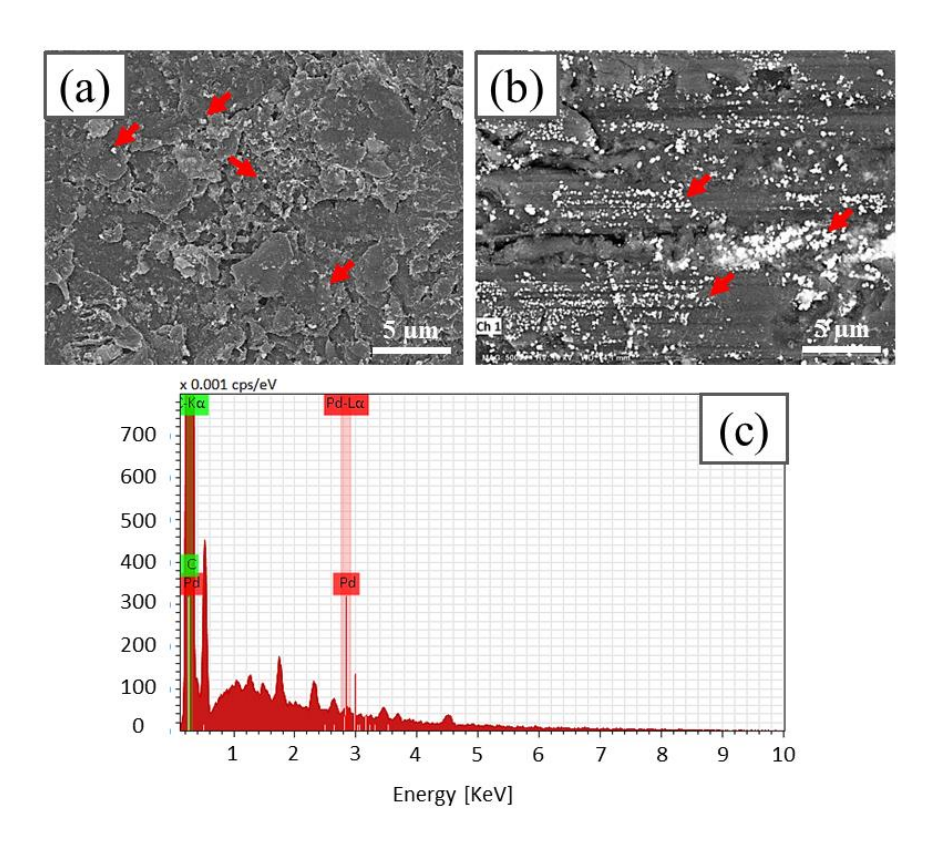


**Figure 5- 6:** SEM images of the CFRP after Pd activation in the (a) epoxy and (b) carbon fiber regions. (c) corresponding EDS data of the image (b).

(Note: bright spots in (a) and (b) indicate Pd particles which are shown by red arrows)

The observed damage to the epoxy in between the carbon fibers and inhomogeneous distribution of Pd particles could mainly be supported by the surface profile of the CFRP. The surface profile of the epoxy-CFRP substrate was characterized over an area of  $6008 \times 6008 \,\mu\text{m}^2$  to study a potential relationship between the substrate surface roughness, accumulation of Pd nanoparticles and the adhesion behavior of the EN coating. Figure 5-7 shows the surface profile of the CFRP substrate before Pd activation. As shown, epoxy areas (red regions) are at the same level in height; however, carbon fibers (green-yellow regions) have greater depth than the epoxy area and are separated by the epoxy polymer (red regions between green-yellow lines). The maximum height ( $S_z$ ) was measured to be 13.74  $\mu$ m which is the sum of the largest peak height

and the largest pit depth for the given field of view. The surface topology of the CFRP substrate would suggest two distinct regions of 'smooth' epoxy area and 'rough' carbon fiber regions. In previous studies [51], surface etching of the polymeric substrates using aggressive chemicals was attempted prior to Pd activation to introduce micropores on the surface and subsequently to enhance mechanical anchoring of Pd particles to the surface.

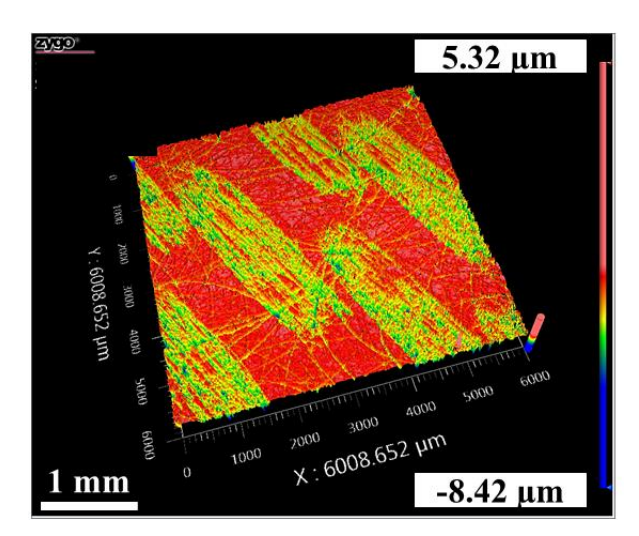


Figure 5-7: Height profile of the epoxy-CFRP substrate before Pd activation

Once the CFRP is activated by Pd particles, nucleation of Ni atoms mainly starts from the activated sites (Pd particles) followed by film growth during electroless Ni deposition [130]. Nickel ions adsorb onto the catalytic CFRP surface and reduce as a result of the oxidation reaction of the reducing agent (hypophosphite anion) to form a Ni-P film (see Eq. (1)) [76]. It is well-established that as-plated EN film is a metastable binary Ni-P alloy [135], formed by:

$$Ni^{2+} + 4H_2PO_2^- + H_2O \rightarrow Ni + 3H_2PO_3^- + P + H^+ + \frac{3}{2}H_2$$
 Eq. (1)

Figure 5-8 shows the spherical nodular SEM microstructures of the EN coating after 15 s, 1 min, and 15 min of deposition. After 15 s of deposition, when there were still gaps between the

particles (Fig 5-8 (a)), Ni particles with an average size of  $34 \pm 6$  nm nucleated and grew in the vicinity of previously dispersed active Pd particles (indicated by red arrows). Nickel islands were then uniformly distributed and formed on the catalytic surface until the catalytic sites were covered by the Ni particles. Since Ni itself is a catalyst metal, Ni ions can be continuously reduced to Ni atoms and deposited on the previously formed layer or fill the gaps between the islands. After 1 min of self-continuing chemical reactions, the isolated islands grew by joining the subsequent Ni particles through self catalytic effect, leading to the formation of a dense, homogeneous, and uniform nodular Ni-P film on the surface (Fig 5-8 (b)).

In Fig 5-8 (c), it can be seen that the EN coating was initially formed on the carbon fibers (shown by the white arrows), where greater Pd intensity was located. After 15 min of EN deposition, larger particles were formed through a lateral/vertical growth mechanism, leading to the formation of nodular microstructure, as has been reported previously [55].

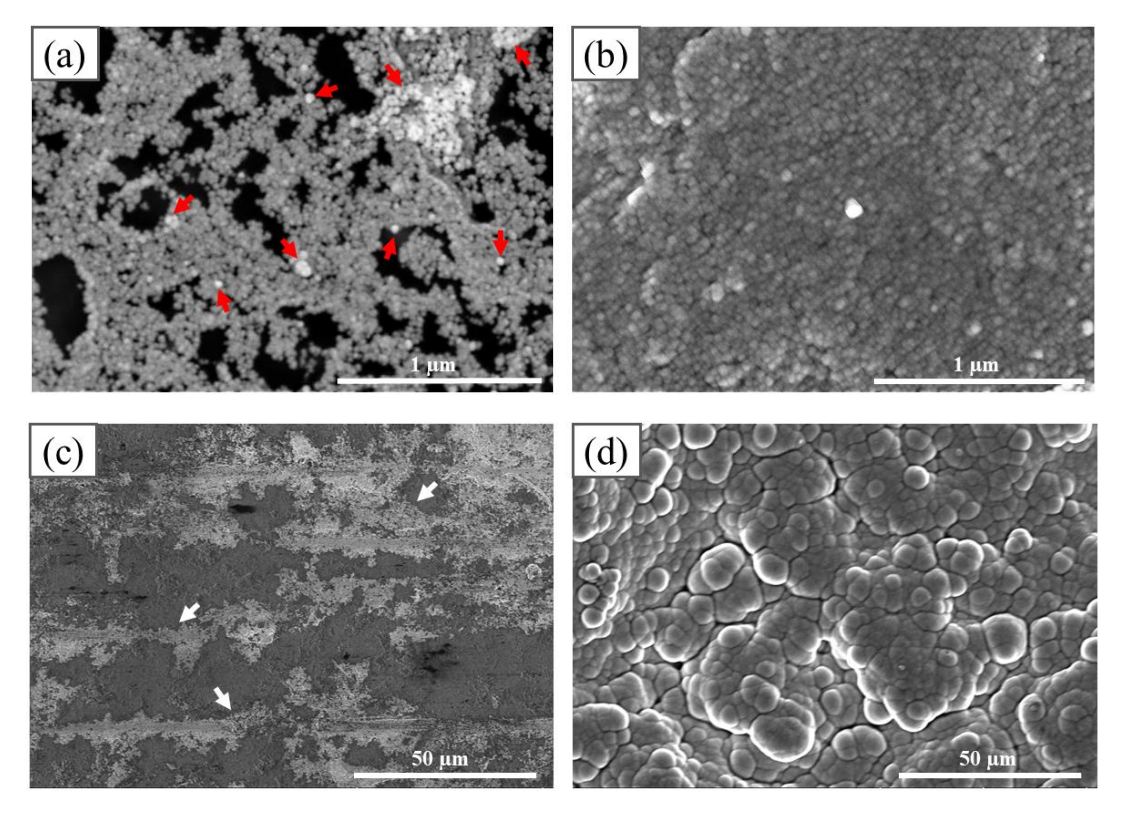


**Figure 5- 8:** High magnification SEM images of EN coating fabricated for (a) 15 s and (b) 1 min. Low magnification SEM images of the EN coating fabricated on carbon fibers after (c) 15 s and (d) 15 min. (Note: the red and white arrows indicate Pd particles and EN coating in (a) and (c), respectively)

# 5.3.4 Characterization of fractured surfaces in the EN-Cu<sub>1</sub>-Cu<sub>2</sub> coating configuration

Figure 5-9 shows the SEM observations of the backside of the removed coatings (a, b, and c) and of the corresponding remains of the Cu coatings (d, e, and f) cold-sprayed at 60, 65, and 68 psi, respectively. As shown, plastically deformed Cu particles are spread out over the surface and no dimpling of the surface is observed. No significant change in the splat diameter was apparent after varying the gas pressure due to the small gas pressure range, despite the slight increase in the cohesion strength of the cold-sprayed Cu coating, rising from 1.45 MPa to 2.95 MPa.

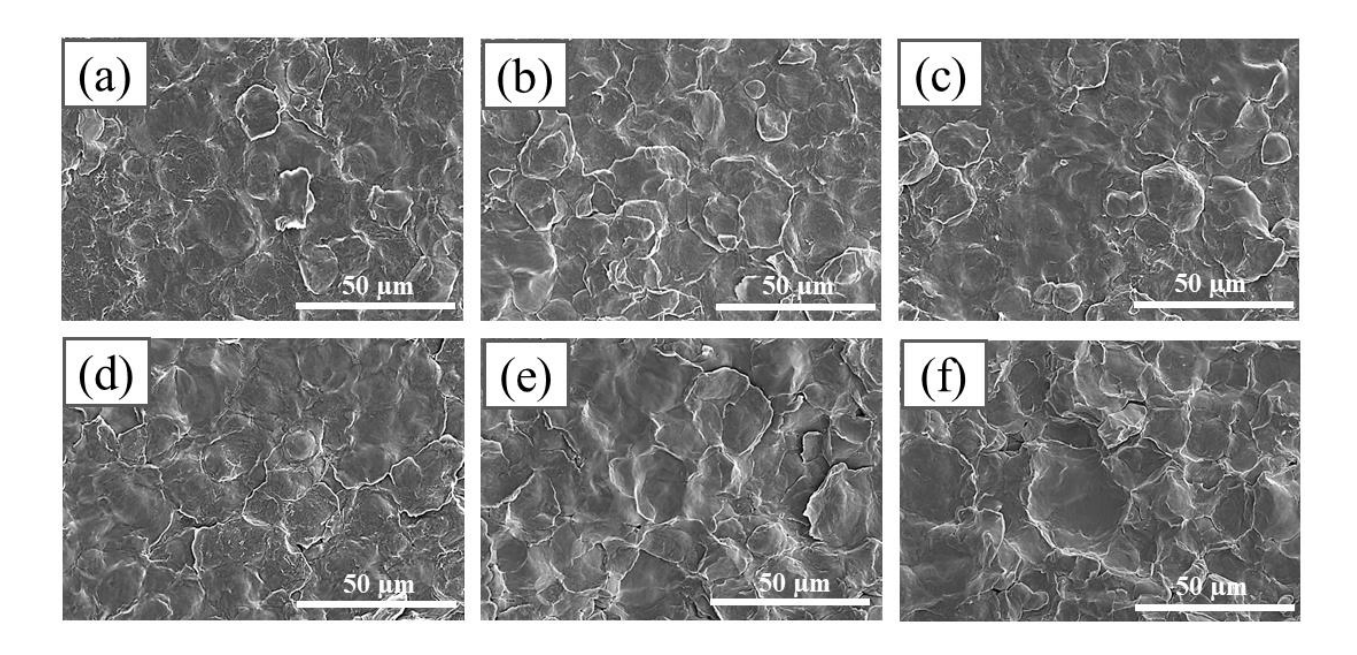


**Figure 5- 9:** (a-c) SEM images of the backside of the removed coatings and (d-f) corresponding remained Cu coatings cold-sprayed at 60, 65, and 68 psi, respectively

## 5.3.5 Scratch adhesion bond strength

Scratch adhesion testing was performed on cross-sections of the coatings. According to ISO/WD 27307, two types of failure can be generated as a result of scratch adhesion testing. The type of failure can be identified by observing the damage generated within/around the scratch track [136, 137]. Adhesive failure occurs when cracks are initiated and propagated at the coating/substrate or coating/coating interfaces and cone-shaped fracture occurs at the interfaces. In cohesive failure, cone-shaped fracture and crack generation take place in the coating [138].

For the scratch testing load used, there was no adhesive failure at the interfaces for all coatings. However, cone-shaped fractures and cracks occurred inside the cold-sprayed coatings, indicating the cohesive failure. Therefore, scratch testing was used to characterize cohesive failure mechanisms. Figure 5-10 shows the SEM and OM images of the scratch tracks obtained from the cross-sections of cold-sprayed and electroplated coatings at which the stylus was drawn starting

from the substrate towards the cold-sprayed coating. In Figs 5-10 (a) and (b), the presence of cracks within the cold-sprayed coatings indicates cohesive failure (shown by the white arrows). This type of failure (through crack generation) has been reported in previous studies for ductile coatings such as Cu [136].

Figures 5-10 (c) and (d) show the OM images of the cone-shaped fracture occurred in the cold-sprayed coatings. Cold-sprayed coatings showed almost similar projected cone areas, suggesting almost similar cohesion bond strength by increasing the pressure from 60 to 68 psi. The similarity of the cohesive failure behavior of these cold-sprayed Cu coatings was likely due to the small gas pressure difference. In addition, Cu flakes can also be observed within both cold-sprayed Cu coatings (Fig 5-10 (a) and (b)), which might be an indication of particle decohesion in this region. In this case, the damage was transferred to the material adjacent (shown by red arrows) as a result of the particle decohesion.

No cracks were observed at the electroplated/cold-sprayed interface for both coatings sprayed at 60 and 68 psi gas pressures. An improved bonding at the Cu<sub>1</sub>/Cu<sub>2</sub> interface is likely due to the hardness similarity of the particle to the underlying electroplated coating that allowed for mutual plastic deformation of both material couples, resulting in an enhanced mechanical/metallurgical bonding [105, 125]. In this stage, the very first layer of particles adheres to the substrate and determines the adhesive strength of the coating to the substrate. In Figs 5-10 (e) and (f), no sign of failure was observed within the electroplated coatings, neither on the scratch track nor on the surrounding.

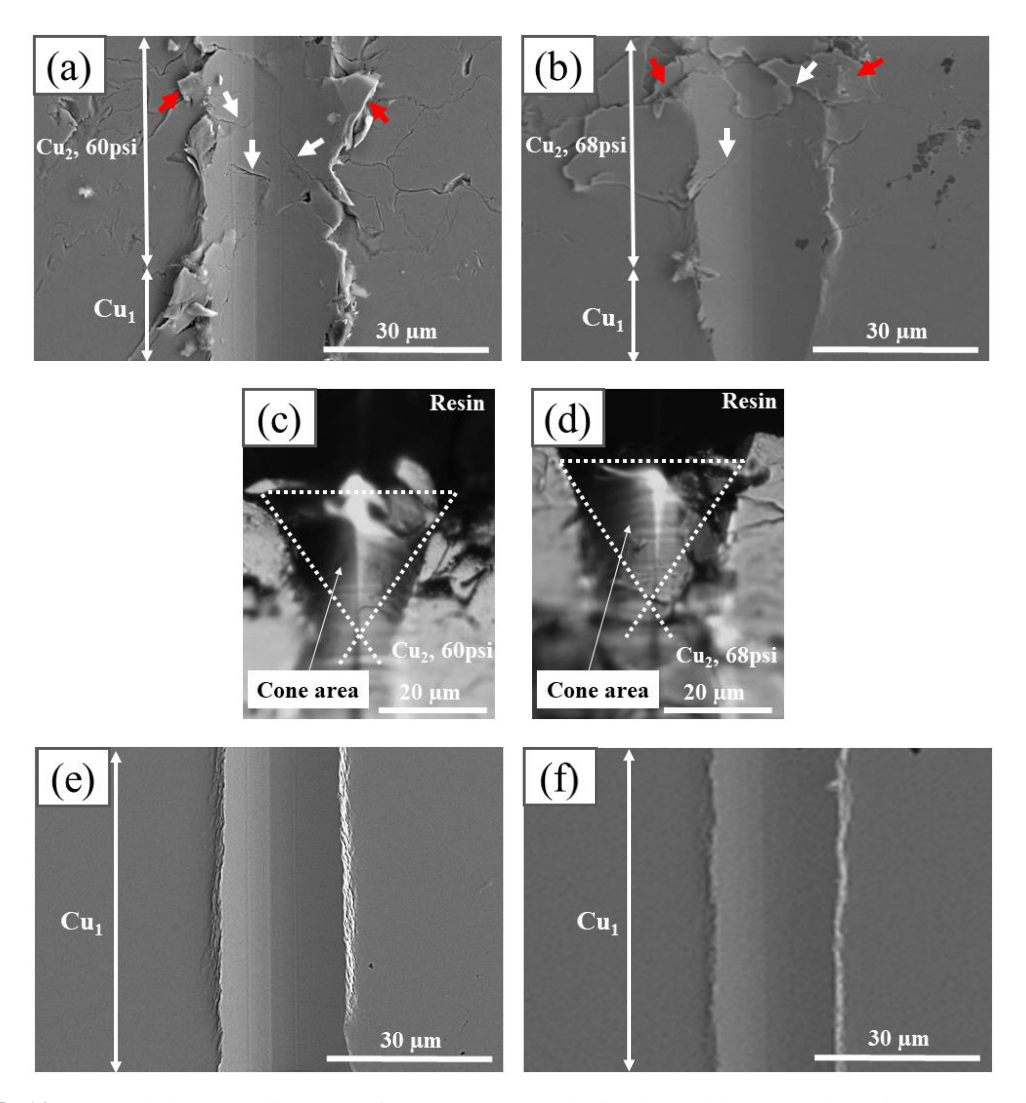


**Figure 5- 10:** (a) and (b) SEM images of the scratch tracks in the cold-sprayed coatings, (c) and (d) OM images of the cone-shaped fracture in the cold sprayed coatings, (e) and (f) SEM images of the scratch tracks in the electroplated regions after cold spraying at 60 and 68 psi, respectively

# 5.3.6 Microstructure analysis

ECCI was performed on cross-sections of the feedstock Cu powder, electroplated, and cold-sprayed Cu coatings to reveal initial and deformed microstructures. Figure 5-11 shows the ECC images of the cross-sectioned Cu powder with low and high magnifications. As is shown, the grain structure of the Cu powder reveals an equiaxed grain microstructure with a grain size ranging from 1 to 4  $\mu$ m with an average grain size of 2  $\pm$  1  $\mu$ m (Fig 5-11 (b)).

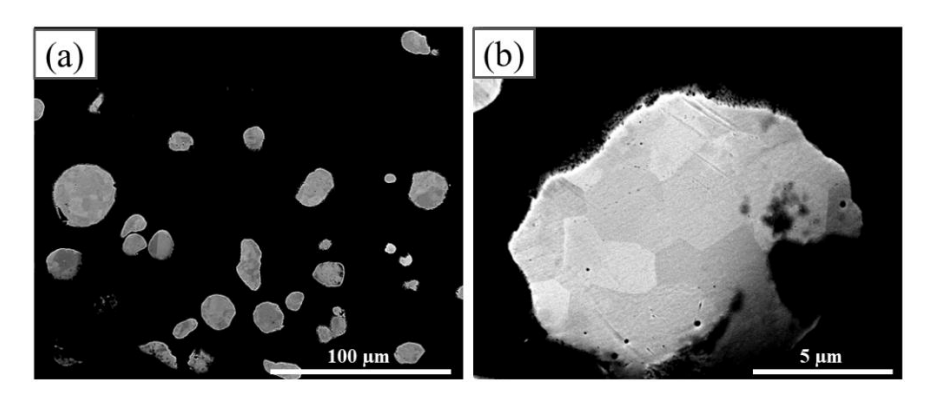


**Figure 5- 11:** ECCI micrographs of the cross-section of the feedstock Cu powder with (a) low and (b) high magnifications

Figure 5-12 illustrates the ECC images of the cross-sectioned Cu coatings electroplated (Fig. 5-12 (a)) and cold-sprayed at pressures of 60 and 68 psi (Fig 5-12 (c) and (e), respectively). Figure 5-12 (b), (d), and (f) are the enlarged views of the rectangles indicated in Fig 5-12 (a), (c), and (e), respectively. A more uniform microstructure was observed for the electroplated Cu coating compared to the cold-sprayed Cu coatings. For electroplated Cu coating, the average grain size was  $900 \pm 150$  nm. However, inhomogeneous microstructures were observed for cold-sprayed Cu coatings fabricated at 60 and 68 psi gas pressures. For both cold-sprayed Cu coatings (Fig 5-12 (c) and (e)), the microstructure near the splat interfaces is fine-grained, indicating the occurrence of dynamic recrystallization [31, 139], while a coarser structure can be observed in the central area of the particles (fine and coarse sub-structures are indicated by yellow and white arrows, respectively.) For the cold-sprayed Cu coating fabricated at 60 psi (Fig 12 (c)), the average grain size of the refined and coarse structures was  $217 \pm 75$  nm and  $700 \pm 270$  nm, respectively, which is significantly lower than that of feedstock Cu powder ( $2 \pm 1 \mu m$ ). By increasing the pressure from 60 to 68 psi, a decrease in the average grain size of the two sub-structures was obtained. For the cold-sprayed Cu coating fabricated at 68 psi (Fig 12 (e)),  $530 \pm 170$  nm and  $160 \pm 60$  nm were the average grain size of the coarse and refined structures, respectively.

It should be noted that combining ECCI and EBSD analysis may lead to a better understanding of the dynamic recrystallization and crystallographic orientation of materials which will be studied in a future work.

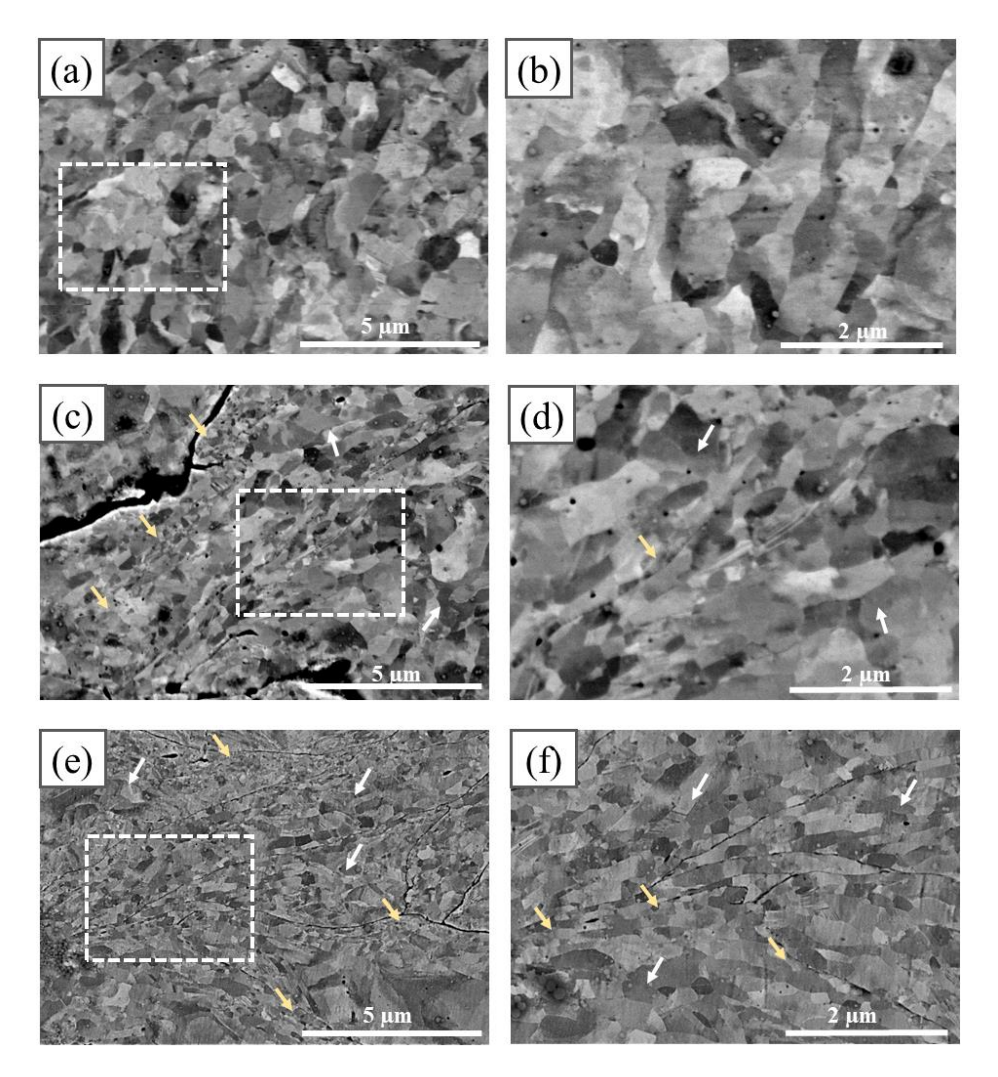


**Figure 5- 12:** ECC images of cross-sections of (a) Cu electroplated coating, (c) and (e) Cu coatings sprayed at 60 and 68 psi, respectively. (b), (d), and (f) are enlarged views of the white rectangles in (a), (c), and (e), respectively. (Note: the impact direction of the Cu powder is from top to the bottom)

### **5.4 Discussion**

## 5.4.1 Adhesion/Cohesion Bond Strengths of Multilayered Coatings

The primary influencing features observed in the fractured surfaces for the EN and EN-Cu<sub>1</sub> coatings were exposed carbon fibers and the associated epoxy regions. Damaged or removed epoxy in areas where exposed carbon fibers were present and locally broken carbon fibers (Fig 5-5 (c)) indicate an enhanced mechanical bonding between the EN coating and the carbon fiber areas relative to the pure epoxy region. Inhomogeneous surface topology of the CFRP (i.e., the presence of "rough" carbon fiber regions and "smooth" epoxy area) may possibly affect the overall adhesion strength of the Ni coating to CFRP. However, it is not possible to investigate the contribution of these two surface features as the tensile adhesion test is being conducted on a certain surface area that includes both epoxy and carbon fiber regions. Therefore, the measured adhesion strength is a result of contributions of both surface features.

The presence of peaks and valleys on the exposed carbon fiber regions relative to the smooth epoxy area where carbon fibre is not exposed, allowed for an enhanced anchoring of Pd nanoparticles to micropores of the carbon fiber regions and the subsequent enhanced mechanical bonding between the EN coating and these areas (Fig 5-6 (a) and (b)). The little-observed presence of Ni (Fig 5-5 (c)) on the CFRP surface after the adhesion test indicated that the bonding between EN coating and CFRP is mostly adhesive. These results suggest that the adhesion by mechanical anchoring between the EN coating and the CFRP could be enhanced by increasing the areal fraction of exposed carbon fibres.

After cold spray deposition of Cu at 60 to 68 psi, weak cohesion strengths were obtained in the Cu<sub>2</sub> part of the EN-Cu<sub>1</sub>-Cu<sub>2</sub> coating configuration (Fig 5-3). Fractured surfaces (Fig 5-9) showed no dimpling of the surface, indicating a lack of metallurgical bonding between the

deformed particles, thus leading to cohesive failure within cold-sprayed coatings for all gas pressures. It was previously reported that the velocity of Cu particles sprayed at 60 to 68 psi was close to the critical velocity of Cu (on the order of 500 m/s) [38, 125]. Weak inter-particle bonding is likely attributed to the low kinetic energy of the particles sprayed close to this velocity. However, applying higher gas pressure than 68 psi and temperatures higher than 482 °C was not possible in this study due to the observed coating delamination [105]. Delamination was hypothesized to be due to the insufficient coating adhesion to the CFRP substrate, and thermal stress being introduced to the coating because of the difference in thermal expansion coefficient. There are several ways to increase the adhesion bond strength of the coating to the polymeric substrates such as chemical, mechanical and plasma treatments of the substrate before the metallization step [140]. It would be expected that microscopic voids, peaks and valleys would be generated on the surface, promoting the mechanical anchoring between the metallic coating and the polymeric substrate. Another method to tackle delamination would be to increase the interlayer thickness to enhance energy absorption and facilitate heat dissipation.

From scratch adhesion testing, it was found that for the given scratch condition, the obtained results correlate with those obtained from the tensile adhesion testing (Fig 5-10). Note that both tensile and scratch testing conditions may affect the failure mechanism behavior of the coatings. In a previous study [138], a direct correlation between the results obtained from scratch and tensile adhesion testing was not obtained and the type of failure for the same coating was different when both methods were employed. However, scratch testing is a practical, efficient, and quick method to identify the type of bond strength (adhesive/cohesive) that can be used as a supplement to ASTM Standard C-633-13 adhesion testing.

## 5.4.2 Coating Microstructure

As observed in the ECC images of the coatings (Fig 5-12), the non-uniform microstructure within cold-sprayed coatings is associated with an inhomogeneous plastic deformation of the cold-sprayed Cu particles. In cold spray, particle interfacial regions experience more severe plastic deformation, strain rate, and associated temperature rise, resulting in recrystallization and an inhomogeneous coating microstructure [31, 141]. In a recent study [125], the temperature profile of the Cu particle impacted onto a Cu interlayer at a gas pressure of 65 psi was analyzed and reported using finite element simulation. The temperature profile of the impacted Cu particle revealed an increase in temperature from 200°C (central region of the particle) to 700°C (particle interfacial region), leading to an inhomogeneous degree of recrystallization within the particle.

A decrease in the grain size of the cold-sprayed coating by increasing the pressure is attributed to the higher degree of plastic deformation and increase in dislocation density. Similar microstructural features have been reported for cold-sprayed coatings [31, 139, 142]. In a previous study [105], the microhardness of the feedstock Cu powder, electroplated and cold-sprayed Cu coatings were measured and reported. The copper powder had a microhardness of  $65 \pm 5$  HV, which was lower than that of cold-sprayed Cu coatings. The average microhardness of the cold-sprayed Cu coatings fabricated at pressures of 60 and 68 psi was found to be  $100 \pm 5$  and  $118 \pm 5$  HV, respectively. An increased microhardness of the cold-sprayed Cu coatings relative to the Cu powder is related to the extensive plastic deformation, increased dislocation density, and grain refinement [143]. An increased microhardness of the coating cold-sprayed at 68 psi compared to that of 60 psi is due to the more severe plastic deformation and consequently smaller average grain size of both sub-structures. It can also be found that the smaller average grain size of the cold-

sprayed coatings as compared to the electroplated Cu coating led to an increase in the hardness of the cold-sprayed coating relative to the electroplated coating (75 HV vs. 100 and 118 HV).

### **5.5 Conclusion**

The adhesion/cohesion bond strength of multilayered metallic coatings fabricated onto CFRP substrate was studied through tensile and scratch adhesion testing, and fracture surfaces characterization. The results indicated that failure was almost completely adhesive at the EN/CFRP interface in the EN and EN-Cu<sub>1</sub> coatings. Damaged epoxy and broken carbon fibers indicated enhanced mechanical anchoring between the EN coating and carbon fiber regions. This enhanced bonding was possibly due to the increased roughness leading to the large accumulation and anchoring of Pd nanoparticles in these areas. From the scratch adhesion testing of the EN-Cu<sub>1</sub>-Cu<sub>2</sub> coating, cone-shaped fractures and cracks were observed within cold-sprayed Cu coatings, indicating cohesive failure. Failure of the cold sprayed Cu coatings was likely due to the poor inter-particle bonding, absence of dimpling and limited plastic deformation of the particles at low gas pressures. A direct correlation between the tensile and scratch adhesion testing was obtained.

Microstructural analysis of the cold-sprayed Cu coatings through ECC imaging revealed inhomogeneous microstructure with grain refinement at the splat boundaries due to the higher degree of plastic deformation. However, a more uniform microstructure was achieved for the electroplated Cu coating with a larger average grain size as compared to that of cold-sprayed Cu coatings. The lower hardness of the electroplated Cu coating compared to the cold-sprayed Cu coatings was attributed to the larger average grain size and different microstructural characteristics.

# 5.6 Acknowledgement

The authors would like to acknowledge the financial support of the Natural Sciences and Engineering Research Council of Canada (NSERC) through the Green Surface Engineering for Advanced Manufacturing (Green SEAM) Strategic Network [grant number NETGP 493955-16]. In addition, the industrial partner, Bombardier Aerospace, is gratefully acknowledged. We wish to thank the National Research Council Canada and Mr. Kevin Bricault for their assistance with the cold spray experiments. Dr. Lise Guichaoua from the McGill Materials Services Electron Microscopy Labs is gratefully acknowledged for her help with the SU8230.

# Chapter 6: Development of a Duplex Sn-Cu Coating on Carbon Fiber-Reinforced Polymers (CFRPs) using Cold Spray and Electrodeposition Processes

### Preface

In previous chapters, a multilayered metallic coating (i.e., EN-Cu<sub>1</sub>-Cu<sub>2</sub>) was successfully fabricated onto an epoxy-CFRP substrate though three subsequent coating processes. This chapter aims to investigate the feasibility of the fabrication of a duplex coating onto an epoxy-CFRP using cold spray and electrodeposition processes. Adhesion properties and electrical conductivity of the coatings were evaluated and compared with those obtained for the previously fabricated multilayered coatings in Chapters 3 and 5.

# This chapter is ready for submission and will be credited to the following authors:

Panteha Fallah, André McDonald, Stephen Yue, "Development of a Duplex Sn-Cu Coating on Carbon Fiber-Reinforced Polymers (CFRPs) through Cold Spray and Electrodeposition Processes".

## **Abstract**

Direct cold spray deposition of Cu was not possible on carbon fiber-reinforced polymers (CFRPs) due to the substrate erosion. In a recent study, epoxy-CFRPs were successfully metallized through a hybrid coating process that involves three consecutive coating steps: (i) electroless deposition, followed by (ii) electrodeposition, and finally (iii) cold spray. In this present study, to

reduce the number of coating steps, a duplex metallic coating was developed on CFRPs by cold spray deposition of tin (Sn) to fabricate a continuous metallic interlayer, followed by Cu electrodeposition (i.e., Sn<sub>cs</sub>-Cu<sub>ep</sub>). The Cu was selected for electrodeposition on Sn interlayer due to its superior electrical conductivity, which makes it suitable as a lightning strike protection coating material. Tensile adhesion bond strength of the duplex Sn<sub>cs</sub>-Cu<sub>ep</sub> coating was measured in accordance with ASTM Standard C-633-13. Fractured surfaces after tensile adhesion testing were examined by using a scanning electron microscope (SEM) and an optical microscope (OM). The electrical resistivity of the fabricated coatings was evaluated using the 4-point probe method. It was found that cold-sprayed Sn coating failed adhesively in the absence of the electrodeposited Cu coating. After electrodeposition of Cu, cohesive failure of the cold-sprayed Sn coating took place. A "dissolution-deposition" mechanism has been established to explain the weakening of the cold-sprayed Sn coating after electrodeposition. Despite the weakening effect, the cohesive strength of the Sn coating is slightly higher than that of the previously fabricated three-step coating system. Electrical resistivity of the electrodeposited Cu coating was found to be close to that of bulk Cu. These results suggest that a duplex Sn<sub>cs</sub>-Cu<sub>ep</sub> coating can be fabricated on CFRPs with significantly improved electrical conductivity and slightly enhanced adhesion properties as compared to multilayered coatings fabricated using a three-step electroless depositionelectrodeposition-cold spray processes.

**Keywords:** Adhesive failure; Cohesive failure; Dissolution-deposition; Duplex coating; Electrical resistivity; Tensile adhesion bond strength

### **6.1 Introduction**

Carbon fiber-reinforced polymers (CFRPs) have been considered suitable materials for aerospace applications (i.e., load-bearing components for aircraft) since they have low density and high strength [4]. However, the use of CFRP is hindered due to its high electrical resistivity as compared to aluminium [144] which may cause structural damage during the lightning strike. Thus, metallization of CFRP materials is necessary to ensure the structural safety.

Various coating methods have been used to apply metallic coatings on polymeric substrates such as physical vapor deposition (PVD) and chemical vapor deposition (CVD), but low deposition rates and high expense of these processes would limit their applications [63, 64, 115]. Among thermal spray processes, cold spray has been widely used to metallize polymers or polymer-based composites as it uses relatively low temperatures [116], which makes it suitable for heat-sensitive materials such as CFRPs. As a result, oxidation of metallic powders and accumulation of tensile residual stress are minimized [65]. In the cold spray process, particles are accelerated to a high velocity (ranging from 500-1200 m/s) through a converging-diverging nozzle onto a substrate to form a dense metallic coating [26]. In the case of a metallic substrate, metallurgical and/or mechanical interlocking are responsible for the bonding of the particles [117]. However, development of cold sprayed metallic coatings on polymeric substrates is challenging as these substrates suffer from poor erosion resistance when subjected to cold spraying [12, 69].

It was reported that Cu causes substrate erosion due to its high impact energy [46] and cannot be cold sprayed onto CFRP, but Sn can be cold sprayed onto CFRP and form a continuous coating due to its relatively low critical velocity [12]. A "crack-filling" mechanism has been previously established, explaining the bonding of cold sprayed Sn particles with the CFRP substrate [12]. Tin has also been mixed with various secondary components to understand the effect of secondary

component properties on deposition efficiency and properties of the mixed coatings (adhesion and electrical conductivity performance) [123]. It was found that nature of the substrate, impact energy and hardness of the secondary components affected the adhesion properties of the mixed coatings, leading to the variety of the failure behaviors such as adhesive, cohesive and a mixed adhesive cohesive. In case of an epoxy-CFRP, no notable improvement in adhesion strengths was observed as compared to that of pure Sn coating. The lowest electrical resistivity of the mixed coating was measured to be 85% of the bulk Sn when tin was mixed with aluminum alloys.

In this present study, the feasibility of fabrication of a duplex Sn-Cu coating onto an epoxy-CFRP substrate using cold spray and electrodeposition processes were investigated. Duplex Sn-Cu coating will be abbreviated as Sn<sub>cs</sub>-Cu<sub>ep</sub> (cold sprayed Sn - electroplated Cu). The adhesion/cohesion properties, fractured surfaces, as well as the electrical conductivity performance of the duplex coating were evaluated through tensile adhesion testing (i.e., pull-off test) and 4-point probe method, respectively.

# **6.2 Experimental Methodology**

# 6.2.1 Materials, Metallization Steps, and Conditions

Tin powder (SST-S6001, CenterLine, SST, Windsor, ON, Canada) was used in this study as the feedstock powder to produce a metallic interlayer prior to Cu electrodeposition [125]. Its properties were examined previously [125] and are summarized in Table 6-1. The particle size of the Sn powder was assessed using a laser scattering particle size analyzer (LA-920, Horiba, Japan), and the distribution was presented elsewhere [125]. A scanning electron microscope (SEM, Hitachi SU 3500, Japan) was used to obtain images of the Sn powder particles from the top and

cross-section views (see Fig 6-1). The Sn powder was roughly spherical, and its average particle size ( $D_{50}$ ) was 12  $\mu$ m, where 50% of the particles was smaller than 12  $\mu$ m.

**Table 6- 1:** Properties of the feedstock Sn powder

Powder	Morphology	Supplier	$D_{50}$ , $\mu \mathrm{m}$	Microhardness, HV <sub>0.01</sub>
Sn	Roughly spherical	CenterLine, SST	12	$10 \pm 1 \ (n = 7)$

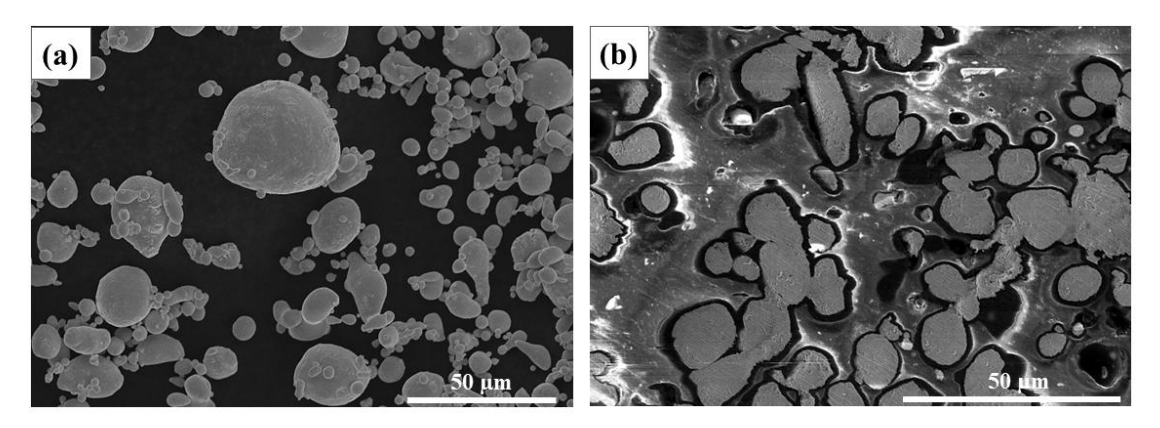


Figure 6-1: SEM images of the feedstock Sn powder from (a) top and (b) polished cross-section views

The substrate materials were epoxy-CFRPs, manufactured by Bombardier Aerospace (Montreal, Canada), consisting of a thermosetting epoxy matrix with continuous carbon fiber reinforcements. The CFRP panels were made of four plies of 5276-1/G30-500 epoxy carbon prepreg ([0/90]2s). The CFRP substrates were 1.7 x 1.7 cm<sup>2</sup> with a thickness of 1.7 mm and were degreased with methanol prior to coating.

CFRP substrates were first cold spray deposited with Sn to obtain a metallic interlayer for the subsequent electrodeposition step. Tin was selected for cold spray deposition since it is the only metal that can produce a uniform and continuous coating onto an epoxy-CFRP [12]. A Sn-coated CFRP was then electrodeposited with Cu in a solution containing 0.5 M CuSO<sub>4</sub>. 5H<sub>2</sub>O and

1M H<sub>2</sub>SO<sub>4</sub> for about an hour to achieve a Cu coating of 25 μm thickness. The electrodeposition process has been fully described in a previous study [105].

Cold spray of Sn at low pressure was conducted with a commercially available CenterLine SST system (Supersonic Spray Technologies, CenterLine Windsor Limited, Windsor, ON, Canada). The cold spray process parameters for Sn-coated CFRP substrates are listed in Table 6-2. Only one pass was sprayed under the gas pressure of 68 psi. A step size of 1 mm (17 steps) was selected, and the feeding rate was measured to be  $10 \pm 2$  g/min for three measurements. The cold spray parameters were chosen based on the previously successful cold spay experiments [12, 125].

**Table 6- 2:** Sn cold spray parameters for CFRP substrates

Powder	Carrier gas	Gas temperature,	Gas pressure,	Stand-off distance,	Nozzle travel speed,
		$^{\circ}\mathrm{C}$	psi	mm	mm/s
Sn	$N_2$	320	68	18	25

# 6.2.2 Coating Characterization and Properties

Microstructures of the coatings were analyzed from the top surface and the polished cross-sections of the coated CFRPs with SEM. Coated CFRPs were cold mounted, mechanically ground, and polished using 9, 3, and 1  $\mu m$  diamond pastes.

The pull-off strength of the coatings was evaluated according to ASTM standard C-633-13 [126]. Square specimens of 1.7 x 1.7 cm<sup>2</sup> were sectioned (Delta Abrasimet, Buehler, Illinois, USA) from CFRP panel to mostly cover all the circular surface area. Similarly, other researchers used the modified standard to assess the bond strength of various coatings fabricated on CFRP specimens [12, 121, 122]. A room temperature curing epoxy glue (J-B weld original cold weld, USA) was used to adhere the coated CFRPs between two steel cubic blocks with a dimension of

1.7 x 1.7 cm<sup>2</sup> and a height of 1 cm, which was machined on a cylindrical steel block with a 2.5 cm diameter. The test was performed using an MTS servo-hydraulic pressure machine at a constant crosshead speed of 1.0 mm/min. The pull-off strength of the cold sprayed Sn before and after electrodeposition was measured; three measurements were performed, and the average strength value was reported. The fractured surfaces were then analyzed with a digital microscope (Keyence VHX-5000, IL, USA) and SU3500. Compositional analysis of the fractured surfaces was conducted using Energy-Dispersive X-ray Spectroscopy (EDS) in the SEM.

To understand the correlation between the adhesion/cohesion behavior of the duplex Sn-Cu coating and the chemical reactions happening between the Sn coating and the plating solution, a Sn-coated CFRP with coating dimensions of  $1.7 \times 1.7 \text{ cm}^2$  and a coating thickness of approximately 200  $\mu$ m was immersed into a 50 mL of plating solution for 30 min without applying a current/voltage (i.e., immersion test). A Microwave-Plasma Atomic Emission Spectroscopy (4210 MP-AES, Agilent, CA, USA) was then used to characterize the plating solution after the immersion test to quantify the concentration of dissolved Cu and Sn elements. Similar analysis was conducted for a 50 mL of plating solution after 30 min of Cu electrodeposition and the results were then compared with that of the immersion test. Solution analysis was performed three times (n=3) for both immersion and electrodeposition tests and the average values have been reported.

Electrical resistivity of the cold-sprayed Sn and the electrodeposited Cu coatings were evaluated using the four-point probe method (Everbeing Int'l Corp, Hsinchu City, Taiwan). According to this method, the current was applied to the coating using the two outer probes and the voltage drop was measured using the two inner probes. A Xantrex power supply and a Keithley multimeter (199 system DMM scanner, Cleveland, Ohio, USA) with a precision of 0.001 mV were used to apply current and measure the voltage drop, respectively. Eight measurements ranging

from 50 mA to 120 mA with a 10-mA step were performed on both Sn and Cu coatings and the average of the electrical resistivity was determined for each coating. The electrical resistivity of the coatings was measured according to Eq. (1) [77]:

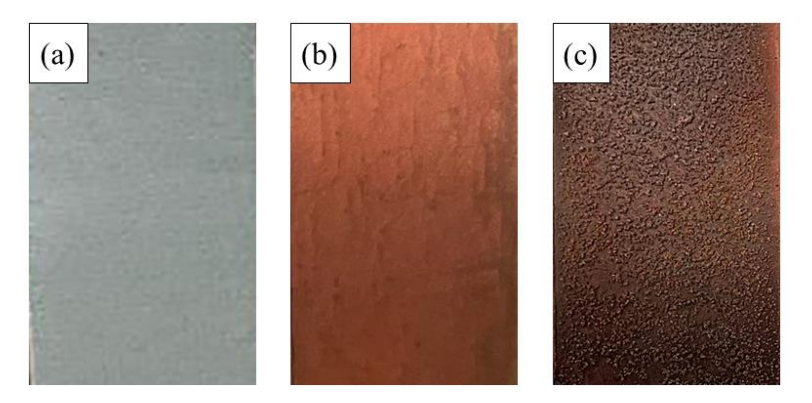
$$\rho_{\rm R} = \frac{\pi}{\ln(2)} t \frac{V}{I} f.$$
 Eq. (1)

where  $\rho_R$  is the resistivity, t the coating thickness, V the measured voltage, I the applied current, and f the finite width correction factor varying depending on the dimensional characteristics of the sample and probe spacing. In this study, the distance between all four probes was fixed at 1 mm and f was estimated to be 0.95.

## 6.3 Results and Discussion

## 6.3.1 Coating microstructure

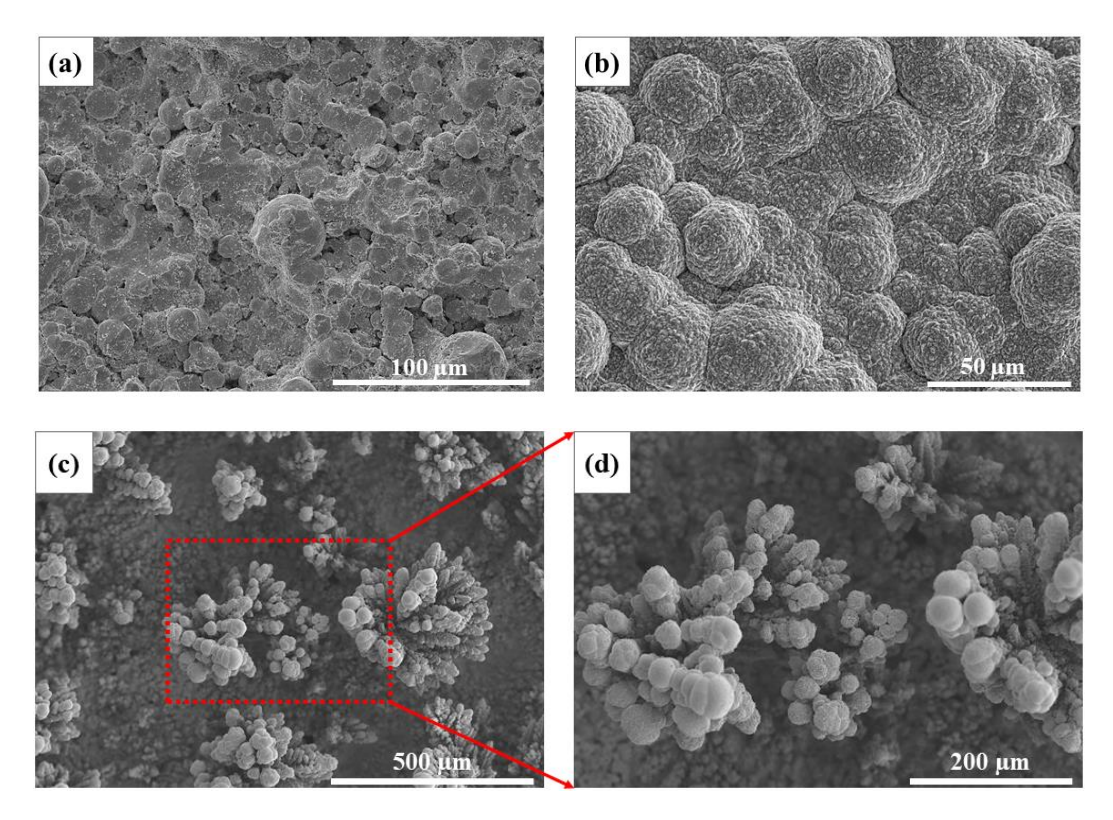
Figure 6-2 shows the top surface views of the Sn coating before and after electrodeposition and immersion. After electrodeposition of Cu, a smooth and continuous Cu coating was deposited on the Sn coating (Fig 6-2 (b)). However, in the absence of current/voltage (Fig 6-2 (c)), a poorly adhered and powdery-like Cu coating was formed on the Sn-coated CFRP. A comprehensive mechanism associated with these coating microstructures is described in Section 6.3.4.



**Figure 6- 2:** Top surface images of the (a) Sn coating, Sn coating after (b) electrodeposition, and (b) after the immersion test

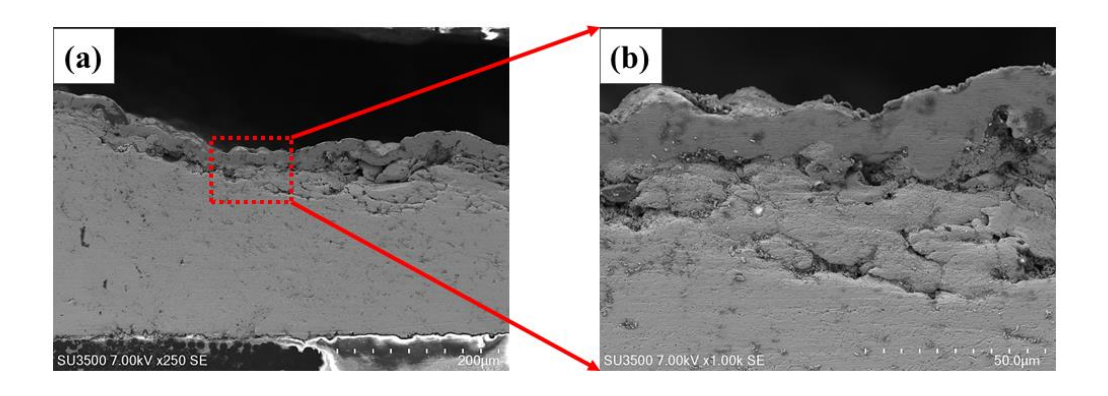
Figures 6-3 (a) and (b) show the top view SEM images of the cold sprayed Sn and the subsequent electrodeposited Cu coatings, respectively. In Fig 6-3 (a), Sn particles on the coating surface that retained their original shape can be observed, leading to the formation of subsurface interparticle voids, allowing for the penetration of the plating solution inside the Sn coating. After electrodeposition on Sn coating, dense and cauliflower-like Cu coating was obtained as shown in Fig 6-3 (b).

Figures 6-3 (c) and (d) show the top surface of the Sn coating after the immersion test in the plating solution and the enlarged view of the rectangle, respectively. As shown, a non-homogeneous Cu coating with dendrite-like structure was obtained. Copper dendrites exhibited a relatively weak adhesion to the underlying Sn coating and this type of morphology was observed in a previous study [145]. The formation of dendrites might be due to the preferred and faster growth of Cu on the sharper area of the coating. These results suggest that Cu coating with different characteristics can be formed on porous Sn coating through different mechanisms of electrodeposition and immersion processes.



**Figure 6- 3:** Top view SEM images of the (a) cold sprayed Sn, (b) electrodeposited Cu coatings, and (c and d) Sn coating after the immersion test in the plating solution

Figure 6-4 shows the cross-section SEM images and EDS mapping results of the  $Sn_{cs}$ - $Cu_{ep}$  coating fabricated onto CFRP. As shown, thicknesses of the Sn and Cu coatings are approximately 200  $\mu$ m and 25  $\mu$ m, respectively. The Cu coating followed the topography of the underlying Sn coating and the EDS results indicated 75 wt% Sn and 7.2 wt% Cu for the given field of view.



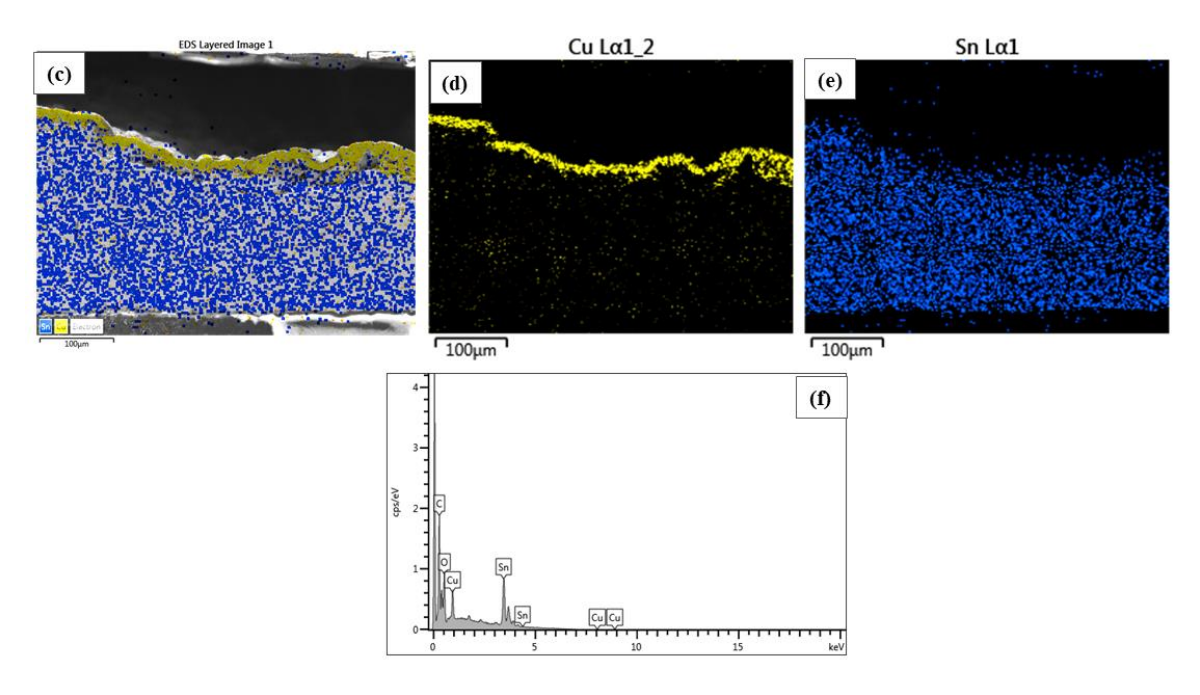


**Figure 6- 4:** (a) and (b) cross-sectional SEM images of the Sn<sub>cs</sub>-Cu<sub>ep</sub> coating and (c)-(f) EDS maps and results of the image (a)

## 6.3.2 Tensile Adhesion/Cohesion Bond Strength

The pull-off strength results of the deposited coatings before and after electrodeposition and immersion test are shown in Fig 6-5. The glue adhesion strength was determined to be 13 MPa.

In the adhesion strength test, cold-sprayed Sn coating failed at the Sn/CFRP interface with an adhesion strength of 8.45 MPa, indicating adhesive failure. After electrodeposition of Cu, adhesion strength test led to the failure of the cold-sprayed Sn coating, suggesting cohesive failure with cohesion bond strength of 3.59 MPa. After the immersion test in the plating solution, cold-sprayed Sn coating cohesively failed, and the corresponding cohesion bond strength was 2.7 MPa, which was slightly lower than that after Cu electrodeposition. This lower cohesion strength is possibly attributed to the different deposition mechanisms of electrodeposition and immersion plating, which will be explained in the following section 6.3.4. It can be found from the pull-off

strength results that the transition of adhesive failure to cohesive failure of the Sn coating after electrodeposition resulted from the plating solution.

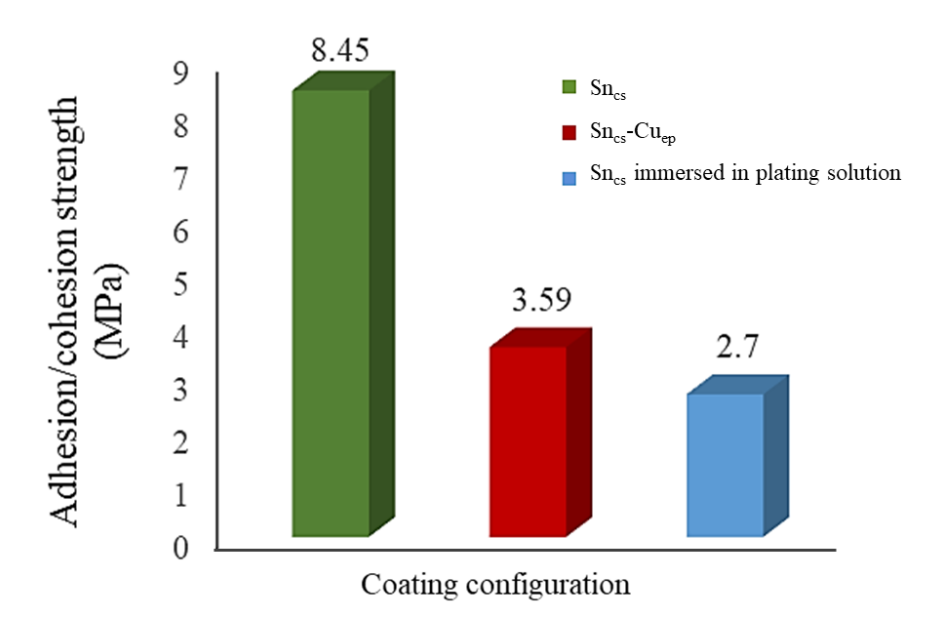


**Figure 6- 5:** Adhesion/cohesion bond strength of the cold sprayed Sn coating before and after electrodeposition of Cu and immersion test in the plating solution

# 6.3.3 Fractured surfaces

Figures 6-6 and 6-7 show the OM and SEM images of the fractured surfaces in the absence of the electrodeposited Cu coating where adhesive failure took place at the Sn/CFRP interface. As shown in Fig 6-6, carbon fiber areas were roughened, and remnants of Sn (indicated by white arrows) from the peeled Sn coating can be observed on these regions. Adhesive failure of the Sn coating with the CFRP substrate was reported previously [123]. It was reported in the literature [12] that Sn can be successfully cold spray deposited onto the CFRP surface through the "crack-filling" mechanism. According to this mechanism, partially melted or softened Sn particles impact onto a substrate, generating micro-cracks by the hard core of the particles. Subsequently, the

molten part of the particles is squeezed into the cracks area, allowing for mechanical interlocking between the particles and the substrate.

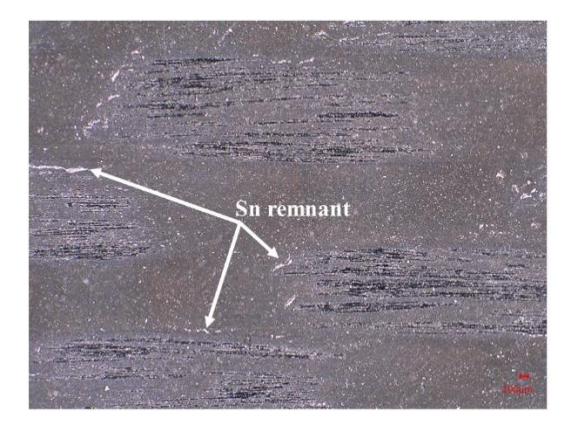
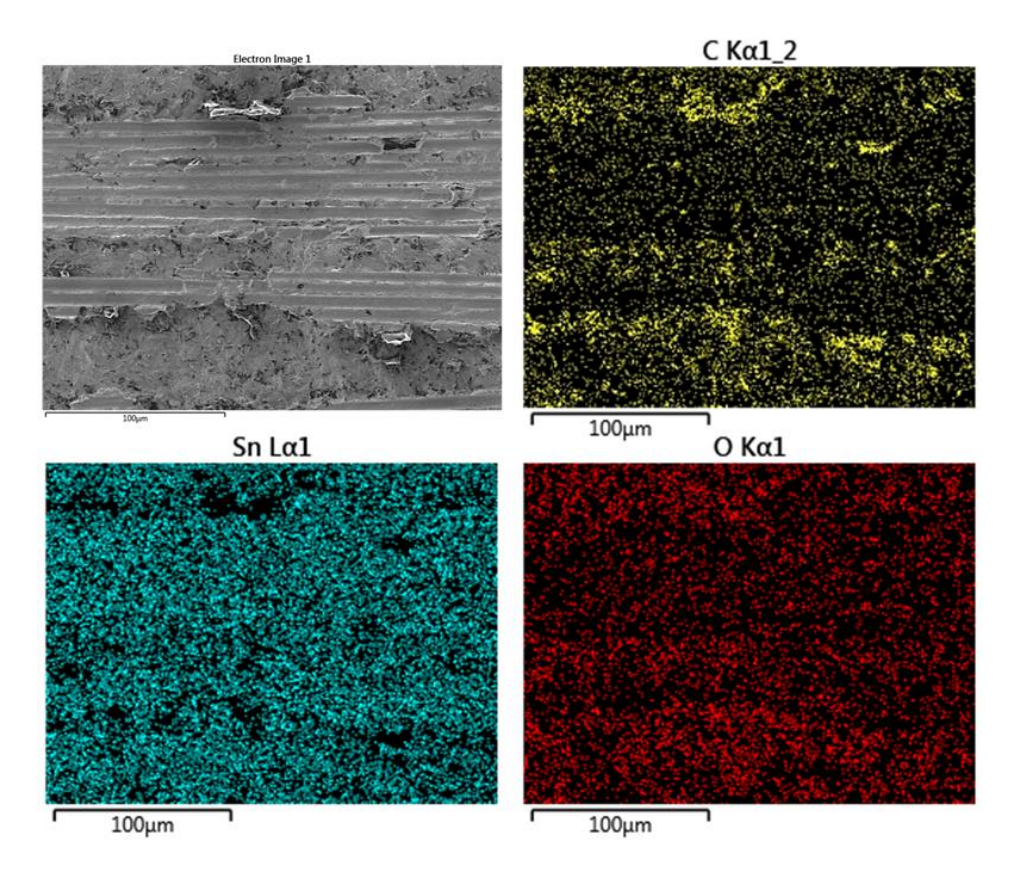


Figure 6- 6: OM image of the substrate side of a tested Sn coating on epoxy-CFRP

In Fig 6-7 that shows the coating side of the fractured surfaces, an homogeneous continuous structure was obtained, and topography of the exposed carbon fibers was printed on the backing surface of the Sn coating. The EDS results indicate the 90.8 wt% Sn, 5.1 wt% C, and 4.2 wt% O. The presence of carbon on the backing surface of the Sn coating possibly suggests the detachment of carbon fibers from the CFRP substrate, where bonding is more favorable in these regions, and their attachment to the peeled Sn coating.



**Figure 6- 7:** SEM image and EDS mapping of the coating side of a tested Sn coating in the absence of the Cu coating

Figures 6-8 (a-c) and (d-f) show the SEM images and EDS mapping of the fractured surfaces after Cu electrodeposition for both coating and the substrate sides, respectively. The SEM images of both sides show Sn particles, indicating cohesive failure within Sn coating. The EDS mapping of these areas indicated the presence of Cu on both coating and the substrate sides of the fractured surfaces. These areas are mostly tin with 38.3 wt% and 6.7 wt% Cu on the coating and the substrate sides, respectively. These results suggest that the plating solution penetrated inside the Sn coating through the subsurface voids, resulting in either dissolution of Sn and deposition of Cu inside the Sn coating or trapping the solution inside the porous Sn coating. The occurrence of cohesive failure is due to the poor bonding between the Sn particles and further weakened through the penetration of the solution inside the coating.

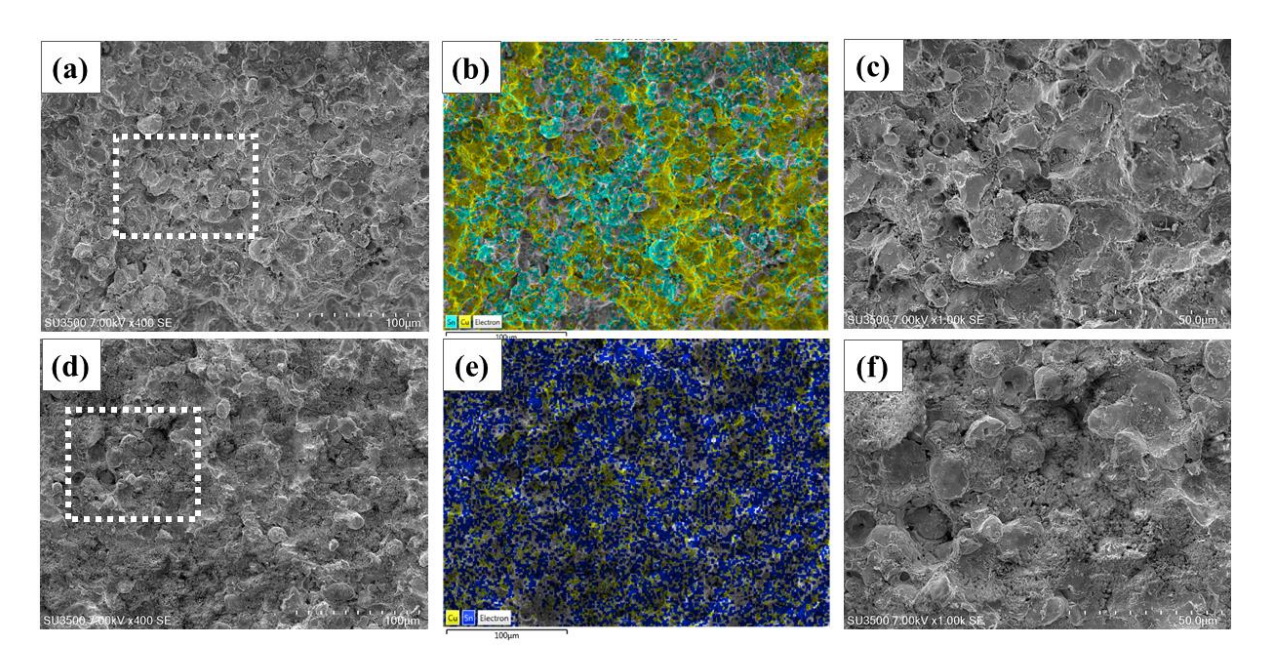


**Figure 6- 8:** (a) and (d) SEM images of the coating and substrate sides of the tested Sn<sub>cs</sub>-Cu<sub>ep</sub> coating on CFRP, respectively (b) and (e) EDS mapping of the image (a) and (b), respectively, (c) and (f) enlarged views of the rectangles in images (a) and (d), respectively

# 6.3.4 Dissolution-deposition mechanism

To understand the chemical reactions happening in the immersion plating, and to correlate the corresponding chemical reactions to the adhesion results, it is necessary to consider the standard redox potentials of the involved species. Standard redox potentials of Cu<sup>2+</sup>/Cu and Sn<sup>2+</sup>/Sn are +0.34 V and -0.14 V, respectively [53]. Since Sn<sup>2+</sup>/Sn has a lower redox potential than Cu<sup>2+</sup>/Cu, Sn reduces Cu<sup>2+</sup> ions from the solution to Cu metal atoms. Tin from the substrate dissolves into the solution and supplies electrons necessary for the reduction reaction of Cu. In this process, thickness of the deposited metal is self-limiting since an exposed free surface of Sn is required to proceed with the deposition.

A mechanism behind this process is called "dissolution-deposition" since it involves simultaneous dissolution of the Sn metal and deposition of the Cu from the solution onto the Sn

coating. A schematic diagram of the dissolution-deposition mechanism is presented in Fig 6-9 and the corresponding reactions are shown below.

According to the equation (3) which is the sum of the two partial anodic and the cathodic reactions of (1) and (2), dissolution of Sn took place and the PH of the solution increased from 1.5 to 2.5 due to the formation of the basic Sn(OH)<sub>2</sub>. Dissolution of Sn is accompanied by hydrogen evolution, and once a surface layer of Sn is dissolved, Cu from the solution (equations 4 and 5) is deposited and grows on a fresh exposed active surface.

(1) 
$$Sn \rightarrow Sn^{2+} + 2e^{-}$$

(2) 
$$2H_2O + 2e^- \rightarrow H_2 + 2OH^-$$

(3) 
$$Sn + 2H_2O \rightarrow Sn(OH)_2 + H_2$$

(4) 
$$Cu^{2+} + 2e^{-} \rightarrow Cu$$

(5) 
$$H_2 + 20H^- \rightarrow 2e^- + 2H_20$$

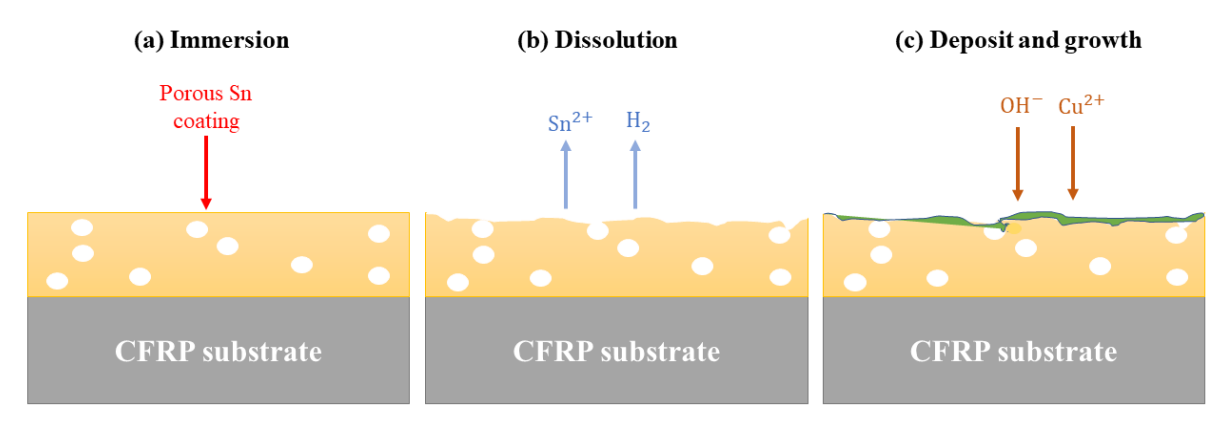


**Figure 6- 9**: Schematic of the immersion, dissolution, and deposition mechanism in the absence of current

Table 6-3 shows the concentration of the dissolved Cu and Sn elements in three plating solutions of as-prepared, after immersion, and after plating. As shown, the concentration of Cu in the as-prepared solution corresponded to the original concentration of Cu (i.e., 0.5 M CuSO<sub>4</sub>). After the immersion, the concentration of Cu in the solution decreased from 0.5 M to 0.48 M due to the formation of a Cu layer and the presence of 0.007 M Sn in the solution suggested the dissolution of Sn coating. However, after the plating, more Cu from the solution has been deposited on Sn as the concentration of Cu in the solution has been reduced to 0.44 M from 0.5 M and less dissolution of Sn occurred (0.001 M).

These results suggest that in electrodeposition, Cu can be continuously deposited on a Sn-coated CFRP as the required electrons for the reduction of the Cu ions can be supplied by the external power supply. The minimal concentration of Sn in the solution was possibly a result of the dissolution of Sn after the immersion prior to applying current/voltage. However, in the immersion plating, there is no external current to supply electrons and deposition is dependent on the dissolution of Sn to provide electrons for the reduction reactions and the available free surfaces.

**Table 6- 3:** Solution analysis of the plating solution before and after immersion and electrodeposition for 30 min

Solution	Cu (324.75 nm)	Sn (303.41 nm)
	ppm (M)	ppm (M)
As prepared	32500 (0.5)	0
After immersion	30782 (0.48)	890 (0.007)
After plating	27939 (0.44)	186 (0.001)

In both deposition processes (i.e., immersion and electrodeposition), Sn coating was cohesively failed due to the penetration of the solution and consequently weakening of the Sn coating. The lower cohesive strength of the Sn coating after immersion test is due to the greater dissolution of Sn, more penetration of the solution and weakening of the coating. However, in electrodeposition, penetration of the solution can be avoided once a first layer of the Cu coating is formed and by reducing the initiation time.

#### 6.3.5 Electrical resistivity

Electrical resistivity of the cold sprayed Sn and electrodeposited Cu coatings were measured and reported in Fig 6-10. The electrical resistivity of the cold sprayed Sn coating was found to be  $18~\mu\Omega$ .cm which is approximately 60% higher than that of bulk Sn material. In a previous study [123], electrical resistivity of the cold sprayed pure Sn coating was measured to be in the range of 13 to 22  $\mu\Omega$ .cm. After electrodeposition of Cu, electrical resistivity of Cu was measured to be 1.9  $\mu\Omega$ .cm, which is close to that of bulk Cu. This 'good level' of conductivity is likely due to the presence of dense, void free and minimal amount of oxygen content in the Cu coating (appx 1wt%). These results suggest that the electrical performance of the cold sprayed Sn coating can be significantly enhanced by depositing a Cu layer on a Sn coating through electrodeposition process.

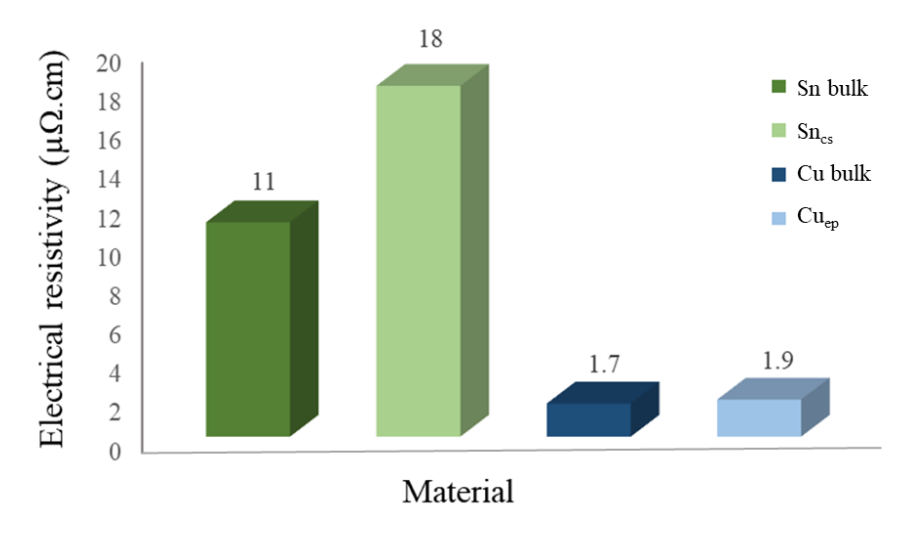


**Figure 6- 10:** Electrical resistivity of the cold sprayed Sn, electrodeposited Cu coatings on CFRP substrate, bulk Cu and Sn materials

#### **6.4 Conclusion**

A duplex Sncs-Cuep coating was successfully developed onto an epoxy-CFRP through cold spray and electrodeposition processes. Adhesion properties of the duplex Sncs-Cuep coating were studied through tensile adhesion testing, and the fractured surfaces were then characterized. An immersion test (i.e., absence of current) was performed to understand the correlation between the adhesion/cohesion properties of the Sn coating and the chemical reactions. The results showed an adhesive failure at the Sn/CFRP interface in the absence of a Cu electrodeposited coating. Corresponding fractured surfaces revealed roughened carbon fiber regions and the presence of carbon on the backing surface of the peeled Sn coating. Electrodeposition of Cu led to the cohesive failure of the Sn coating due to the penetration of the plating solution in the porous Sn coating. A "dissolution-deposition" mechanism was proposed to explain how the Cu coating was formed during the immersion plating and its relation to the adhesion strength results was discussed. The penetration issue can be minimized by producing a denser coating with minimal subsurface pores,

avoiding the subsequent cohesive failure. However, the cohesion strength of the Sn coating after electrodeposition is slightly higher than that of the cold sprayed Cu coating fabricated previously in a three-step coating system (3.59 MPa vs. 2.95 MPa). Electrical resistivity of the electrodeposited Cu coating was significantly lower than that of cold-sprayed Sn coating and was close to the electrical resistivity of the bulk Cu. Duplex Sn<sub>cs</sub>-Cu<sub>ep</sub> coating showed improved performance in terms of adhesion and electrical properties as compared to the previously fabricated multilayered EN-Cu<sub>1</sub>-Cu<sub>2</sub> coatings.

# **6.5** Acknowledgement

The authors would like to acknowledge the financial support of the Natural Sciences and Engineering Research Council of Canada (NSERC) through the Green Surface Engineering for Advanced Manufacturing (Green SEAM) Strategic Network [grant number NETGP 493955-16]. In addition, the industrial partner, Bombardier Aerospace, is gratefully acknowledged. We wish to thank the National Research Council Canada and Dr. Phuong Vo for his assistance with the cold spray experiments. Dr. Zhao Lu and Mr. Peng Yang from the McGill Nanotools Microfab are gratefully acknowledged for their help with the electrical resistivity measurements.

# **Chapter 7: Concluding Remarks**

#### 7.1 Global discussion and conclusions

The aim of this study is to examine the feasibility of the cold spray deposition of Cu onto an epoxy-CFRP. Previous studies [12, 105] suggested that cold spraying Cu onto carbon fiber-reinforced polymers with epoxy as the matrix material resulted in substrate erosion and formation of a coating was not possible. Thus, the main method was through a hybrid coating process involving fabrication of a metallic interlayer before cold spraying. In this process, an interlayer of electroless Ni film followed by electrodeposited Cu coating was fabricated onto an epoxy-CFRP prior to cold spraying. Relative hardness of the powder to the substrate, surface topography of the substrate, and thermal conductivity were found to be influential parameters affecting the cold spray deposition of Cu and its deposition efficiency. Higher gas pressure than 68 psi was not possible due to the coating delamination. These results reinforced the importance of the interlayer adhesion and the thermal expansion coefficient difference between the coating layers and the substrate. Electrical conductivity of the cold sprayed Cu coating was found to be almost two times lower than that of bulk Cu.

It was possible to build-up a coating when cold spraying onto an EN-Cu interlayer under a two-step gas pressure, but with lower DE in the second deposition layer as compared to the first cold sprayed layer. This lower DE in the second pass was attributed to the higher hardness and work hardening effect of the previously deposited Cu coating. Hardness similarity of the powder to the Cu interlayer led to the co-deformation of both material couple and consequently successful deposition. It was not possible to cold spray Cu onto Ni and Sn interlayer due to the insufficient deformation and erosion of the interlayers, respectively.

The pull-off strength of the electroless Ni and electroless Ni plus electroplated Cu coatings revealed adhesive failure. The fracture surfaces revealed damaged epoxy and broken carbon fibers suggesting that adhesion strength is affected by the exposed carbon fibres. It appears that the electroless Ni plating begins at Pd nano particles which cluster around the exposed C fibers, and this may positively affect the adhesion strength. However, the pull off properties of the hybrid (i.e., Cu cold sprayed) coatings revealed much lower strengths due to cohesive failure of the coatings. Fractography analysis showed poor interparticle bonding within the cold sprayed Cu coating, due to the low velocity of the cold spray process, which was also confirmed with scratch adhesion testing. As noted above, the particle velocity was restricted by a delamination effect above a certain velocity (i.e., almost the critical velocity of Cu), leading to achieving relatively low deposition efficiencies (approximately from 6% to 10%). However, the obtained deposition efficiencies in this study are orders of magnitude higher than that of acquired in the literature, when cold spraying Cu onto an epoxy-CFRP (i.e., no deposition was possible due to substrate erosion) [12].

Ultimately, since Cu is of a great interest to be used as the coating material on CFRP, a final hybrid approach was to electrodeposit Cu on a cold sprayed Sn interlayer, with the main goal being to reduce the number of processing steps. This hybrid coating was relatively straightforward to achieve, but the electrodeposited Cu coating led to the cohesive failure of the Sn coating that led to the development of a so-called "dissolution-deposition" mechanism. Making a denser, more defect free cold sprayed Sn interlayer would possibly alleviate this problem, but deploying higher velocities to achieve this leads to erosion and DE reductions.

In summary, the two-step hybrid coating approach (i.e., electroplated Cu of cold sprayed Sn) is superior to the three-step coating process (i.e., cold sprayed Cu on electroless Ni and electroplated Cu intermediate layers) because of process step reduction, higher conductivities, and

a slightly higher pull-off strength. At present, the limitation is that the electroplated Cu is much thinner than the cold sprayed Cu coating, but it is not clear what type of problems this would cause in lightning strike protection.

Based on this study, the following conclusions can be drawn:

- 1) Cold spray of Cu onto a Cu-coated CFRP substrate resulted in formation of a continuous and uniform coating due to the hardness similarity of the Cu particle with the Cu interlayer.
- 2) Maximum DE was achieved at a gas pressure of 68 psi and applying higher gas pressure than 68 psi was not possible due to the coating delamination.
- 3) Surface roughness, hardness of both substrate and the particle, and thermal conductivity of the substrate were found to be the primary parameters affecting the deposition efficiency when cold spraying on both Cu-coated CFRP and bulk Cu.
- 4) Deposition mechanism and deposition efficiency of the cold sprayed Cu particle was explicitly studied numerically and experimentally for the first deposition layer and the build-up phase (i.e., two-step gas process).
- 5) From the FE simulations, it was found that a shared plastic deformation between the particle and the substrate is necessary for a successful cold spray deposition and the increased hardness of the first cold sprayed layer resulted in higher strain energy and lower substrate penetration; thus, hindering the particle retention.

- 6) Single particle impact experiment results indicated co-deformation of the Cu particle with the Cu interlayer, leading to the successful cold spray deposition of Cu. However, in case of Ni and Sn interlayers, cold spray deposition of Cu was not possible due to the insufficient interlayer deformation and interlayer erosion, respectively.
- 7) Cohesive failure of the cold sprayed Cu coating was observed which was possibly due to the poor interparticle bonding and the absence of metallurgical bonding under the gas pressure range of 60 to 68 psi.
- 8) A non-uniform microstructure within cold-sprayed Cu coatings was obtained. This non-uniform microstructure was associated with an inhomogeneous plastic deformation of the cold-sprayed Cu particles, leading to the formation of two substructures: fine and coarse structures.
- 9) Nickel was preferentially electroless-deposited on substrate areas with exposed carbon fibers due to the accumulation of Pd particles on these regions. Improved adhesion bond was obtained on carbon fiber regions due to the observed damaged epoxy and carbon fibers in carbon fiber regions.
- 10) A duplex Sn<sub>cs</sub>-Cu<sub>ep</sub> coating was successfully fabricated onto the CFRP substrate using cold spray and electrodeposition. Electrodeposition of Cu led to the cohesive failure of the Sn coating as a result of the "dissolution-deposition" mechanism.

11) Electrical conductivity of the cold sprayed Cu and electrodeposited Cu coatings were found to be two times lower and almost similar to that of bulk Cu, respectively.

# 7.2 Suggestions of future work

Based on the results and discussions, the following suggestions for future work could be made:

- Cold spraying at various gas temperature and pressure could be performed to develop the window of cold sprayability and to understand the effect of a broad range of cold spray process parameters on deposition efficiency of the Cu particle and possible coating delamination.
- 2) It is recommended to cold spray Cu at higher gas pressure than 68 psi as electrical performance of the cold sprayed Cu coating might be enhanced as a result of an improved consolidation/densification effect and subsequently reduced interparticle pores. The delamination caused by higher pressures is addressed in point 3 below.
- 3) Applying higher gas pressure may be accomplished through the bonding enhancement between the electroless Ni coating and the CFRP substrate. Chemical etching, plasma, and mechanical treatments could possibly increase the roughness of the CFRP surface, resulting in an enhanced mechanical interlocking between the electroless film and the CFRP surface.
- 4) The obtained low deposition efficiencies bring a question about the economics of the proposed hybrid coatings which needs to be quantitatively investigated.

- 5) It is of interest to cold spray Cu onto a greater thickness of the Cu interlayer than 100 μm and to study its effect on deposition characteristics and properties of the coating. It is expected that the heat dissipation and energy absorption would be facilitated by increasing the interlayer thickness, preventing/delaying the delamination problem by increasing the gas pressure.
- 6) More experiments are needed to fully understand the effect of substrate properties such as thermal conductivity and surface roughness when cold spraying metals onto metallic substrates/interlayers.
- 7) Environmental Life Cycle Assessment (LCA) should be used to compare the environmental performance of the developed hybrid coating systems with that of current LSP approaches.
- 8) Annealing of the multilayered metallic coatings could be performed to investigate its effect on adhesion properties and electrical conductivity of the coatings.
- 9) Cold spray deposition of Sn at higher gas pressures could be conducted to fabricate a denser coating with enhanced interparticle bonding for the subsequent electrodeposition. Therefore, it is expected to avoid/minimize the solution penetration inside the Sn coating, preventing the occurrence of cohesive failure.
- 10) Performing a lightning strike test on the successfully fabricated coatings is needed to thoroughly examine their potential as LSP materials.

### 7.3 Contributions to original knowledge

The following contributions to original knowledge were made through the work conducted in this present study:

- 1) For the first time, cold spraying of Cu on an epoxy-CFRP was successfully performed using electrochemically fabricated metallic interlayers to protect the CFRP from any possible damage and to enable cold spray Cu.
- 2) It was shown that the cold spray deposition of Cu powder in the build-up phase would be more difficult (i.e., lower DE) as compared to the first-layer deposition due to the work hardening effect of the previously cold spray deposited layer.
- 3) From the interlayer hardness effect on cold sprayability of the Cu particle, a correlation between the particle deformation and deposition behavior was proposed.
- 4) The importance of CFRP surface characteristics on electroless Ni coating formation was highlighted and enhanced adhesion strength of the electroless Ni coating to the carbon fiber regions relative to the epoxy area was associated with the presence of micro voids and accumulation of Pd nanoparticles on these regions.
- 5) For the first time, a two-step coating process that involves cold spray of Sn followed by Cu electrodeposition was developed on CFRP substrate to achieve a high electrically conductive coating (i.e., almost similar to that of bulk Cu).

6)	A "dissolution-deposition" mechanism was proposed to explain the cohesive failure of the		
	cold sprayed Sn coating after electrodeposition and immersion.		

# References

- [1] Gonzalez, R., H. Ashrafizadeh, A. Lopera, P. Mertiny, and A. McDonald, *A Review of Thermal Spray Metallization of Polymer-Based Structures*, Journal of Thermal Spray Technology, 2016. **25**(5): p. 897-919.
- [2] Faupel, F., V. Zaporojtchenko, T. Strunskus, J. Erichsen, K. Dolgner, A. Thran, and M. Kiene. *Metallization of Polymers 2. in ACS Symposium Series (Kluwer Academic/Plenum, New York, 2002).* 2002.
- [3] Rahimi, A., M. Hojjati, A. Dolatabadi, and C. Moreau, *Thermal Spray Coating on Polymeric Composite for De-Icing and Anti-Icing Applications*, Journal of Manufacturing Science and Engineering, 2021. **143**(10).
- [4] Archambault, G., B. Jodoin, S. Gaydos, and M. Yandouzi, *Metallization of carbon fiber reinforced polymer composite by cold spray and lay-up molding processes*, Surface and Coatings Technology, 2016. **300**: p. 78-86.
- [5] Gagné, M. and D. Therriault, *Lightning strike protection of composites, Progress in Aerospace Sciences*, 2014. **64**: p. 1-16.
- [6] Che, H., M. Gagné, P.S.M. Rajesh, J.E. Klemberg-Sapieha, F. Sirois, D. Therriault, and S. Yue, *Metallization of Carbon Fiber Reinforced Polymers for Lightning Strike Protection*, Journal of Materials Engineering and Performance, 2018. **27**(10): p. 5205-5211.
- [7] Black, S., *Lightning Strike Protection Strategies for Composite Aircraft, in High-Performace Composites*. 2013, Composites World. p. 52-61.
- [8] Affi, J., H. Okazaki, M. Yamada, and M. Fukumoto, *Fabrication of Aluminum Coating onto CFRP Substrate by Cold Spray*, Materials Transactions, 2011. **52**(9): p. 1759-1763.
- [9] Hussain, T., D.G. McCartney, P.H. Shipway, and D. Zhang, *Bonding Mechanisms in Cold Spraying: The Contributions of Metallurgical and Mechanical Components*, Journal of Thermal Spray Technology, 2009. **18**(3): p. 364-379.
- [10] Li, W., K. Yang, S. Yin, X. Yang, Y. Xu, and R. Lupoi, *Solid-state additive manufacturing and repairing by cold spraying: A review*, Journal of Materials Science & Technology, 2018. **34**(3): p. 440-457.
- [11] Zhang, D., P.H. Shipway, and D.G. McCartney, *Cold Gas Dynamic Spraying of Aluminum: The Role of Substrate Characteristics in Deposit Formation*, Journal of Thermal Spray Technology, 2005. **14**(1): p. 109-116.
- [12] Che, H., P. Vo, and S. Yue, *Metallization of carbon fibre reinforced polymers by cold spray*, Surface and Coatings Technology, 2017. **313**: p. 236-247.
- [13] Ganesan, A., M. Yamada, and M. Fukumoto, *Cold Spray Coating Deposition Mechanism on the Thermoplastic and Thermosetting Polymer Substrates*, Journal of Thermal Spray Technology, 2013. **22**(8): p. 1275-1282.

- [14] Małachowska, A., M. Winnicki, Ł. Konat, T. Piwowarczyk, L. Pawłowski, A. Ambroziak, and M. Stachowicz, *Possibility of spraying of copper coatings on polyamide 6 with low pressure cold spray method*, Surface and Coatings Technology, 2017. **318**: p. 82-89.
- [15] Gibson, R.F., *Principles of Composite Material Mechanics*. 4 ed. 2016, Boca Raton: CRC Press. 700
- [16] Skoczylas, J., S. Samborski, and M. Kłonica, *The application of composite materials in the aerospace industry*, Journal of Technology and Exploitation in Mechanical Engineering, 2019. **5**(1).
- [17] MIL-STD-1757, Lightning Qualification Test Techniques for Aerospace Vehicles and Hardware, Document Center, Inc. https://www.document-center.com/standards/show/MIL-STD-1757, 2022.
- [18] US Department of Transportation, F.A.A., *Handbook-Airframe, Aviation Maintenance Technician* Vol. 1. 2018, Oklahoma City, OK.
- [19] Gardiner, G., Lightning Strike Protection for Composite Structures, in High-Performance Composites. 2006, Composites World. p. 44-50.
- [20] Feraboli, P. and H. Kawakami, *Damage of Carbon/Epoxy Composite Plates Subjected to Mechanical Impact and Simulated Lightning*. Journal of Aircraft, 2010. **47**(3): p. 999-1012.
- [21] Ebneth, H., L. Preis, H. Giesecke, and G.D. Wolf, *Metallized carbon fibres and composite materials containing these fibres*. 1984, Google Patents.
- [22] Bobzin, K., W. Wietheger, and M.A. Knoch, *Development of Thermal Spray Processes for Depositing Coatings on Thermoplastics*, Journal of Thermal Spray Technology, 2021. **30**(1-2): p. 157-167.
- [23] Wypych, A., P. Siwak, D. Andrzejewski, and J. Jakubowicz, *Titanium Plasma-Sprayed Coatings on Polymers for Hard Tissue Applications*, Materials, 2018. **11**(12): p. 2536.
- [24] Gonzalez, R., A. McDonald, and P. Mertiny, *Effect of flame-sprayed Al–12Si coatings on the failure behaviour of pressurized fibre-reinforced composite tubes*, Polymer Testing, 2013. **32**(8): p. 1522-1528.
- [25] Assadi, H., H. Kreye, F. Gärtner, and T. Klassen, *Cold spraying A materials perspective*, Acta Materialia, 2016. **116**: p. 382-407.
- [26] Papyrin, A., V. Kosarev, S. Klinkov, A. Alkhimov, and V.M. Fomin, *Cold spray technology*, 2006: Elsevier.
- [27] Dykhuizen, R., M. Smith, D. Gilmore, R. Neiser, X. Jiang, and S. Sampath, *Impact of high velocity cold spray particles*, Journal of Thermal Spray Technology, 1999. **8**(4): p. 559- 564.
- [28] Wong, W., E. Irissou, A.N. Ryabinin, J.-G. Legoux, and S. Yue, *Influence of Helium and Nitrogen Gases on the Properties of Cold Gas Dynamic Sprayed Pure Titanium Coatings*, Journal of Thermal Spray Technology, 2010. **20**(1-2): p. 213-226.
- [29] Yin, S. and R. Lupoi, *Introduction to Cold Spray Additive Manufacturing, in Cold Spray Additive Manufacturing: From Fundamentals to Applications*, 2021, Springer International Publishing: Cham. p. 1-7.

- [30] Stoltenhoff, T., H. Kreye, and H. Richter, *An analysis of the cold spray process and its coatings*, Journal of Thermal Spray Technology, 2002. **11**(4): p. 542-550.
- [31] Rokni, M.R., S.R. Nutt, C.A. Widener, V.K. Champagne, and R.H. Hrabe, *Review of Relationship Between Particle Deformation, Coating Microstructure, and Properties in High-Pressure Cold Spray*, Journal of Thermal Spray Technology, 2017. **26**(6): p. 1308-1355.
- [32] Assadi, H., F. Gärtner, T. Stoltenhoff, and H. Kreye, *Bonding mechanism in cold gas spraying*, Acta Materialia, 2003. **51**(15): p. 4379-4394.
- [33] Schmidt, T., H. Assadi, F. Gärtner, H. Richter, T. Stoltenhoff, H. Kreye, and T. Klassen, *From Particle Acceleration to Impact and Bonding in Cold Spraying*, Journal of Thermal Spray Technology, 2009. **18**(5-6): p. 794-808.
- [34] Thesis | Cold spray characteristics of mixed 316L stainless steel and commercial purity Fe powders | ID: qn59q8729 | eScholarship@McGill. https://escholarship.mcgill.ca/concern/theses/qn59q8729 (accessed Jul. 28, 2022).
- [35] Grujicic, M., C.L. Zhao, W.S. DeRosset, and D. Helfritch, *Adiabatic shear instability based mechanism for particles/substrate bonding in the cold-gas dynamic-spray process*, Materials & Design, 2004. **25**(8): p. 681-688.
- [36] Van Steenkiste, T.H., J.R. Smith, and R.E. Teets, *Aluminum coatings via kinetic spray with relatively large powder particles*, Surface and Coatings Technology, 2002. **154**(2): p. 237- 252.
- [37] Gärtner, F., T. Stoltenhoff, T. Schmidt, and H. Kreye, *The Cold Spray Process and Its Potential for Industrial Applications*, Journal of Thermal Spray Technology, 2006. **15**(2): p. 223-232.
- [38] Schmidt, T., F. Gärtner, H. Assadi, and H. Kreye, *Development of a generalized parameter window for cold spray deposition*, Acta Materialia, 2006. **54**(3): p. 729-742.
- [39] Kang, K., S. Yoon, Y. Ji, and C. Lee, *Oxidation dependency of critical velocity for aluminum feedstock deposition in kinetic spraying process*. Materials Science and Engineering: A, 2008. **486**(1-2): p. 300-307.
- [40] Askeland, D.R., P.P. Phulé, W.J. Wright, and D. Bhattacharya, *The science and engineering of materials*. 2003.
- [41] Schultheiß, D., Permeation barrier for lightweight liquid hydrogen tanks, in Faculty of Mathematics, Natural Sciences and Materials Engineering. 2008, University of Augsburg: Augsburg.
- [42] Campbell, F. C., *Manufacturing Technology for Aerospace Structural Materials*, 2006. p. 273–368.
- [43] Barkoula, N.-M. and J. Karger-Kocsis, *Review Processes and influencing parameters of the solid particle erosion of polymers and their composites*, Journal of Materials Science, 2002. **37**(18): p. 3807-3820.
- [44] Arjula, S. and A.P. Harsha, *Study of erosion efficiency of polymers and polymer composites*, Polymer Testing, 2006. **25**(2): p. 188-196.

- [45] Stachowiak, G. and A.W. Batchelor, *Abrasive, erosive and cavitation wear*, in Engineering Tribology, 1993. p. 557-612.
- [46] Lupoi, R. and W. O'Neill, *Deposition of metallic coatings on polymer surfaces using cold spray*, Surface and Coatings Technology, 2010. **205**(7): p. 2167-2173.
- [47] Robitaille, F., M. Yandouzi, S. Hind, and B. Jodoin, *Metallic coating of aerospace carbon/epoxy composites by the pulsed gas dynamic spraying process*, Surface and Coatings Technology, 2009. **203**(19): p. 2954-2960.
- [48] Paunovic, M. and M. Schlesinger, *Fundamentals of Electrochemical Deposition*, John Wiley & Sons, 2006.
- [49] Mallory. G. and J. Hajdu, *Electroless Plating: Fundamentals and Applications*, William Andrew, 1990.
- [50] Ohno, I, *Electrochemistry of electroless plating*, Materials Science and Engineering: A, 1991. **146** (1–2): p. 33–49.
- [51] Charbonnier, M and M. Romand, *Polymer pretreatments for enhanced adhesion of metals deposited by the electroless process*, International Journal of Adhesion and Adhesive, 2003. **23**(4): p. 277-285.
- [52] Di, L., B. Liu, J. Song, D. Shan, and D. A. Yang, Effect of chemical etching on the Cu/Ni metallization of poly (ether ether ketone)/carbon fiber composites, Applied Surface Science, 2011. **257**(9): p. 4272-4277.
- [53] Schlesinger, M. and M. Paunovic, *Modern Electroplating: Fifth Edition*, 2011. p. 1-32.
- [54] Ghosh, S., *Electroless copper deposition: A critical review*, Thin Solid Films, 2019. **669**: p. 641-658.
- [55] Shang, W., X. Zhan, Y. Wen, Y. Li, Z. Zhang, F. Wu, and C. Wang, *Deposition mechanism of electroless nickel plating of composite coatings on magnesium alloy*, Chemical Engineering Science, 2019. **207**: p. 1299–1308.
- [56] Bindra, P. and J. Tweedie, *Mechanisms of Electroless Metal Plating*, Journal of The Electrochemical Society, 1983. **130** (11): p. 1112.
- [57] Ma, L., Y. Chen, P. Renner, D. Parkinson, A. Fang, and H. Liang, *Synthesis and morphological characterization of electroless-deposited Ni-P coatings on diamond abrasives*, Lubricants, 2021. **9**(2): p. 20.
- [58] Kanani, N., Electroplating: Basic Principles, Processes and Practice, Elsevier, 2004.
- [59] Lelevic, A. and F. C. Walsh, Electrodeposition of NiP alloy coatings: A review, Surface and Coatings Technology, 2019. **369**: p. 198–220.
- [60] Che, H., X. Chu, P. Vo, and S. Yue, *Metallization of Various Polymers by Cold Spray*, Journal of Thermal Spray Technology, 2017. **27**(1-2): p. 169-178.

- [61] Zhou, X.L., A.F. Chen, J.C. Liu, X.K. Wu, and J.S. Zhang, *Preparation of metallic coatings on polymer matrix composites by cold spray*, Surface and Coatings Technology, 2011. **206**(1): p. 132-136.
- [62] Liang, J., H. Jiang, J. Zhang, X. Wu, X. Zhang, G. Li, and J. Cui, *Investigations on mechanical properties and microtopography of electromagnetic self-piercing riveted joints with carbon fiber reinforced plastics/aluminum alloy 5052*, Archives of Civil and Mechanical Engineering, 2019. **19** (1): p. 240-250.
- [63] Siegel, J. and V. Kotal, *Preparation of Thin Metal Layers on Polymers*, Acta Polytechnia, 2007. **47**(1).
- [64] Duguet, T., F. Senocq, L. Laffont, and C. Vahlas, *Metallization of polymer composites by metalorganic chemical vapor deposition of Cu: Surface functionalization driven films characteristics*, Surface and Coatings Technology, 2013. **230**: p. 254-259.
- [65] Chen, C., X. Xie, Y. Xie, X. Yan, C. Huang, S. Deng, Z. Ren, and H. Liao, *Metallization of polyether ether ketone (PEEK) by copper coating via cold spray*, Surface and Coatings Technology, 2018. **342**: p. 209-219.
- [66] Katsoulis, C., B. K. Kandola, P. Myler, and E. Kandare, *Post-fire flexural performance of epoxy-nanocomposite matrix glass fibre composites containing conventional flame retardants*, Composites Part A: Applied Science and Manufacturing, 2012. **43**(8): p. 1389-1399.
- [67] Huonnic, N., M. Abdelghani, P. Mertiny, and A. McDonald, *Deposition and characterization of flame-sprayed aluminum on cured glass and basalt fiber-reinforced epoxy tubes*, Surface and Coatings Technology, 2010. **205**(3): p. 867-873.
- [68] Sturgeon, A., B. Dunn, S. Celotto, and B. O'Neill, *Cold Sprayed Coatings for Polymer Composite Substrate*, in Proceedings of the 10th ISMSE, 8th ICPMSE, B. Battrick, Editor. 2006: Collioure, France.
- [69] Barletta, M., A. Gisario, and V. Tagliaferri, *Electrostatic spray deposition (ESD) of polymeric powders on thermoplastic (PA66) substrate*, Surface and Coatings Technology, 2006. **201**(1-2): p. 296-308.
- [70] Ganesan, A., J. Affi, M. Yamada, and M. Fukumoto, *Bonding behavior studies of cold sprayed copper coating on the PVC polymer substrate*. Surface and Coatings Technology, 2012. **207**: p. 262-269.
- [71] ASTM Standard E0384-17, Standard Test Method for Microindentation Hardness of Materials, ASTM International, 2017.
- [72] McDonald, A., M. Lamontagne, S. Chandra, and C. Moreau, *Photographing impact of plasma-sprayed particles on metal substrates*, Journal of Thermal Spray Technology, 2006. **15**: p. 708-716.
- [73] Zygo, Mx Surface Texture Parameters. 2018.
- [74] Fujii, S., H. Hamasaki, H. Takeoka, T. Tsuruoka, K. Akamatsu, and Y. Nakamura, *Electroless nickel plating on polymer particles*, Journal of colloid and interface science, 2014. **430**: p. 47-55.

- [75] Balaraju, J. N., Kalavati, and K. S. Rajam, *Surface morphology and structure of electroless ternary NiWP deposits with various W and P contents*, Journal of Alloys and Compounds, 2009. **486**(1-2): p. 468-473.
- [76] Lee, C. K., Structure, electrochemical and wear-corrosion properties of electroless nickel-phosphorus deposition on CFRP composites, Materials Chemistry and Physics, 2009. **114** (1): p. 125-133.
- [77] Smits, F.M., *Measurement of sheet resistivities with the four-point probe*, The Bell System Technical Journal, 1958. **37**(3): p. 711-718.
- [78] Balaraju, J. N. and K. S. Rajam, *Electroless deposition of Ni-Cu-P, Ni-W-P and Ni-W-Cu-P alloys*, Surface and Coatings Technology, 2005. **195**(2-3): p. 154-161.
- [79] Balaraju, J. N., P. Radhakrishnan, V.Ezhilselvi, A. A. Kumar, Z. Chen, and K.P.Surendran, *Studies on electroless nickel polyalloy coatings over carbon fibers/CFRP composites*, Surface and Coatings Technology, 2016. **302**: p. 389-397.
- [80] Nikolić, N. D., K. I. Popov, L. J. Pavlović, and M. G. Pavlović, The effect of hydrogen codeposition on the morphology of copper electrodeposits. I. the concept of effective overpotential, Journal of Electroanalytical Chemistry, 2006. **588**(1), p. 88–98.
- [81] Nikolić, N. D., L. J. Pavlović, M. G. Pavlović, and K. I. Popov, *Effect of temperature on the electrodeposition of disperse copper deposits*, Journal of the Serbian Chemical Society, 2007. **72**(12): p. 1369-1381.
- [82] Fukumoto, M., M. Mashiko, M. Yamada, and E. Yamaguchi, *Deposition behavior of copper fine* particles onto flat substrate surface in cold spraying, Journal of thermal spray technology, 2010. **19**(1-2): p. 89-94.
- [83] Meng, F., D. Hu, Y. Gao, S. Yue, and J. Song, *Cold-spray bonding mechanisms and deposition efficiency prediction for particle/substrate with distinct deformability*, Materials & Design, 2016. **109**: p. 503-510.
- [84] Bae, G., Y. Xiong, S. Kumar, K. Kang, and C. Lee, *General aspects of interface bonding in kinetic sprayed coatings*, Acta Materialia, 2008. **56**(17): p. 4858-4868.
- [85] Christoulis, D. K., S. Guetta, V. Guipont, and M. Jeandin, *The influence of the substrate on the deposition of cold-sprayed titanium: An experimental and numerical study*, Journal of Thermal Spray Technology, 2011. **20**: p. 523-533.
- [86] Yin, S., X. Suo, J. Su, Z. Guo, H. Liao, and X. Wang, *Effects of substrate hardness and spray angle on the deposition behavior of cold-sprayed ti particles*, Journal of Thermal Spray Technology, 2014. **23**: p. 76-83.
- [87] McDonald, A. G., A. N. Ryabinin, E. Irissou, and J. G. Legoux, *Gas-substrate heat exchange during cold-gas dynamic spraying*, Journal of Thermal Spray Technology, 2013. **22**: p. 391-397.
- [88] Fukumoto, M., H. Wada, K. Tanabe, M. Yamada, E. Yamaguchi, A. Niwa, M. Sugimuto, and M. Izawa, *Effect of substrate temperature on deposition behavior of copper particles on substrate surfaces in the cold spray process*, Journal of Thermal Spray Technology, 2007. **16**: p. 643-650.

- [89] Lopera-Valle, A., and A. McDonald, *Application of Flame-Sprayed Coatings as Heating Elements for Polymer-Based Composite Structures*, Journal of Thermal Spray Technology, 2015. **24**: p. 1289-1301.
- [90] McCune, R. C., W. T. Donlon, O. O. Popoola, and E. L. Cartwright, *Characterization of copper layers produced by cold gas-dynamic spraying*, Journal of Thermal Spray Technology, 2000. **9**: p. 73-89.
- [91] Arabgol, Z., M. Villa Vidaller, H. Assadi, F. Gärtner, and T. Klassen, *Influence of thermal properties and temperature of substrate on the quality of cold-sprayed deposits*, Acta Materialia, 2017. **127**: p. 287-301.
- [92] Koivuluoto, H., A. Coleman, K. Murray, M. Kearns, and P. Vuoristo, *High pressure cold sprayed* (HPCS) and low pressure cold sprayed (LPCS) coatings prepared from OFHC Cu feedstock: Overview from powder characteristics to coating properties, Journal of Thermal Spray Technology, 2012. **21**: p. 1065-1075.
- [93] Webster, J. G., Electrical measurement, signal processing, and displays, 2003.
- [94] Tejero-Martin, D., M. Rezvani Rad, A. McDonald, and T. Hussain, *Beyond Traditional Coatings:* A Review on Thermal-Sprayed Functional and Smart Coatings, Journal of Thermal Spray Technology, 2019. **28**: p. 598–644.
- [95] Champagne, V.K., *The cold spray materials deposition process: fundamentals and applications*. 2007: Elsevier.
- [96] Assadi, H., F. Gärtner, T. Klassen, and H. Kreye, *Comment on 'Adiabatic shear instability is not necessary for adhesion in cold spray'*. Scripta Materialia, 2018.
- [97] Champagne, V. K., D. Helfritch, P. Leyman, S. Grendahl, and B. Klotz, *Interface material mixing formed by the deposition of copper on aluminum by means of the cold spray process*, Journal of Thermal Spray Technology, 2005. **14**: p. 330-334.
- [98] Fernandez, R. and B. Jodoin, *Cold Spray Aluminum–Alumina Cermet Coatings: Effect of Alumina Content*, Journal of Thermal Spray Technology, 2018. **27**(4): p. 603-623.
- [99] Yin, S., X. Wang, W. Li, H. Liao, and H. Jie, *Deformation behavior of the oxide film on the surface of cold sprayed powder particle*, Applied Surface Science, 2012. **259**: p. 294-300.
- [100] Ernst, K.R., J. Braeutigam, F. Gaertner, and T. Klassen, Effect of Substrate Temperature on Cold-Gas-Sprayed Coatings on Ceramic Substrates, Journal of Thermal Spray Technology, 2013.
  22(2): p. 422-432.
- [101] Xiong, Y., G. Bae, X. Xiong, and C. Lee, *The Effects of Successive Impacts and Cold Welds on the Deposition Onset of Cold Spray Coatings*, Journal of Thermal Spray Technology, 2010. **19**(3): p. 575-585.
- [102] Hassani, M., D. Veysset, Y. Sun, K.A. Nelson, and C.A. Schuh, *Microparticle impact-bonding modes for mismatched metals: From co-deformation to splatting and penetration*, Acta Materialia, 2020. **199**: p. 480-494.

- [103] Wang, X., and M. Hassani, *Ultra-High strain rate constitutive modeling of pure titanium using particle impact test*, Journal of Applied Mechanics, Transactions ASME, 2020. **87**(9): p. 091007.
- [104] King, P.C., G. Bae, S.H. Zahiri, M. Jahedi, and C. Lee, *An Experimental and Finite Element Study of Cold Spray Copper Impact onto Two Aluminum Substrates*, Journal of Thermal Spray Technology, 2009. **19**(3): p. 620-634
- [105] Fallah, P., S. Rajagopalan, A. McDonald, and S. Yue, *Development of hybrid metallic coatings on carbon fiber-reinforced polymers (CFRPs) by cold spray deposition of copper-assisted copper electroplating process*, Surface and Coatings Technology, 2020. **400**: p. 126231.
- [106] E. Broitman, *Indentation Hardness Measurements at Macro-, Micro-, and Nanoscale: A Critical Overview*, Tribology Letters, 2017. **65**.
- [107] Ning, Z., Y. He, and W. Gao, *Mechanical attrition enhanced Ni electroplating*, Surface and Coatings Technology, 2008. **202**(10): p. 2139-2146.
- [108] Abaqus, "ABAQUS/Standard analysis user's manual v14.2," SIMULIA, 2014.
- [109] Li, W. Y., S. Yin, and X. F. Wang, Numerical investigations of the effect of oblique impact on particle deformation in cold spraying by the SPH method, Applied Surface Science, 2010.
   256(12): p. 3725-3734.
- [110] Kumar, S., G. Bae, and C. Lee, *Influence of substrate roughness on bonding mechanism in cold spray*, Surface and Coatings Technology, 2016. **304**: p. 592-605.
- [111] G. R. Johnson and W. H. Cook, A Constitutive modeling and data for metals subjected to large strain rates and high temperatures, Proceedings of 7th international symposium on ballistics, 1983.
- [112] Cahoon, J. R., W. H. Broughton, and A. R. Kutzak, *The determination of yield strength from hardness measurements*, Metallurgical Transactions, 1971.
- [113] Manap, A., O. Nooririnah, H. Misran, T. Okabe, and K. Ogawa, *Experimental and SPH study of cold spray impact between similar and dissimilar metals*, Surface Engineering, 2014. **30**(5): p. 335-341.
- [114] Yin, S., X. F. Wang, W. Y. Li, and H. E. Jie, *Effect of substrate hardness on the deformation behavior of subsequently incident particles in cold spraying*, Applied Surface Science, 2011. **257**(17): p. 7560-7565.
- [115] Kuroda, S., J. Kawakita, M. Watanabe, and H. Katanoda, *Warm spraying-a novel coating process based on high-velocity impact of solid particles*, Science and technology of advanced materials, 2008. **9**(3): p. 033002-033002.
- [116] S Kuroda, S., M. Watanabe, K. Kim, and H. Katanoda, *Current Status and Future Prospects of Warm Spray Technology*, Journal of Thermal Spray Technology, 2011. **20**(4): p. 653-676.
- [117] Champagne, V.K., *The cold spray materials deposition process: fundamentals and applications*. 2007: Elsevier.

- [118] Lomonaco, P., S. Weiller, I. Feki, A. Debray, F. Delloro, M. Jeandin, B. Favini, and C. Rossignol, Cold Spray Technology to Promote Conductivity of Short Carbon Fiber Reinforced Polyether-Ether-Ketone (PEEK), Key Engineering Materials, 2019. **813**: p. 459-464.
- [119] Gillet, V., E. Aubignat, S. Costil, B. Courant, C. Langlade, P. Casari, W. Knapp, and M.P. Planche, *Development of low pressure cold sprayed copper coatings on carbon fiber reinforced polymer (CFRP)*, Surface and Coatings Technology, 2019. **364**: p. 306-316.
- [120] Della Gatta, R., A. Viscusi, A.S. Perna, A. Caraviello, and A. Astarita, *Feasibility of steel powder deposition on composites through cold spray*, Materials and Manufacturing Processes, 2020. **36**(3): p. 281-291.
- [121] Thesis | Surface preparation of polymeric substrates for cold spraying coatings | ID: 6h440z60f | eScholarship@McGill. https://escholarship.mcgill.ca/concern/theses/6h440z60f (accessed Apr. 29, 2022).
- [122] Thesis | Mechanisms affecting the metallization of carbon fiber reinforced polymers through the cold spraying of Sn-based mixed metal powders | ID: 76537606p | eScholarship@McGill. https://escholarship.mcgill.ca/concern/theses/76537606p (accessed Apr. 29, 2022).
- [123] Liberati, A.C., H. Che, P. Fallah, P. Vo, and S. Yue, *Pull-off Testing and Electrical Conductivity of Sn-Based Metal Powder Mixtures Cold Sprayed on Carbon Fiber-Reinforced Polymers*, Journal of Thermal Spray Technology, 2022. **31**: p. 1792–1812.
- [124] Rezzoug, A., S. Abdi, A. Kaci, and M. Yandouzi, *Thermal spray metallisation of carbon fibre reinforced polymer composites: Effect of top surface modification on coating adhesion and mechanical properties*, Surface and Coatings Technology, 2018. **333**: p. 13-23.
- [125] Fallah, P., R. Chakrabarty, J. Song, A. McDonald, and S. Yue, *Effect of Metallic Interlayer Hardness on Deposition Characteristics of Cold-Sprayed Copper Particles on Carbon Fiber-Reinforced Polymers*, Journal of Thermal Spray Technology, 2022. **31**(3): p. 559–573.
- [126] International, A., ASTM C633-13, Standard Test Method for Adhesion or Cohesion Strength of Thermal Spray Coatings. 2017: West Conshohocken, PA.
- [127] ISO ISO 27307:2015 Thermal spraying Evaluation of adhesion/cohesion of thermal sprayed ceramic coatings by transverse scratch testing.
- [128] M. Cailler and G. H. Lee, Scratch adhesion test of magnetron-sputtered copper coatings on aluminium substrates: Effects of the surface preparation, Thin Solid Films, 1989. **168**(2): p. 193–205.
- [129] Yu, S. J., L. X. Song, Y. S. Huang, R. G. Zhao, and X. F. Hu, *Electroless Ni-P-SiC composite coating*, Wuji Cailiao Xuebao/Journal of Inorganic Materials, 2004.
- [130] Agarwala, R., V. Agarwala, and R. Sharma, *Electroless Ni-P based nanocoating technology A review*, Synthesis and Reactivity in Inorganic, Metal-Organic and Nano-Metal Chemistry, 2006. **36**(6): p. 493-515.
- [131] Yamagishi, K., N. Okamoto, N. Mitsumata, N. Fukumuro, S. Yae, and H. Matsuda, *Reaction process of two-step Catalysation Pre-treatment for Electroless Plating on Non-conducting Substrates*, Transactions of the Institute of Metal Finishing, 2004. **82**(3–4): p. 114-117.

- [132] H. Jüntgen, *Activated carbon as catalyst support: A review of new research results*, Fuel, 1986. **65**(10): p. 1436–1446.
- [133] Luty-Błocho, M., M. Wojnicki, K. Pacławski, and K. Fitzner, *The synthesis of platinum nanoparticles and their deposition on the active carbon fibers in one microreactor cycle*, Chemical Engineering Journal, 2013. **226**: p. 46–51.
- [134] Lam, E., and J. H. T. Luong, *Carbon materials as catalyst supports and catalysts in the transformation of biomass to fuels and chemicals*, ACS Catalysis, 2014. **4**(10): p. 3393–3410.
- [135] Van Den Meerakker, J. E. A. M., On the mechanism of electroless plating. II. One mechanism for different reductants, Journal of Applied Electrochemistry, 1981. 11(3): p. 395–400.
- [136] S. J. Bull, *Failure modes in scratch adhesion testing*, Surface and Coatings Technology, 1991. **50**(1): p. 25–32.
- [137] Váz, R. F., A. Silvello, P. D. Cavalière, S. Dosta, I. G. Cano, L. Capodieci, A. Rizzo, and D. Valerini, *Fretting Wear and Scratch Resistance of Cold-Sprayed Pure Cu and Ti*, Metallography, Microstructure, and Analysis, 2021. **10**(4): p. 496–513.
- [138] Vencl, A., S. Arostegui, G. Favaro, F. Zivic, M. Mrdak, S. Mitrovic, and V. Popovic, *Evaluation of adhesion/cohesion bond strength of the thick plasma spray coatings by scratch testing on coatings cross-sections*, Tribology International, 2011. **44**(11), p. 1281–1288.
- [139] Liu, T., J. D. Leazer, and L. N. Brewer, *Particle deformation and microstructure evolution during cold spray of individual Al-Cu alloy powder particles*, Acta Materialia, 2019. **168**: p. 13–23.
- [140] M. Hamdi, M. N. Saleh, and J. A. Poulis, *Improving the adhesion strength of polymers: effect of surface treatments*, Journal of Adhesion Science and Technology, 2020. **34**(17): p. 1853–1870.
- [141] Borchers, C., F. Gärtner, T. Stoltenhoff, H. Assadi, and H. Kreye, *Microstructural and macroscopic properties of cold sprayed copper coatings*, Journal of applied physics, 2003. **93**(12): p. 10064-10070.
- [142] Munagala, V. N. V., V. Akinyi, P. Vo, and R. R. Chromik, *Influence of Powder Morphology and Microstructure on the Cold Spray and Mechanical Properties of Ti6Al4V Coatings*, Journal of Thermal Spray Technology, 2018. **27**(5): p. 827–842.
- [143] Zou, Y., D. Goldbaum, J. A. Szpunar, and S. Yue, *Microstructure and nanohardness of cold-sprayed coatings: Electron backscattered diffraction and nanoindentation studies*, Scripta Materialia, 2010. **62**(6): p. 395–398.
- [144] Aviation Handbooks & Manuals | Federal Aviation Administration. https://www.faa.gov/regulations\_policies/handbooks\_manuals/aviation (accessed May 06, 2022).
- [145] Nikolić, N. D., K. I. Popov, Lj. J. Pavlovic, and M. G. Pavlovic, *Morphologies of copper deposits obtained by the electrodeposition at high overpotentials*, Surface and coatings technology, 2006. **201**(3-4): p. 560-566.

# **Appendix A**

1) Figure 3-15 in chapter 3 is presented here with an enhanced clarity of the legends and coordinates.

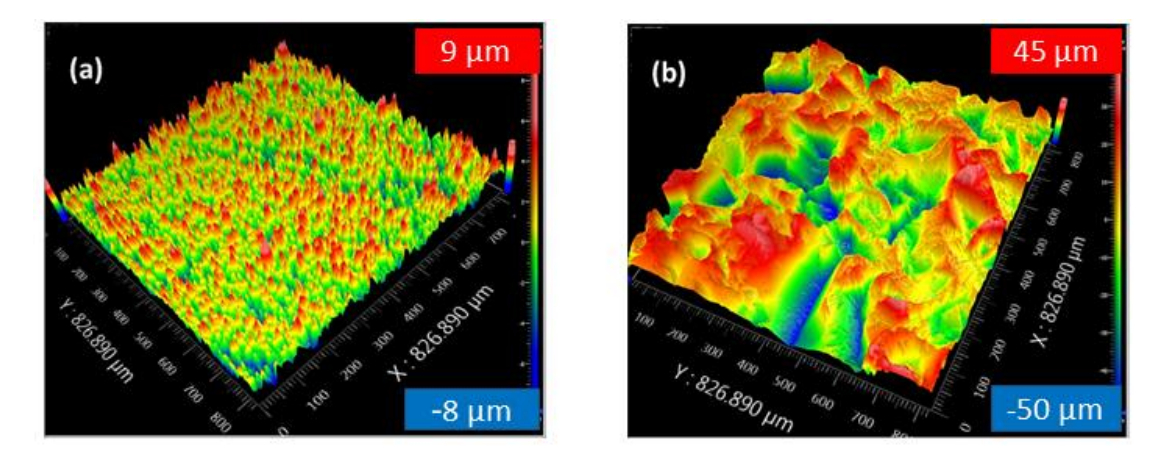


Figure 3-15: Surface topologies of (a) Cu electroplated interlayer, and (b) grit-blasted copper panel

2) In chapter 4, the standard deviation of the particle velocities in Table 4-8 is approximately  $\pm 45$  m/s for all the three gas pressures.